Mémoire

Auteur : Delguste, Romane
Promoteur(s) : Delrez, Laetitia; Pozuelos Romero, Francisco José
Faculté : Faculté des Sciences
Diplôme : Master en sciences spatiales, à finalité approfondie
Année académique : 2021-2022
URI/URL : http://hdl.handle.net/2268.2/16199

FACULTY OF SCIENCES, UNIVERSITY OF LIÈGE

Searching for multi-planet systems in TESS data

Romane Delguste

Master in Space Sciences, Research Focus

Supervisors: Laetitia Delrez - Francisco Pozuelos

Academic year 2021-2022

Acknowledgements

I would like to thank my supervisors Laetitia Delrez and Francisco Pozuelos for the proposal of this subject, on which I really enjoyed working throughout this year, and above all for their availability, their advice and all the time they spent to help me in carrying out this master thesis.

I would also like to thank Juliette and Lisa for our working sessions together that helped me to keep going, even on the bad days, and my stepfather for his language corrections on this work and on many others.

Contents

List of Figures

List of Tables

Abbreviations

BLS	Box Least Squares
BTJD	TESS Barycentric Julian Day
CHEOPS	CHaracterising ExOPlanet Satellite
ExoFOP	Exoplanet Follow-up Observing Program
FAP	False Alarm Probability
FOV	Field Of View
FPP	False Positive Probability
MAST	Mikulski Archive for Space Telescope
NFPP	Nearby False Positive Probability
RMS	Root-Mean-Square
SDE	Signal Detection Efficiency
SHERLOCK	Searching for Hints of Exoplanets fRom Lightcures Of spaCe-based seeKers
SNR	Signal-to-Noise Ratio
SPOC	TESS Science Processing Operations Center
TCE	Threshold Crossing Event
TESS	Transiting Exoplanet Survey Satellite
TFOPWG	TESS Follow-up Observing Program Working Group
TIC	TESS Input Catalog
TLS	Transit Least Squares
TOI	TESS Object of Interest
TRICERATOPS	Tool for Rating Interesting Candidate Exoplanets and Reliability Analysis of Transits Originating from Proximate Stars

Chapter 1

Introduction

1.1 Context

The search for exoplanets is a burgeoning field. To date, 5069 confirmed exoplanets have been discovered, and most of them during the last decade. Among those planets, 3912 are transiting planets, meaning that these planets pass in front of their host star as seen from the Earth. The transit method is the most effective to discover new planets, mostly thanks to the Kepler mission which is at the origin of many detections. [32]

Figure 1.1 illustrates the cumulative detections per year with the detection methods detailed.

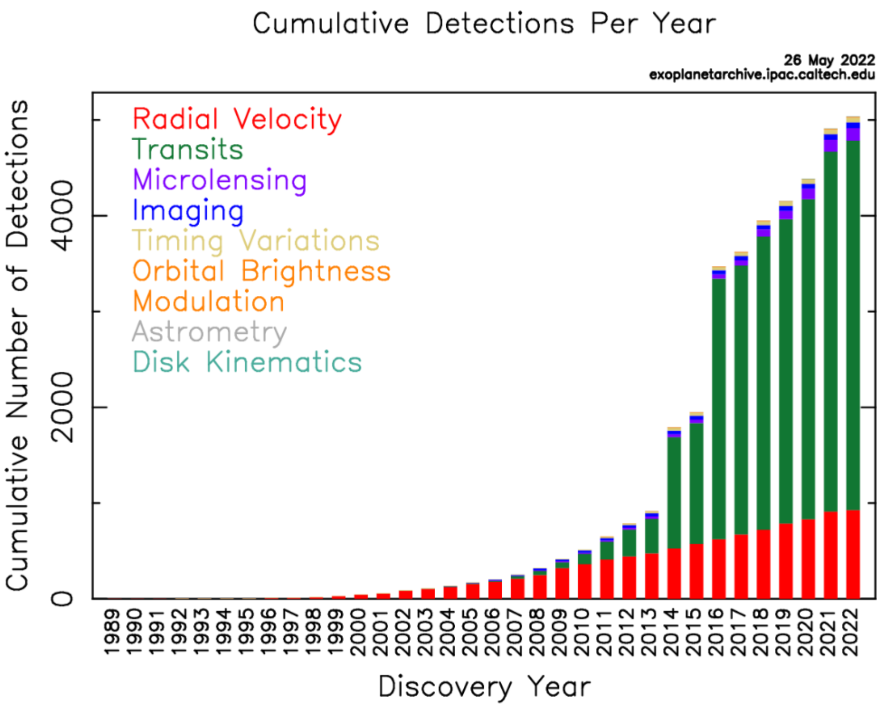

Figure 1.1: Cumulative exoplanet detections per year [32].
The different colors indicate the detection method used.

In this work, we focus on systems where there is already at least one transiting planet candidate. Assuming that planets in a system have similar orbital planes, if one of the planets is transiting it increases the probability that the other planets, if any, are also transiting their star. Moreover, systems with several transiting planets are of particular interest. Indeed, multi-planetary systems allow a better characterization of their planet's interiors by exploiting the correlations between the data of the different planets. [6] They also enable a direct comparison of the planets with one another to study for example the evolution of some properties (interiors, atmospheres) with the orbital distance to the star. Since the planets in the same system have been formed in the same protoplanetary disk, their formation and evolution models are also better constrained. [1]

The goal of this master thesis is to look in TESS (section 1.3) data of systems with already at least one transiting planet candidate, called "TESS Object of Interest" (TOI), and to scrutinize their brightness over a period of time (lightcurve) using SHERLOCK (described in chapter 2) to identify some possible transit-like signals that can hint at the presence of additional planets. The planets we are looking for may have been missed by TESS automatic detection pipeline, if they produce transit signals that are below the set detection threshold (SNR=7.1). We thus need to perform our own transit search using a lower detection threshold in order to find them. Those planets may have long orbital periods, meaning not many transits observed, and/or small radii, resulting in shallow transits.

In addition to the condition of systems with already at least one TOI, the targets were also selected to be compatible with follow up observation by CHEOPS (section 1.4). Ultimately, a selection of 100 targets have been analysed within the framework of this master thesis.

1.2 Transits

Since we are using transits to identify planetary signals in TESS data, it is worth defining some important concepts [30].

We call an eclipse the obscuration of a celestial body by another one. When the apparent sizes of the two bodies are very different, we talk about transits and occultations. The situation where the smaller body passes in front of the larger one corresponds to a transit, while the reverse configuration is called an occultation. In the latter case, the smallest body is completely hidden behind the other one. If we consider a circular orbit, transits and occultations always go together, but for an eccentric orbit, we could observe only transits or only occultations.

In order to describe transits, we also need to introduce the contact times. The four contact points $t_I - t_{IV}$ are illustrated in figure 1.2. We can then define the total duration as $T_{tot} = t_{IV} - t_I$, the full duration (when the entire disk of the smaller body is in front of the larger one) as $T_{full} = t_{III} - t_{II}$, the ingress duration as $\tau_{ing} = t_{II} - t_I$, and the egress duration as $\tau_{egr} = t_{iv} - t_{III}$. Note that for a grazing transit, corresponding to the situation where the disks of the two bodies do not overlap completely, the second and third contact points do not occur.

The impact parameter "b" is also illustrated in figure 1.2. This quantity is defined as the sky-projected distance between the centre of the stellar disc and the centre of the planetary disk at conjunction (i.e. when the two objects are most closely aligned as seen from Earth). The impact parameter can take values between 0 and 1, corresponding respectively to situations where the planet crosses the centre or the edge of the stellar disk. The total transit duration will thus depend on the impact parameter, with a longer duration for $b = 0$ and a shorter transit duration for $b = 1$.

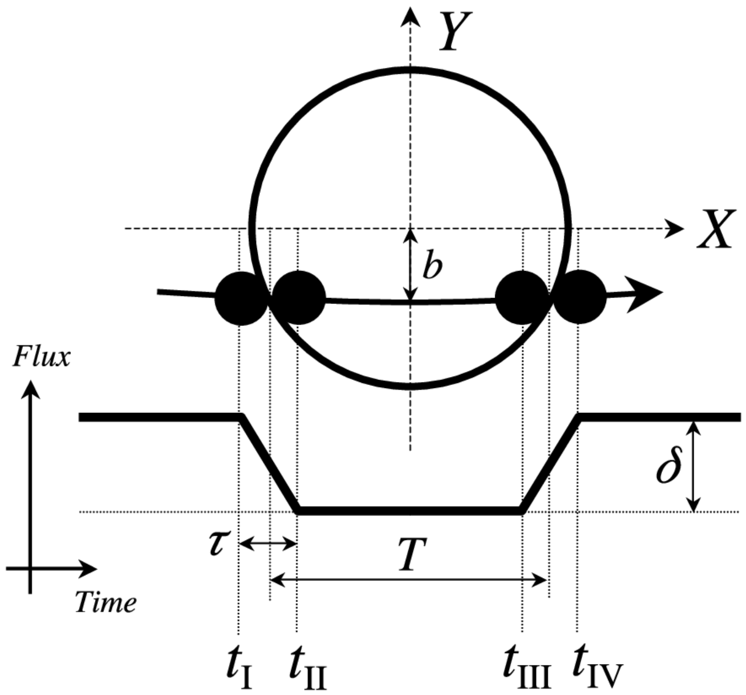

Figure 1.2: Illustration of a transit with the four contact points $t_I - t_{IV}$ along with the idealized lightcurve produced [30].

The condition for an observer to see an eclipse (or transit) is to be positioned in such a way that the orbital plane of the planet is seen nearly edge-on. More specifically, as the planet orbits its star, its shadow describes a cone that sweeps out a band on the celestial sphere, and transits are only visible by observers within this band (figure 1.3). The cone is called the "penumbra" and has an opening angle Θ with $\sin\Theta = \frac{(\mathrm{R_s}+\mathrm{R_p})}{\mathrm{r}}$ where R_s is the radius of the star, R_p the radius of the planet, and r the instantaneous distance between the star and the planet.

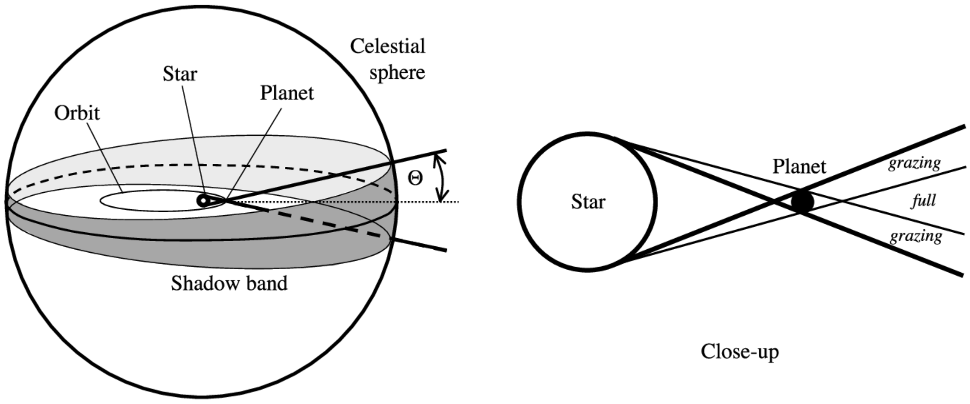

Figure 1.3: Shadow band on the celestial sphere and close-up on the penumbra cone [30].

From geometrical considerations, assuming we are in the case of a circular orbit and that $R_p << R_s$ (which is usually the case for a planet transiting a star), the probability to have a transit can be written:

$$p_{tra} = \frac{R_s}{a}$$

where a is the semi-major axis of the orbit. Therefore, the probability to get a transit increases when the value of a decreases. Using Kepler's third law, this means that the transit method favours the detection of short-period exoplanets.

When we want to observe transits of exoplanets, we cannot actually see the darker disk of the planet against the bright disk of the star, like it is the case for instance for Venus in our solar system. The way to detect those events is then to observe the variation of the flux of the star. Obviously, the measured flux is the combined flux of the star and the planet. During a transit, the observed flux decreases since the planet blocks a part of the light coming from the star. The flux will then increase after the transit and decreases again during the occultation (however this decrease is much smaller than during the transit). Note that there are two contributions to the flux coming from the planet: its own (thermal) emission, and the light of the star reflected on its surface. The general shape of the observed flux during one complete orbit of the transiting planet is illustrated in figure 1.4.

Assuming that the flux from the planetary disk is negligible compared to the stellar flux, the relative flux decrease during a transit is given by:

$$\frac{\Delta F_s}{F_s} = \frac{\pi R_s^2 - (\pi R_s^2 - \pi R_p^2)}{\pi R_s^2} = \frac{R_p^2}{R_s^2}$$

This quantity is the transit depth, corresponding to the δ parameter in figure 1.2.

The relation obtained means that the observation of a transit provides us with a direct measurement of the planet's radius relative to the radius of the star. Therefore, if one knows R_s, one may determine R_p. Furthermore, if one can estimate the mass of the planet (typically by using radial velocity measurements), one can also determine the mean density of the planet, which gives a first indication about its bulk composition.

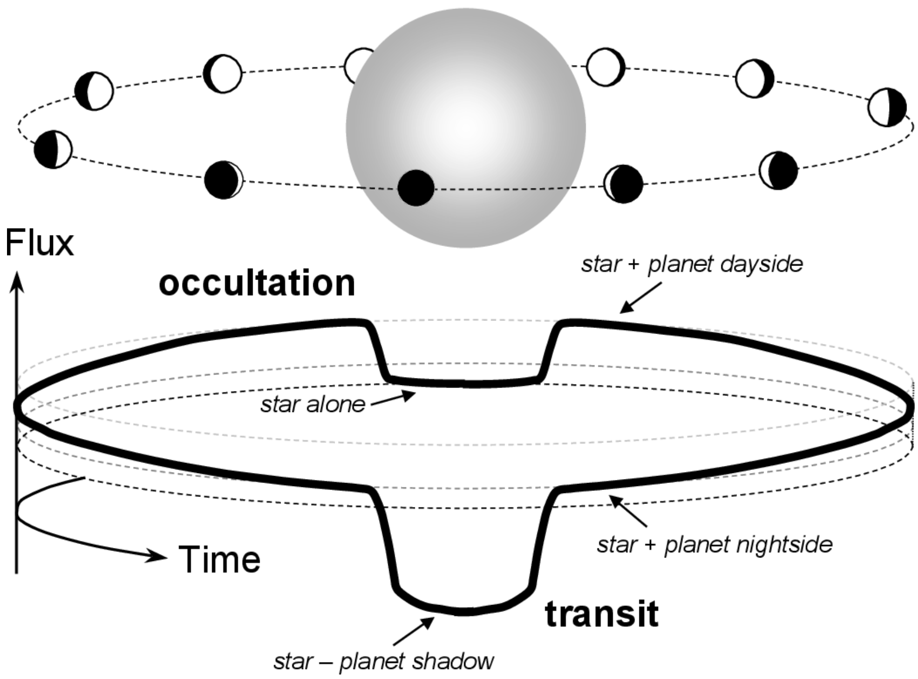

Figure 1.4: Variations of the combined flux of the star and planet (measured flux) during one full orbit of a transiting planet [30].

In order to have a first look at the order of magnitude of the relative flux decrease, we can make the calculation for some planets of our solar system.

For the Earth:

$$\frac{R_p^2}{R_s^2} = \frac{(6.3781 \times 10^6)^2}{(6.957 \times 10^8)^2} \approx 0.008\%$$

For Jupiter:

$$\frac{R_p^2}{R_s^2} = \frac{(7.1492 \times 10^7)^2}{(6.957 \times 10^8)^2} \approx 1.06\%$$

The detection of Earth-like planets around Sun-like stars can thus be difficult with the transit method but can still be achieved with space telescopes.

Some important observables from a transit light curve are:

- The recurrence of the transit (period)
- The relative change of the stellar flux (transit depth)

- The duration of the transit (transit width)
- The mid-transit time (T0)

The period, the transit depth and the transit width are illustrated on a lightcurve, extracted from TESS data (TOI 34077285), in figure 1.5.

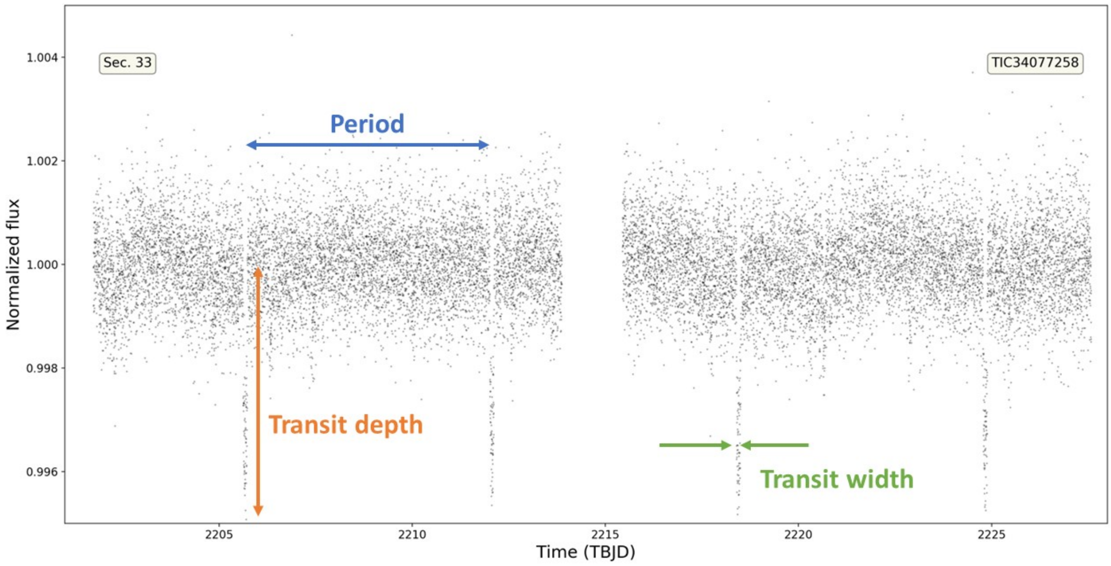

Figure 1.5: Transit parameters.
Period, transit depth and transit width illustrated on the lightcurve of TOI 34077285, for which transits are clearly visible.

The main drawback when using the transit method is that periodic variations of the flux can have other causes than a transiting planet, like eclipsing binaries or variability of the star itself. The false positive scenarios considered are described in section 2.3.

1.3 TESS

As mentioned in section 1.1, the data used to carry out this work come from the TESS mission [25]. In this section, I will briefly describe this mission and its observation strategy.

TESS stands for "Transiting Exoplanet Survey Satellite". This mission focuses on the discovery of transiting exoplanets around bright nearby stars, allowing follow-up measurements of the mass and atmospheric composition of the planets. In particular, TESS concentrates on main-sequence stars with spectral types between F5 and M5. Indeed, stars with earlier spectral types are larger, making more difficult the detection of transiting planets, while stars with spectral types later than

M5 are less abundant and optically faint. Since those bright stars are nearly evenly distributed in the sky, the choice of an all-sky survey has been made.

TESS uses a 600 to 1000 nm bandpass. The width of 400 nm corresponds to the largest practical choice for the optical design. This bandpass is centered on the I_C band but is wider. Since small planets are more easily detected around small stars, which are cool and red, this explains the choice of an enhanced sensitivity to red wavelengths.

TESS is in a highly elliptical orbit around the Earth, with a period of 13.7 days. This orbit prevents the satellite from passing into the Earth's radiation belt, which could damage the CCDs. This orbit is also in a 2:1 resonance with the Moon, implying that lunar perturbations are roughly averaged to zero with the Moon leading or lagging TESS at apogee by $\sim$90°.

TESS has a "stare and step" observation strategy. The satellite points antisolar and observes a sector with a size of 24° x 96° continuously for about 27 days (corresponding to two orbits). It takes two years (26 sectors) to observe the entire sky. Each star is observed between 1 month and 1 year, depending on its position on the sky. In this way, stars located where the observation sectors overlap (e.g. at the ecliptic poles) benefit the longer observation periods.

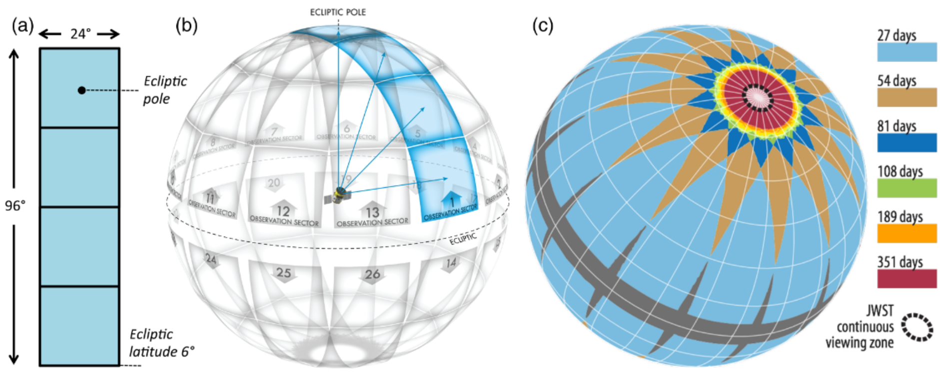

Figure 1.6: TESS division of the sky in sectors [25].
The left panel represents a single sector divided into the respective fields of view of the four CCD cameras. The middle panel illustrates the division of the sky into 26 sectors. And the right panel shows the duration of observations, taking into account the overlap of the sectors.

TESS cameras have an exposure time of 2 seconds. Pixels in postage stamps around 200,000 preselected stars will be downloaded at 2 minute cadence, meaning that images are summed in groups of 60 into 120-second stacks. This cadence is short enough to resolve the ingress and egress for the brighter planet candidates. Full frame images will also be collected at 30 minute cadence, allowing to perform general variability studies of the other stars in the field of view.

It is worth mentioning that TESS have large pixels (21 arcsec), which can lead to some contamination of the target's photometry by nearby stars. If one, or more, of those nearby objects show some variability, it can result in a false positive signal (see section 2.3).

Since TESS was launched in April 2018, we are currently in the fifth year of observation. Basically, the observation plan year-by-year [33] is:

- Year 1 (July 2018-July 2019): southern ecliptic hemisphere (sectors 1-13)
- Year 2 (July 2019-July 2020): northern hemisphere observed (sectors 14-26)
- Year 3 (July 2020-July 2021): southern ecliptic hemisphere re-observed (sectors 27-39)
- Year 4: (July 2021-September 2022): part of northern hemisphere re-observed and observation of the ecliptic (sectors 40-55)
- Year 5: observation of northern hemisphere will be completed, and a new observation of the southern hemisphere will begin (sectors 56-69)

All TESS data are automatically processed by the SPOC pipeline. They are calibrated, and from the calibrated data are generated the photometric results for each target. The Planet Search pipeline is then run and transit signals are searched with a SNR $>= 7.1$ [16].

If the transit detection threshold is exceeded and if transit consistency checks are satisfied, a Threshold Crossing Event (TCE) is generated. A suite of validation tests is then performed on each TCE and the light curves are searched for additional TCEs, after modeling and removing transit signatures. Then, a suite of diagnostic tests is performed on all candidates to aid in discrimination between genuine transiting planets and instrumental or astrophysical false positives [28].

All the TESS data products are publicly available on the MAST (Mikulski Archive for Space Telescope) archive [31]. The most promising planet candidates are then given a TOI name and released publicly on the ExoFOP website [34] with some basic information about the star, planet candidate(s), follow-up observations etc.

TESS already provided numerous exoplanet discoveries, including some terrestrial-sized planets such as : a "hot Earth" orbiting the M dwarf LHS 3844 with a very short period of 11 hours [29], a system of three planets with periods ranging between 2.25 and 7.45 days around the bright M dwarf L 98-59 [18], a Super-Earth transiting the bright solar-type star π Men with an orbital period of 6.27 days [15], a hot rocky super-Earth and a warm puffy super-Earth with respective orbital periods of 4.76 and 17.18 days [7]... To date, 233 confirmed planets have been discovered by TESS. We call "confirmed planets" the ones that have been published in peer-reviewed journals. While the number of TOIs, which are transit-like events that appear to be astrophysical in origin, amounts to 5808 at the time of writing [34].

Beside the search for exoplanets, TESS data also provided material for some publications about other phenomena, such as stellar variability [23] and flares [10].

1.4 CHEOPS

If a new transit-like signal is found in the TESS data analysed in this work, and if it is convincing enough, our ultimate goal would be to perform follow-up observations of the target with the CHEOPS satellite [3]. This mission is briefly described hereafter.

CHEOPS stands for "CHaracterising ExOPlanet Satellite". It was launched in December 2019 and the primary mission is expected to last 3.5 years. While TESS could be compared to Kepler or Corot, there is a fundamental difference between CHEOPS and those missions: its follow-up nature.

CHEOPS focuses on obtaining ultra-high precision photometry of bright stars with magnitudes ranging from 6 to 12 in the V-band, already known to host planets, with a single star being targeted at the time. The goal of this mission is thus not to discover new transiting planets, but to provide or improve radii measurements for interesting targets. It can also identify prime targets for future spectroscopic characterization of exoplanetary atmospheres. Those goals were successfully achieved for example with the hot Jupiter WASP-189b, where an occultation were observed in addition to two transits, providing some information about its atmosphere along with better estimations of the planetary properties [20]. CHEOPS also allowed to refine the planetary parameters of the three low mass planets orbiting HD 136352 [5], and to confirm the orbital configuration of the six planets in TOI-178, where five planets form a chain of Laplace resonances[19]. CHEOPS is therefore complementary to other transit missions such as TESS.

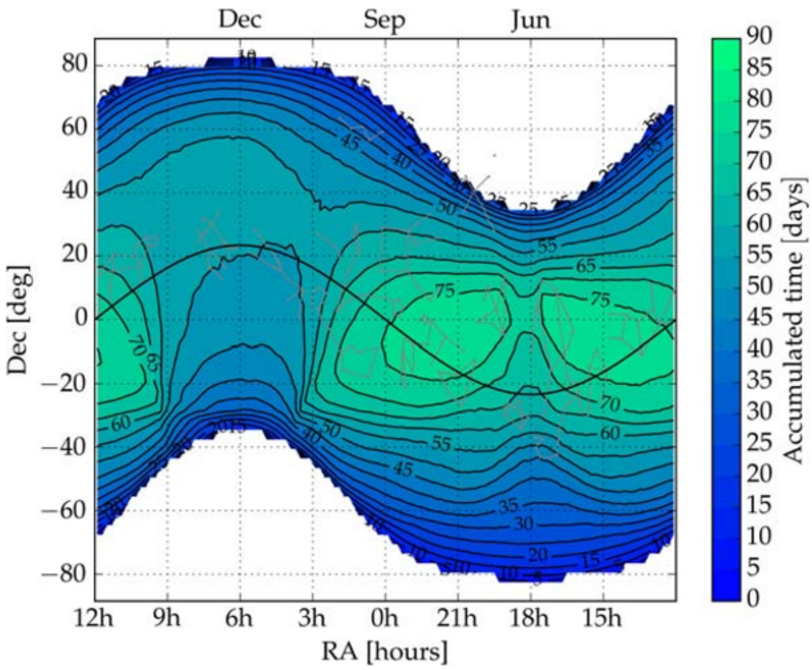

Figure 1.7: CHEOPS visibility map [3].
The color code shows the accumulated observation time in days over one year for each possible pointing direction. The thick black line in the middle is the ecliptic. Zodiacal constellations are also over-plotted in grey with some other constellations for reference. December, September and June are specified to indicate at which time of the year a certain region of the sky is observable.

Chapter 2

SHERLOCK

The main tool used to complete this master thesis is SHERLOCK (Searching for Hints of Exoplanets fRom Lightcurves Of spaCe-based seeKers) [24] [35]. The goal of this pipeline is to ease the process of searching for transiting exoplanet candidates. This is done by minimizing the manipulation of the data by the user.

SHERLOCK has six modules that respectively allow to: acquire and prepare the light curves from their repositories; search for planetary candidates; perform a vetting of the most promising signals; compute a statistical validation; model the signals to refine their ephemerides; and compute the observational windows from ground-based observatories. The search for candidates 2.1, the vetting 2.2, and the statistical validation 2.3 are described in the next sections of this chapter. To execute all these modules, the user only needs to fill an initial `yaml` file with some basics information such as the star ID, the cadence to be used, etc., and use sequentially a few lines of code to pass from one step to the next.

2.1 Search for candidates

SHERLOCK uses a multi-detrend approach. The light curve is detrended a number of times, with different window sizes. This is done with a biweight algorithm from the wotan package. [12]

The idea behind detrending is to remove instrumental and/or stellar noise while preserving the transit signals. The window size used for the detrending should be short enough to remove the stellar/instrumental noise but long enough to preserve the transits. This is can be complicated, especially since we do not know the duration of the transits that we are looking for, and there is always a risk that detrending will alter the transit signals, in particular short and shallow ones. This is the reason why SHERLOCK is exploring different detrendings using various widow sizes.

The search for transits is performed with the TLS (Transit Least Squares) algorithm [13]. TLS searches for transits using a transit-like search function, assuming a realistic shape with ingress, egress and stellar limb darkening. Thus, it approximates the transit shape more accurately than the classical BLS (Box Least Squares) algorithm, which uses box functions. TLS has a more sensitive detection statistic and is optimized to find small planets in large data sets, even if large planets producing deep transits can also be found with this algorithm.

The TLS algorithm searches for periodic transit-shaped signals in flux measurements. The algorithm operates by phase-folding the data over a range of trial periods, transit epochs and transit durations. It then calculates the χ^2 statistic of the phase folded curve between the data points of the respective transit model and the observed values and searches the minimum χ^2.

The search for planetary candidates with SHERLOCK is an iterative process. For each run, the most promising signal is selected. Then, the transits corresponding to this signal are masked, and in the next run we search for a new signal in the remaining portions of the lightcurve. The process stops when the maximum number of runs is reached, or when the selected signal is not good enough to continue.

In order to start the search for candidates, we need to provide SHERLOCK with a `yaml` file containing all the necessary information relative to the target that we want to investigate.

The main parameters that should be included in the `yaml` file are:

- The star ID. Here we use the TIC ID, which is the identifier in the TESS Input Catalog. This catalog is a collection of sources on the sky, for use by the TESS mission to select target stars to observe, and to provide stellar parameters useful for the evaluation of transit signals [27].
- MODE: can be either set to GLOBAL, SECTOR or BOTH. Those three modes respectively mean that, if several sectors are available, SHERLOCK will run all the sectors together, separately or both.
- AUTO_DETREND_ENABLE: allows an initial detrend execution against the original light curve to remove strong periodic trends (due to stellar variability) which might considerably affect the entire execution of SHERLOCK.
- INITIAL_HIGH_RMS_MASK: if enabled, an initial mask for high RMS (root-mean-square) areas is applied only to short cadence light curves.
- INITIAL_SMOOTH_ENABLED: if enabled, an initial Savitzky-Golay filter [26] is applied to smooth and reduce the local noise in the data. This option is only available for the short cadence light curves.
- INITIAL_HIGH_RMS_TRESHOLD: upper limit for the data RMS deviation computed by four-hour binning. Data over this threshold is masked.

- DETREND_L_MIN: minimum detrend window to build the detrends set.
- DETREND_L_MAX: maximum detrend window to build the detrends set.
- DETREND_NUMBER: number of detrend models to be generated from the original light curve.
- DETREND_CORES: number of CPU cores to detrend the original light curve.
- CPU_CORES: number of cores used during the search process.
- MAX_RUNS: maximum number of runs of SHERLOCK.
- SNR_MIN: signal-to-noise ratio threshold for a candidate to be accepted and finish the execution.
- SDE_MIN: SDE (signal detection efficiency) threshold for a candidate to be accepted and finish the execution. SDE characterizes how confident we can be in the detection.
- PERIOD_MIN: minimum period for the search period grid.
- PERIOD_MAX: maximum period for the search period grid.
- INITIAL_MASK: if enabled, a mask is applied to the time ranges specified. It can be used in case of an anomaly in the lightcurve, or to mask deliberately some events.
- INITIAL_MASK_TRANSIT: if enabled, this feature allows to mask manually transiting candidates. We need to provide the epoch, the period and the duration of the transit.
- BEST_SIGNAL_ALGORITHM: this specifies the algorithm used to decide which signal is the best one for each run. Basically, SHERLOCK will select the signal with the highest SDE from all the detrended light curves. The quorum algorithm will also take into account the number of detrends that selected the same signal.

Note that SHERLOCK will use by default parameters of the host star given by the database used. But it is also possible to specify the values that we want to use for the mass, radius and effective temperature of the star.

We can look at an example of this file for TIC 34077285, filled with typical values used for this work.

The SNR and SDE thresholds are deliberately set to low values. The reason is that we are looking for planetary candidates that may have been missed by TESS automatic detection pipelines. Therefore, they probably have rather low SNR and/or SDE.

The signal to noise ratio is defined by $SNR = \frac{d}{\sigma} n^{1/2}$ with d the mean transit depth, σ the standard deviation of the out-of-transit points, and n the number of in-transit points.

```yaml
TARGETS:
 TIC 34077285:
   #MODE: BOTH
   MODE: GLOBAL
   #MODE: SECTORS
   AUTO_DETREND_ENABLED: False
   INITIAL_HIGH_RMS_MASK: False
   INITIAL_SMOOTH_ENABLED: True
   INITIAL_HIGH_RMS_THRESHOLD: 2
   DETREND_L_MIN: 0.2
   DETREND_L_MAX: 1.2
   DETRENDS_NUMBER: 10
   DETREND_CORES: 35
   CPU_CORES: 35
   MAX_RUNS: 5
   SNR_MIN: 5
   SDE_MIN: 5
   PERIOD_MIN: 0.2
   PERIOD_MAX: 30
   BEST_SIGNAL_ALGORITHM: quorum
```

Figure 2.1: An example of the `yaml` file used to analyse the TIC 34077285.

In order to compute the signal detection efficiency, the TLS calculates the signal residue (SR) from the distribution of minimum χ^2 as a function of the period. The signal detection efficiency distribution as a function of the period SDE(P) is then:

$$SDE(P) = \frac{1 - < SR(P) >}{\sigma(SR(P))}$$

With $< SR(P) >$ the arithmetic mean, $\sigma(SR(P))$ the standard deviation and SR_{peak} the peak value of $SR(P)$. An SDE value of x for any given P means that the statistical significance of this period is $x * \sigma$ compared to the mean significance of all other periods.

The maximum number of runs is almost always set to 5. This is because of the iterative nature of the process, which keeps removing for each run the parts of the lightcurve corresponding to transits of the most promising signal. In short, the more we run the search stage, the less data are left.

Concerning the auto detrend, the initial high RMS mask and the initial smooth options: we chose to use them or not on a case-by-case basis. In order to decide, before running the full search process, whether or not those parameters should be enabled, one can only run the preparation stage with the command:

`python3 -m sherlockpipe --properties prop.yaml --explore`

With "prop.yaml" being the `yaml` file containing all the properties.

Once the parameters are adjusted, one can run the whole searching process by using: **`python3 -m sherlockpipe --properties prop.yaml`**

Once this search stage is over, SHERLOCK produces a new directory containing:

- A directory for each run, containing plots of the detrended fluxes and their suggested transits, along with the corresponding lightcurve in csv files
- A directory with the field of view (FOV), if available, to inspect the neighbourhood of the target
- A directory with the RMS masking plots, only if the high RMS mask is enabled
- A directory with plots of the detrending models for each window sizes
- A Lomb-Scargle periodogram and the phase folded over the strongest peak to identify variability that needs to be corrected
- The object report file where the entire log of the object run is written
- The report log containing a summary of the parameters of the most promising candidates for each run.

In order to better understand those items, we show below some examples of what we obtained for some of our targets.

Two fields of view of two different stars from our target list are illustrated in figure 2.2, with our target at the centre, the aperture used by TESS SPOC pipeline to extract the lightcurve and the relative magnitude of the stars in the vicinity.

The left image shows a relatively isolated star with a small nearby star, while in the right image we see the presence of a bright star near the target. Nearby stars can contaminate the flux of the target. Observing an isolated star is thus the ideal scenario.

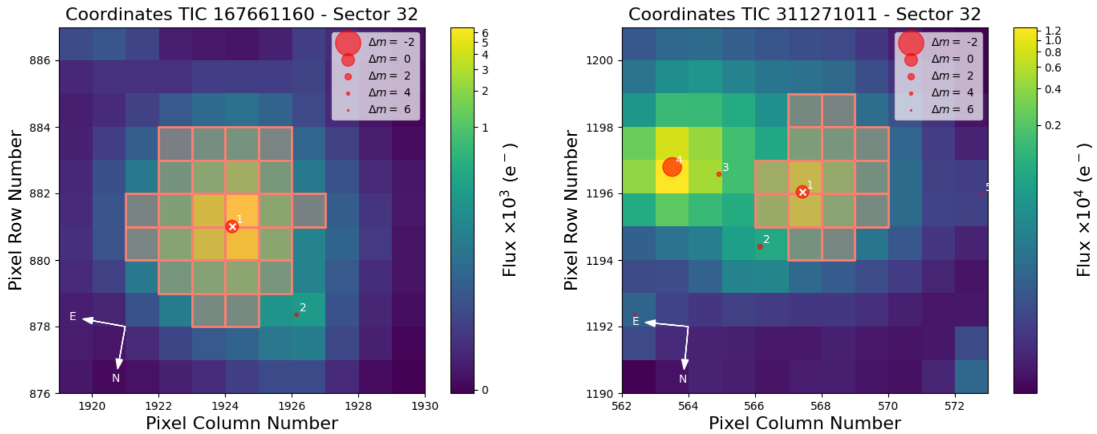

Figure 2.2: Field of view plot examples.
The color code corresponds to the flux in each pixel, the pinkish squares around the target correspond to the extraction aperture used and the red points are nearby stars, with the size of the point indicating the difference in magnitude with the target.

For the following items, we are going to take the example of TIC 34077285. For this star, we obtained in the detrend directory the image in figure 2.3.

In figure 2.3, we see for each window sizes the non-detrended data in black, with the detrending model plotted in orange. The detrended lightcurves are then obtained by dividing the raw, non-detrended, data by the orange curve.

The periodogram plot (figure 2.4) shows a Lomb-Scargle periodogram, used to generate a power spectrum from unevenly-spaced observations. The highest peaks correspond to the strongest periodic components.

We can look at what we obtained in the report log for the first run. This is illustrated in table 2.1.

Each row corresponds to a detrending with a different window size and the columns are:

- Window size used for the detrending (in days)
- Period of the transits in days
- Error on the period in days
- Number of transits observed in the data
- Mean depth of the transits in ppt
- Duration of the transit in minutes

- Epoch of the transit (T0) in BTJD (TESS Barycentric Julian Day)
- SNR: the higher the value, the better it is
- SDE: the higher the value, the more confident in the detection we are
- False alarm probability (FAP): a low value indicates that the event is unlikely of instrumental nature
- Border score: this value ranges from 0 to 1, corresponding respectively to the worst and the best scenario. A border score lower than 1 means that at least one of the transits is on the edge of the dataset. In borders, there are systematics, and therefore any detection matching with them is less reliable.
- Matching OI: if the signal matches a candidate planet of the database (TOI), its ID appears in this column
- Harmonic: this indicates if the period is an harmonic of a previous signal
- Planet radius in Earth radii
- R_p/R_s: planet-to-star radius ratio, calculated from the transit depth under the assumption of zero transit impact parameter
- a: Semi-major axis in astronomical units
- Habitability zone. This zone is calculated using the effective temperature and the luminosity of the star [17]. The possible outputs are: I=inner, HZ-IO=Habitable Zone (Inner Optimistic), HZ=Habitable Zone, HZ-OO=Habitable Zone (Outer Optimistic)

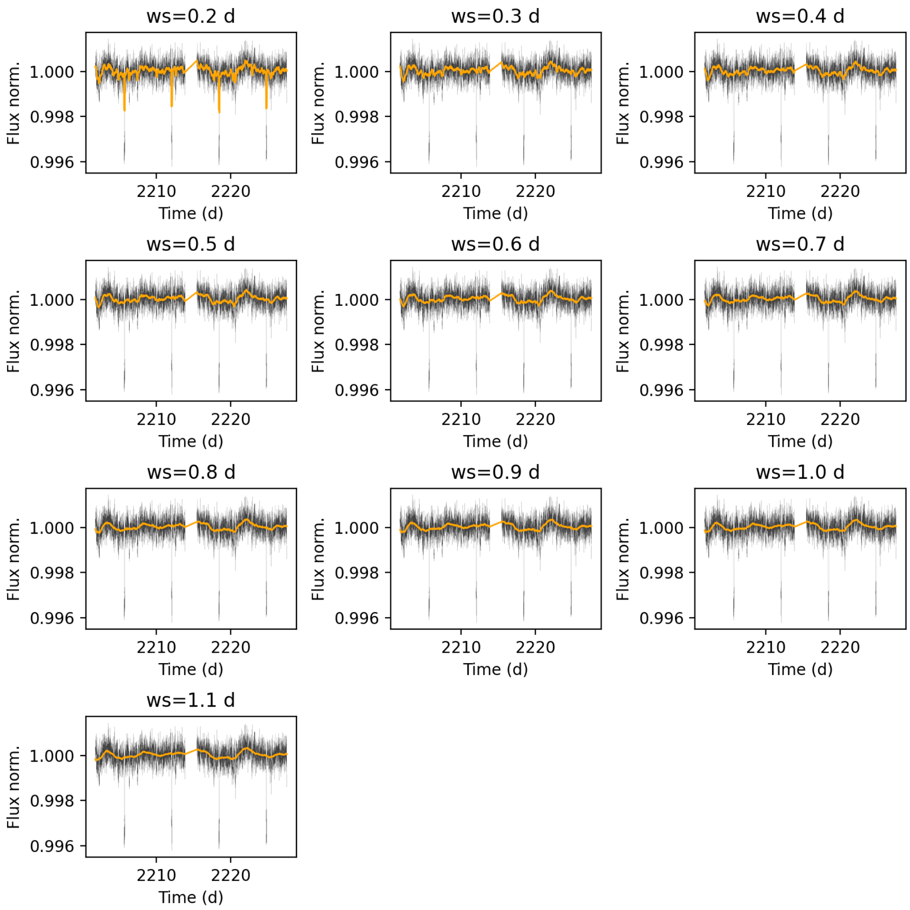

Figure 2.3: TIC 34077285 detrending models for all window sizes.
Fluxes are shown as black data points and the orange lines show the bi-weight detrending models with the corresponding window sizes given above each plot.

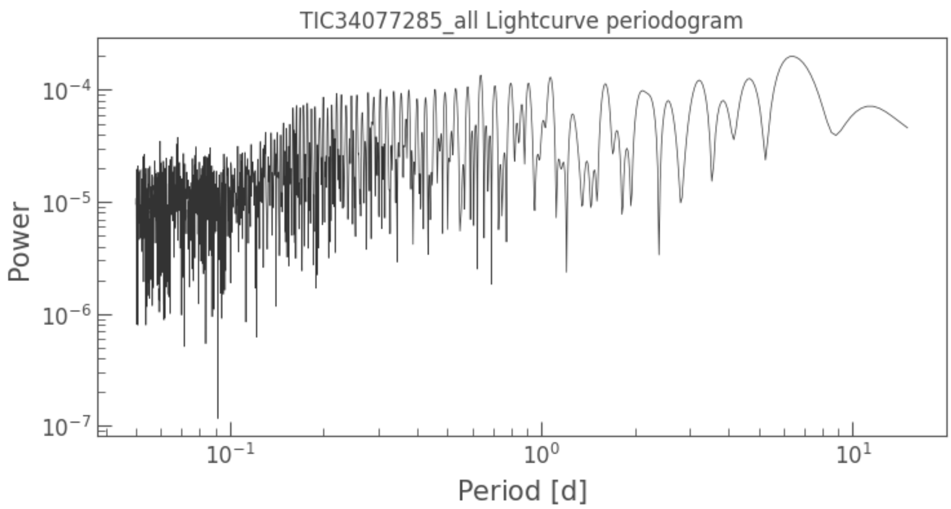

Figure 2.4: TIC 34077285 periodogram.

Win_size	Period	P_err	N.Tra	Depth	T. dur	T0	SNR	SDE	FAP	Border	Match. OI	Harm.	Plan. rad	Rp/Rs	*a*	Habit.
PDCSAP	6.39018	0.030415	4	2.729	176.8	2205.6659	101.761	23.344	8.0032e-05	1.00	TOI 880.01	-	4.66063	0.05174	0.06294	I
0.2000	6.39018	0.030415	4	1.120	176.8	2205.6659	54.093	20.318	8.0032e-05	1.00	TOI 880.01	-	2.98563	0.03356	0.06294	I
0.3000	6.39018	0.030415	4	2.633	176.8	2205.6659	105.361	24.171	8.0032e-05	1.00	TOI 880.01	-	4.57774	0.05084	0.06294	I
0.4000	6.39018	0.030415	4	2.659	176.8	2205.6659	105.509	24.048	8.0032e-05	1.00	TOI 880.01	-	4.60034	0.05108	0.06294	I
0.5000	6.39018	0.030415	4	2.664	176.8	2205.6659	105.357	24.020	8.0032e-05	1.00	TOI 880.01	-	4.60509	0.05114	0.06294	I
0.6000	6.39018	0.030415	4	2.672	176.8	2205.6659	105.213	23.938	8.0032e-05	1.00	TOI 880.01	-	4.61187	0.05121	0.06294	I
0.7000	6.39018	0.030415	4	2.679	176.8	2205.6659	105.254	23.875	8.0032e-05	1.00	TOI 880.01	-	4.61764	0.05128	0.06294	I
0.8000	6.39018	0.030415	4	2.686	176.8	2205.6659	105.196	23.831	8.0032e-05	1.00	TOI 880.01	-	4.62403	0.05134	0.06294	I
0.9000	6.39018	0.030415	4	2.692	176.8	2205.6659	105.115	23.780	8.0032e-05	1.00	TOI 880.01	-	4.62848	0.05139	0.06294	I
1.0000	6.39018	0.030415	4	2.692	176.8	2205.6659	104.934	23.710	8.0032e-05	1.00	TOI 880.01	-	4.62924	0.05140	0.06294	I
1.1000	6.39018	0.030415	4	2.691	176.8	2205.6659	104.800	23.640	8.0032e-05	1.00	TOI 880.01	-	4.62797	0.05138	0.06294	I

Elected signal with QUORUM algorithm from 11 VOTES –> NAME: 1 Period:6.390176035093979 CORR_SDE: 50.540195728062514 SNR: 105.36098310144631 SDE: 24.17139795689946 FAP: 8.0032e-05 BORDER_SCORE: 1.0 Proposed selection with BASIC algorithm was –> NAME: 1 Period:6.390176035093979 SNR: 105.36098310144631 New best signal is good enough to keep searching. Going to the next run.

Table 2.1: TIC 34077285 report log run 1.

Detrend no.	Period	Per_err	Duration	T0	Depth	SNR	SDE	FAP	Border_score	Matching OI	Harmonic	Plan. rad	Rp/Rs	*a*	Habit.
2	6.3902	0.03041	176.76	2205.67	2.633	105.36	24.17	0.000080	1.00	TOI 880.01	-	4.57774	0.05084	0.06294	I
1	2.5724	0.00754	123.28	2202.30	0.347	23.51	17.09	0.000080	1.00	TOI 880.02	-	1.66244	0.01772	0.03432	I
0	14.3220	0.10393	188.69	2206.34	0.629	23.15	24.57	0.000080	1.00	TOI 880.03	-	2.23718	0.02549	0.10779	I
10	1.9874	0.00534	26.08	2203.71	0.221	8.00	9.02	0.000160	1.00	nan	-	1.32717	0.01116	0.02889	I
7	1.5939	0.00398	106.93	2202.69	0.098	8.26	15.25	0.000080	0.93	nan	0.25*SOI1	0.88516	0.00969	0.02494	I

Table 2.2: TIC 34077285 candidates report log.

In our example, we see that a signal with a period of 6.39018 days is retrieved in all the detrendings. Note that we do not always find the same period for all the widow sizes, but it is a sign that the signal is reliable since it does not depend on the detrending. This planetary candidate is already in the database and corresponds to TOI 880.01. The signal here is all the time the same since it is recovered in all the detrends. The elected one, that is, with the window size of 0.3 days, represents the optimum detrend to recover such a planet.

We can look at the image of the corresponding detrended light curve in figure 2.5. On the upper panel, we see the normalized detrended flux for all the sectors available (or selected) along with the suggested transits fitted in red. On the second panel, we have the stacked phase-folded fluxes over the period detected. This gives us a first look at the shape of the transits. On the lower panel, we have a plot of the SDE. The period selected is the one corresponding to the highest peak in the graph. The blue dotted lines are the harmonics of the selected period. In our example, we see that the harmonics are matching some peaks in the plot, which is a hint that the signal is promising.

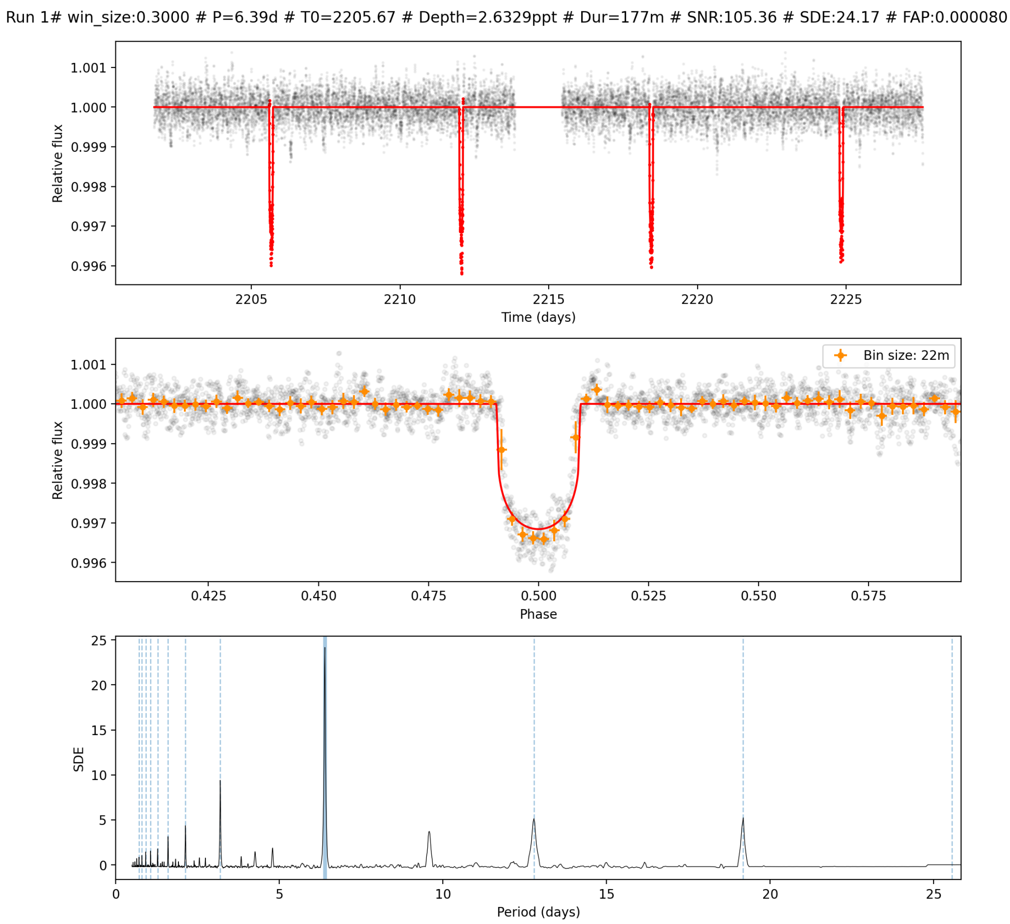

Figure 2.5: TIC 34077285 run 1 win_size 0.3

Those 4 transits will then be masked and SHERLOCK will search a new significant periodic signal in the data that are left. The process continues until we reach the maximum number of runs or until the next signal is below the SDE or SNR thresholds that we fixed in the properties file.

The report log summarizing the signals selected in each of the runs is illustrated in table 2.2.

The signal selected in the second run has a period of 2.5724 days, corresponding to TOI 880.02 and the best signal in the third run matches TOI 880.03 which has a period of 14.32196 days. All three TOIs known for this target are thus retrieved in the first three runs, meaning that all the corresponding transits have been masked. If a signal looks promising in run 4 and/or in run 5, it could then be a new detection, which is what we are looking for.

Unfortunately, in run 4 we do not retrieve the same period for all the detrendings, and the shape of the stacked transits does not look very convincing. And for the run 5, the selected signal is an harmonic of TOI 880.01, meaning that it corresponds to the same signal with an harmonic of the period. Therefore, those signals are not promising enough to take them to the next step.

2.2 Vetting

In case one of the signals looks promising, based on the criteria mentioned in the section 2.1, the next step is to perform the vetting of the corresponding candidate. This stage will allow us to examine the suggested transits individually, and to check if those events could have been caused by external factors, from instrumental or astrophysical origin.

We can run the vetting process by using the command:

```
python3 -m sherlockpipe.vet --candidate ${theCandidateNumber}
```

In this way, the parameters of the transits obtained in the first step will be automatically read and used.

The vetting stage provides us with several graphs and images gathered in a report. In order to have an example of those items, let us imagine that we want to vet the third selected signal in our previous example (TOI 880.03 with P=14.322d).

The first graph in the report document is the transits depth analysis (figure 2.6). Each point corresponds to a single transit (in our example, there are only two of them). We need to check that the depths of all the individual transits are consistent. Indeed, for a transiting planet we should have transits of consistent depths since we observe the same object passing in front of the star. If one transit in particular has a different depth compared to the others, then it may not be related to them or be affected by more systematics. And if we observe that the depth alternates between the even and odd transits, this can be a hint for eclipsing binaries. Indeed in this case, the transit depth will depend on which star is in front of the other and their characteristics.

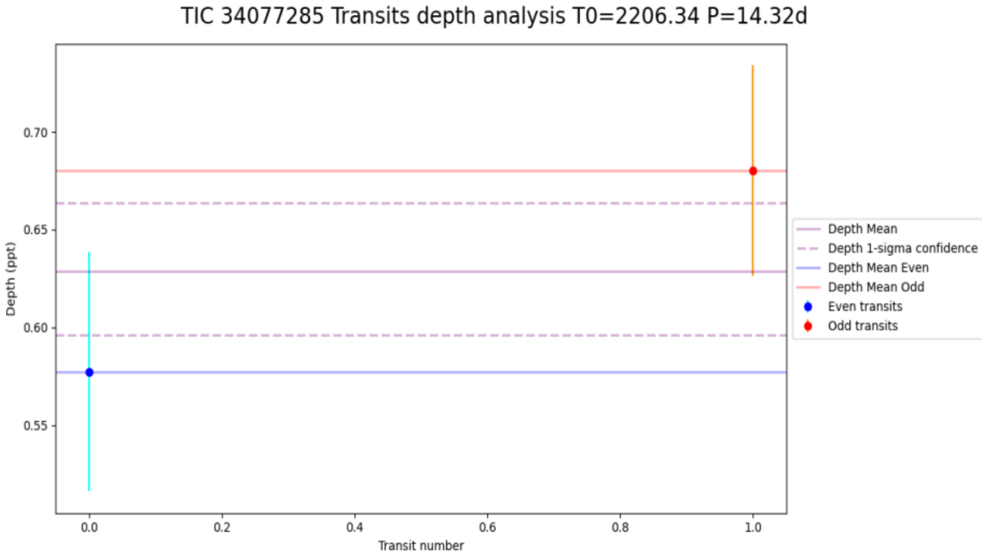

Figure 2.6: TOI 880.03 single-transits depths plot.
The red and blue lines are respectively the depth means of the even and odd transits. The purple line is the depth mean of all the transits, and the doted purple lines indicate the 1-sigma confidence on the depth mean.

The second plot (figure 2.7) is the folded curve at the epoch of the transit T0 (inferior conjunction) and at superior conjunction. This will allow us to check if the period selected is the right one.

In the first row, the selected period for the candidate (P=14.322d) is considered. If this period is correct, we should see a transit in the first graph, and a flat flux for the second graph. Indeed, if transits are observed at superior conjunction, it would mean that the period selected is twice the real one or this could indicate an eclipsing binary.

For the second row, we consider the first harmonic of the period (P*2). If the selected period is correct, we should see a transit in both panels, which is the case here.

The third row shows the folded curve for the first subharmonic (P/2). For this part, we should see on the first panel a superposition of a flat flux with a transit. In the second graph, we should observe a flat light curve.

The next figures of the vetting report will enable us to explore individually each suggested transit. We will look at the graphs generated for the first transit of our example.

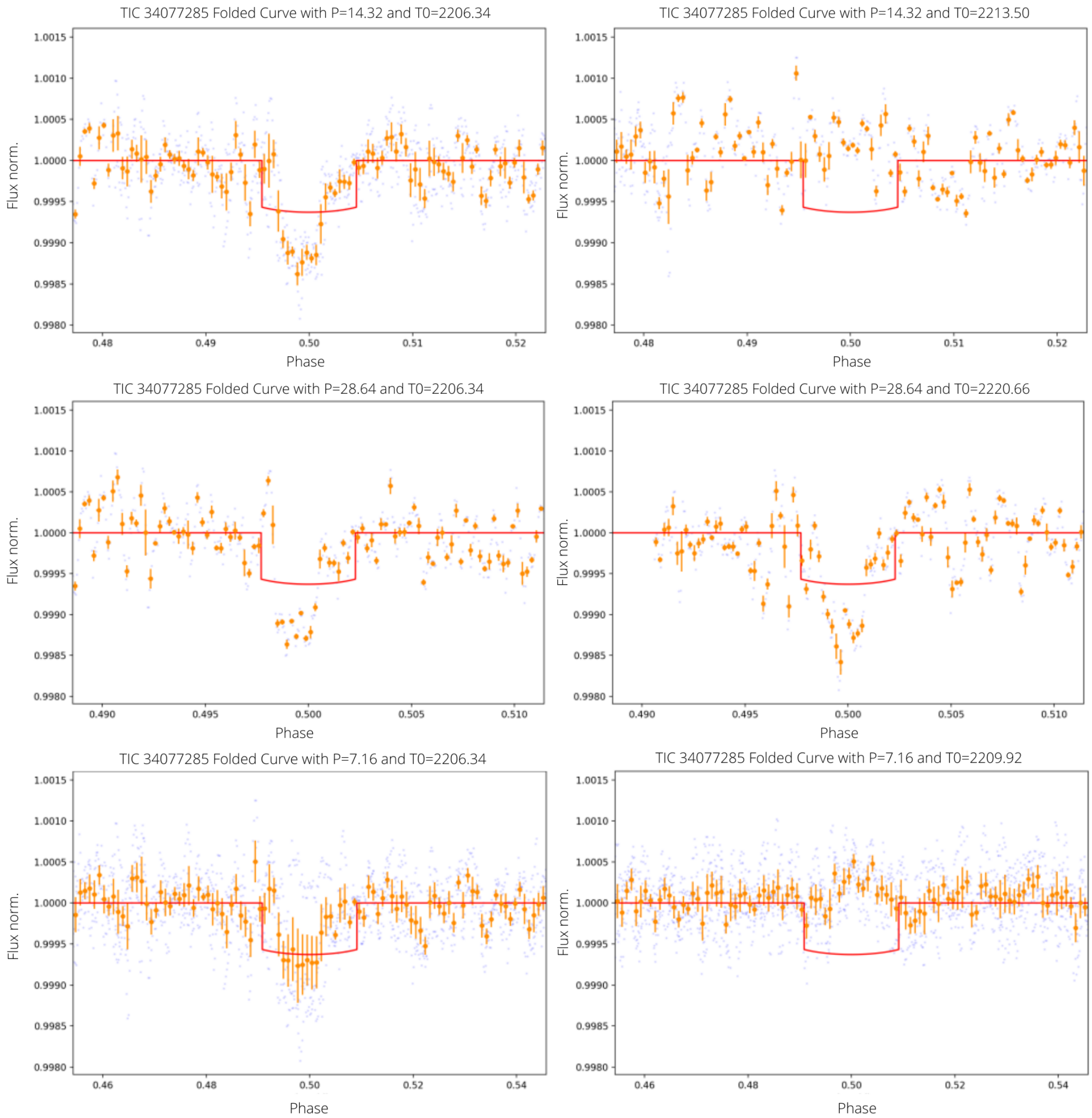

Figure 2.7: TOI 880.03 folded curve at T0 and at superior conjunction.

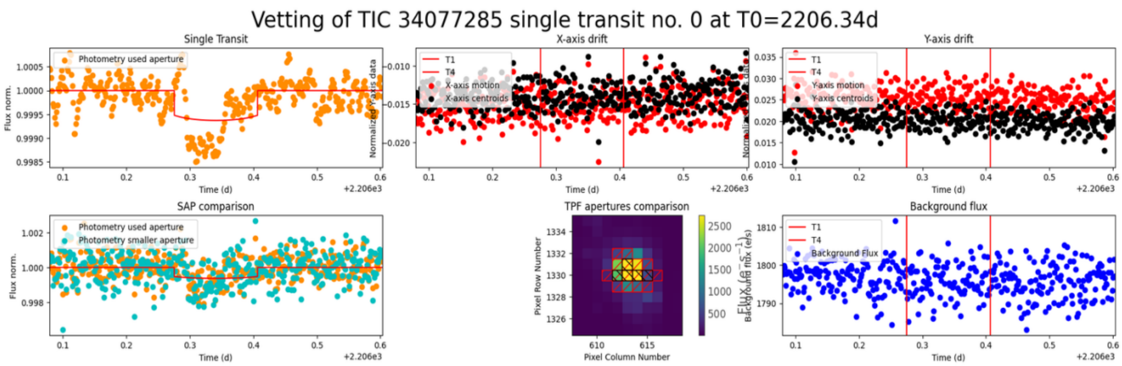

Figure 2.8: TOI 880.03 vetting plots of the first transit.

In figure 2.8, the top-left plot is the photometry of the transit. With this figure, we can look at the shape of each individual transit. This gives us a new hint to rule out, or not, an eclipsing binary. Indeed, eclipsing binaries will lead to V-shaped transits while transiting planets will produce U-shaped transits. This is because for eclipsing binaries, the sizes of the eclipsing bodies are comparable (unlike a transiting planet which is smaller than its host star), the geometry of the eclipse is thus grazing. Therefore we lack the quasi-flat total phase of a planetary transit, and the resulting transit is V-shaped. [4]

If there are any momentum dumps during the time of the transit they will be indicated on this plot by a dashed vertical line. Indeed, the accumulated momentum of the reaction wheels (controlling the spacecraft attitude) needs to be dumped at some point. This is done every 2 – 2.5 days and typically lasts around half an hour. These momentum dumps can affect the satellite pointing and the observed lightcurve. Therefore, we need to check that the transits do not match one of them.

The top-center and top-right figures show the X-axis and Y-axis positions of the centroid. The full duration of the transit is included in between the two red lines, corresponding to the first and the fourth contact points (T1 and T4). We see the changes in position of the brightest point in the aperture, with the black points showing the position of the target's flux-weighted centroid, and the red points showing the local motion. In other words, these graphs show the pointing stability of TESS at the time of the transits. Smooth variations are expected but a large scatter of the points at the time of the transit-like event can be a sign that the transit is not real.

The bottom-left and bottom-center figures show a comparison of lightcurves extracted using different aperture sizes. If the transit-like event is caused by a planet, using different aperture sizes should not change the transit shape or depth. Conversely, the depth and shape are expected to change if the signal is due to a blended eclipsing binary. This is because for blended binaries, the signal is not centered on the target and instead originates from elsewhere in the field of view, thus resulting in different shapes and depths of the signal with different apertures. The orange points in the left plot are extracted using the red aperture in the center plot while the green points are extracted using the smaller black aperture.

The bottom-right plot shows the evolution of the background flux. The transit takes place between the red lines. Smooth variations of the background flux are expected. However, we need to look if there is any sudden change. If a spike is matching the time of the transit, the observed event is probably only due to something happening in the background, like enhanced scattered light or asteroids passing through the field of view. In our example, the background flux looks good.

The last figure that we will find in the vetting report for each transit is the individual pixel lightcurves (figure 2.9). This figure shows individual lightcurves for each pixel at the time of the transit. The red lines are delimiting the photometric extraction aperture. The idea here is that the transit signal should come from pixels that are centered on the target. If the transit-like signal is more prominent in pixels that are not centered on the target star, this could suggest that the signal is caused by a blended eclipsing binary. In our example, most of the lightcurves of the other pixels look good, but we can still note some flux variations in the upper left corner. However, these pixels are relatively far from the photometric aperture and seem to show some periodic stellar variability rather than an eclipse-like event at the expected T0. It is thus unlikely that they are the cause of the transit-like signal observed on the target.

Having all those graphs gathered in a single report is very convenient to rule out transit-like events that are in fact due to external factors. However, the outcome can sometimes be ambiguous and the final decision to rule out, or not, the signal remains at the discretion of the user.

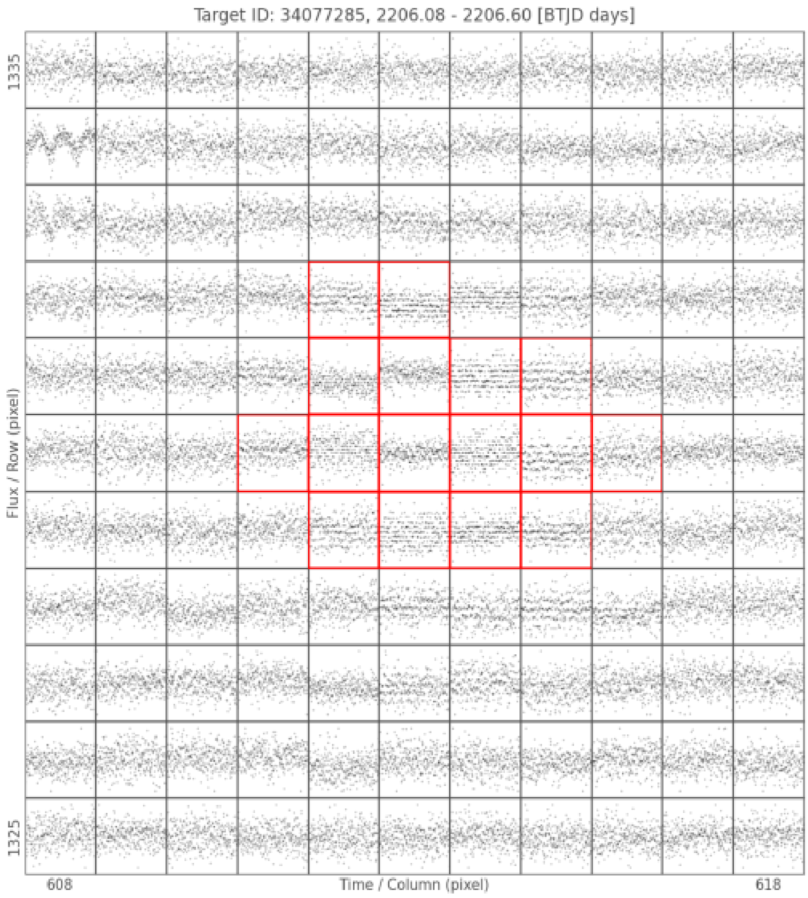

Figure 2.9: TOI 880.03 individual pixel lightcurves.

2.3 Validation

In case our signal still looks promising after the vetting, we can execute a statistical validation with the command:

```
python3 -m sherlockpipe.validate --candidate ${theCandidateNumber}
```

This step is done by using TRICERATOPS (Tool for Rating Interesting Candidate Exoplanets and Reliability Analysis of Transits Originating from Proximate Stars) [9]. The basic idea is to model different astrophysical scenarios that can produce transits, taking into account nearby stars in addition to the target, and see which scenario fits better the observed shape of the transit.

After running this validation step, we obtain two parameters: the false positive probability (FPP) and the nearby false positive probability (NFPP). The criterion to classify a signal as a "likely planet" is: FPP < 0.5 and NFPP $< 10^{-3}$. And to be classified as a validated planet we must have: FPP < 0.015 and NFPP $< 10^{-3}$.

The TRICERATOPS team tested their tool on a sample of 68 TOIs that have been designated as either confirmed planets or astrophysical false positives by members of the TESS Observation Follow-up Program (TFOP) based on follow-up observations. They defined the classifications based on the results of this analysis. They also cross-checked their criteria by comparing their results with another statistical validation tool devoted to Kepler mission (VESPA) [9].

In order to compute those probabilities, TRICERATOPS collects the data of the stars in a radius of 10 pixels around the target and identifies which ones are bright enough to contribute to the observed signal, based on the measured transit depth and the aperture used for the photometric extraction. We can use again the target TIC 34077285 as an example, and perform the validation for the third candidate (P=14.322d). The plot of the 10 pixels radius field of view for our example is shown in figure 2.10. The aperture used for the extraction is plotted in red and our target is represented by the star symbol. The stars are color-coded as a function of their TESS magnitude.

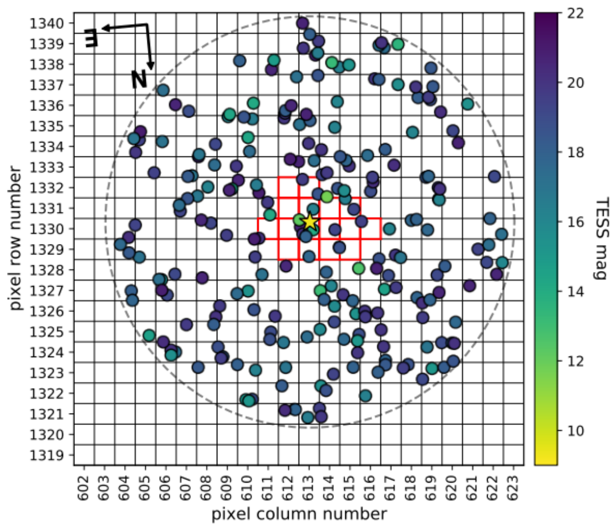

Figure 2.10: Stars within 10 pixels around TIC 34077285.

Scenario	Configuration
TP	No unresolved companion. Transiting planet with P_{orb} around target star.
EB	No unresolved companion. Eclipsing binary with P_{orb} around target star.
EBx2P	No unresolved companion. Eclipsing binary with $2 \times P_{orb}$ around target star.
PTP	Unresolved bound companion. Transiting planet with P_{orb} around primary star.
PEB	Unresolved bound companion. Eclipsing binary with P_{orb} around primary star.
PEBx2P	Unresolved bound companion. Eclipsing binary with $2 \times P_{orb}$ around primary star.
STP	Unresolved bound companion. Transiting planet with P_{orb} around secondary star.
SEB	Unresolved bound companion. Eclipsing binary with P_{orb} around secondary star.
SEBx2P	Unresolved bound companion. Eclipsing binary with $2 \times P_{orb}$ around secondary star.
DTP	Unresolved background star. Transiting planet with P_{orb} around target star.
DEB	Unresolved background star. Eclipsing binary with P_{orb} around target star.
DEBx2P	Unresolved background star. Eclipsing binary with $2 \times P_{orb}$ around target star.
BTP	Unresolved background star. Transiting planet with P_{orb} around background star.
BEB	Unresolved background star. Eclipsing binary with P_{orb} around background star.
BEBx2P	Unresolved background star. Eclipsing binary with $2 \times P_{orb}$ around background star.
NTP	No unresolved companion. Transiting planet with P_{orb} around nearby star.
NEB	No unresolved companion. Eclipsing binary with P_{orb} around nearby star.
NEBx2P	No unresolved companion. Eclipsing binary with $2 \times P_{orb}$ around nearby star.

Table 2.3: Transit-producing scenarios [9].

The transit-producing scenarios tested by TRICERATOPS are listed in table 2.3.

The probability of each of these scenarios is calculated using a Bayesian framework, and thus using the Bayes theorem:

$$p(S_j|D) \propto p(S_j)p(D|S_j)$$

where $p(S_j|D)$ is the posterior probability of the jth scenario S_j given the datat D, $p(S_j)$ is the prior probability of scenario S_j, and $p(D|S_j)$ is the marginal likelihood of the data D given the scenario S_j. After calculating $p(S_j|D)$ for each scenario, the relative probability of each scenario is determined using the equation:

$$P_j = \frac{p(S_j|D)}{\sum_j p(S_j|D)}$$

Using those probabilities, the FPP and NFPP are then calculated. The FPP value is given by:

$$\text{FPP} = 1 - (P_{TP} + P_{PTP} + P_{DTP})$$

Where P_j is the relative probability of scenario j.

This quantity can thus be understood as the probability that the transit is caused by something else than a transiting planet around the target star. The NFPP is given by the sum of all scenarios involving nearby stars:

$$\text{NFPP} = \sum(P_{NTP} + P_{NEB} + P_{NEBx2P})$$

NFPP represents the probability that the observed transit is produced by a resolved nearby star rather than the target star.

For the calculation of the final FPP and NFPP values, five points are drawn from the probability distribution of each scenarios and are used to compute five values of NFPP and FPP, using the equations described previously. The final FPP and NFPP are then the respective mean of those five values.

In addition to FPP and NFPP, two quantities called FPP2 and FPP3+ are provided. These are false positive probabilities taking into account that the candidate for which we are performing the validation is in a system with respectively one or more planets already discovered. Indeed, a transiting planet candidate in a multi-transiting system has a higher prior probability to be a real planet. This is what is called "multiplicity boost" [21], and this is of particular interest for this master thesis since we are focusing on systems with at least one previously known planetary candidate.

Chapter 3

Results

3.1 Target selection

The very first step of this work was to select the targets to analyse. We started from the list of all TOIs (about 5600 objects) and used the ExoFOP website [34] to directly apply filters to this list. This website is a repository allowing the upload and display of exoplanet candidates related resources.

Our list of targets was obtained using the following filters:

- TESS disposition: contains CP (confirmed planet) OR PC (planetary candidate)
- TFOPWG disposition: contains CP OR contains PC
- TESS magnitude: $\leq$ 11.5
- Source: spoc (TESS Science Processing Operations Center)
- Declination: $\geq$ -40° AND $\leq$ 40°
- Planet Radius: $\leq 6\ R_{\oplus}$
- Stellar Teff: $\geq$ 4000 K AND $\leq$ 7000 K

The first two filters ensure that our initial condition to have targets with already one candidate or confirmed planet is fulfilled.

The limitation of the declination arises from the will to perform follow-up observations with CHEOPS, which does not cover the entire sky (see figure 1.7).

The filters about TESS magnitude and stellar Teff are also related to CHEOPS, which was designed to observed V-mag < 12 solar-type (F to K) stars.

The condition on the planet radius aims to rule out hot Jupiters, which tend to be "lonely". Indeed, most of them do not seem to have nearby companion planets [14] (with a few exceptions like WASP-47 [2]). A possible explanation is that companion planets (if they existed) were destroyed during the inward migration process that led the hot Jupiters to their current short-period orbits. [22]

Applying those filters, we obtained a list of 158 TOIs. Among those targets, we prioritized the multiple systems and and the Level 1 candidates, that can be used to complete the TESS Level One Science Requirement, which is to measure masses for 50 transiting planets smaller than 4 Earth radii. On the contrary, the lowest priority was given to potential eclipsing binaries with V-shaped transits. We finally ended up with the 100 targets analysed in this master thesis. All the targets are listed in appendix A, in the order of their analysis.

3.2 Presentation of the results

We performed the search stage (section 2.1) for all the 100 targets of our list. Before searching for new candidates, the first goal is to make sure that SHERLOCK retrieved and masked correctly all the transits corresponding to already known TOIs for each target. If it is not the case, we have two ways to mask the transits manually from the `yaml` file:

- The initial mask, where we can specify directly which intervals we want to mask. This way of proceeding is convenient if we have only a few transits that are deep enough to be easily identified in the lightcurve.
- The initial transit mask, for which we need to provide the epoch, the period and the duration of the transit. To find those parameters, we can either look directly in the ExoFOP database, or "force" SHERLOCK to retrieve the TOI using a reduced period grid centered on the corresponding period, and then use the parameters obtained to mask the TOI.

Once TOIs are masked, by SHERLOCK or manually, the search for new planetary candidates can start. Out of the 100 targets of our list, 20 presented signals interesting enough to run the vetting (section 2.2) and validation (section 2.3) steps. Among those 20 candidates, 7 are classified as "likely planets" based on the FPP and NFPP values obtained at the validation step. In addition, 4 candidates out of the "likely planet zone" are also worth discussing. All the candidates corresponding to color points in figure 3.1 will be discussed hereafter.

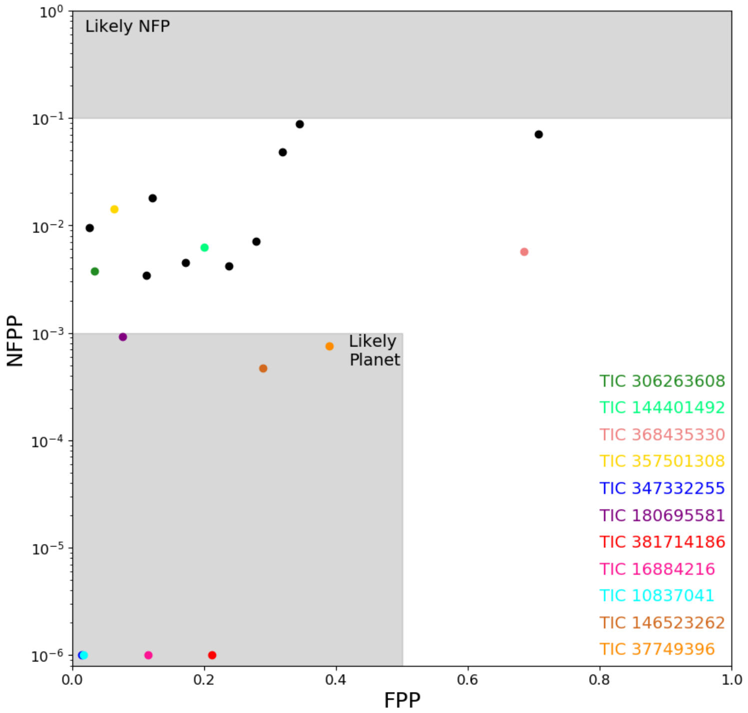

Figure 3.1: FPP and NFPP of the 20 most promising candidates.

TIC ID	Period of the candidate (days)	FPP < 0.5 ?	NFPP $< 10^{-3}$?
357501308	11.24	✓	✗
357501308	15.40	✓	✗
306263608	22.04	✓	✗
144401492	7.97	✓	✗
347332255	12.99	✓	✓
114018671	7.77	✗	✗
368435330	1.04	✗	✗
180695581	21.88	✓	✓
381714186	4.02	✓	✓
16884216	15.78	✓	✓
39200363	14.06	✓	✗
271478281	12.48	✓	✗
425561347	15.29	✓	✗
82452140	14.68	✓	✗
70420766	2.55	✓	✗
10837041	18.76	✓	✓
146523262	4.43	✓	✓
262435954	5.89	✓	✗
167661160	7.17	✓	✗
37749396	2.31	✓	✓

Table 3.1: 20 most promising candidates.

Among the discussed candidates, 4 actually correspond to new planet candidates also found by other teams and that we recovered independently and blindly (i.e. without knowing anything about their existence) during this work. These candidates are discussed in sections 3.2.1 (TIC 347332255), 3.2.8 (TIC 357501308), 3.2.9 (TIC 368435330) and 3.2.11 (TIC 306263608).

All the 20 candidates corresponding to a point in figure 3.1 are listed in table 3.1, with the corresponding orbital period proposed for the candidate.

3.2.1 TIC 347332255

TIC 347332255 already has two known planet candidates: TOI 1835.01 and TOI 1835.02, which have not been confirmed yet. Note that the second planet candidate is proposed to be a single-transit detection. This TOI can thus not be retrieved alone by SHERLOCK, since it searches for periodic signals, and we have to mask it manually. The period of TOI 1835.01 is P = 5.64195 $\pm$ 0.00114 days.

TIC ID	Sector(s)	Mass (M_Sun)	Rad (R_Sun)	Teff (K)	Lum (L_Sun)	Log(g)
347332255	23	0.91	0.782	5297	0.434	4.610

Existing TOI(s)	Period (days)	Radius (R_Earth)
TOI 1835.01	5.642	1.824
TOI 1835.02	/	2.539

Table 3.2: TIC 347332255 stellar and TOI parameters.

On our first attempt to run the search for candidates, TOI 1835.01 is retrieved in the second run. In the first run, the signal selected mixes of new transit-like events with one transit of TOI 1835.01 (which is not masked before the run 2). The period proposed can thus not be correct, and we make a second attempt masking this time the two TOIs.

In figure 3.2, we can see the raw lightcurve and the ranges of time masked manually. We can already see by eye on this plot that there are other potential transits, even if there is some variability in the lightcurve.

Using these masks and running again the search stage, the candidate that we retained is the selected signal of the first run. Its parameters are given in table 3.3.

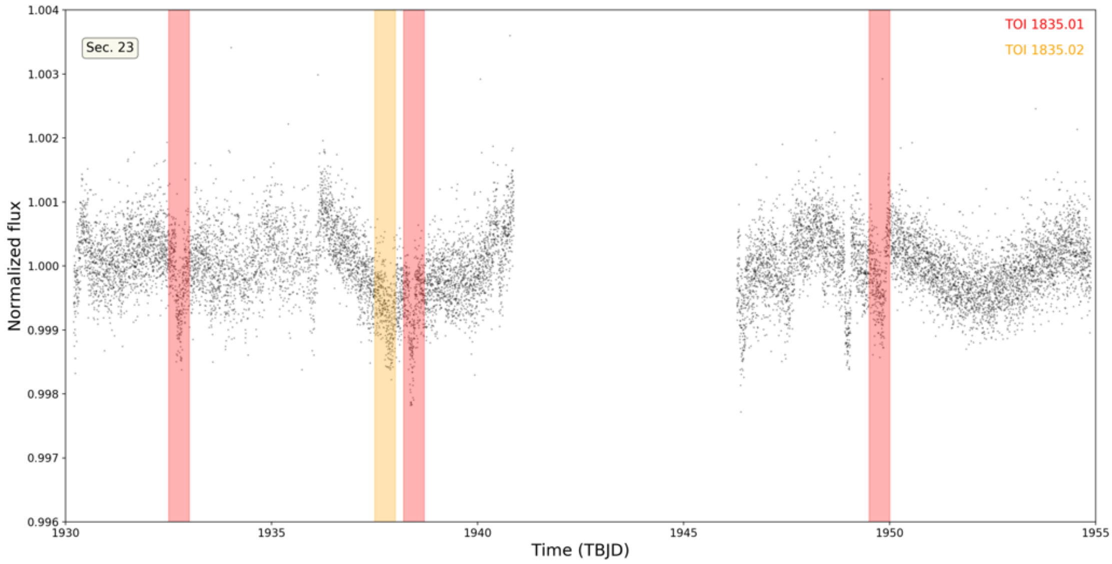

Figure 3.2: TIC 347332255 initial masks.

Win_size.	Period	Per_err	N.Tran	Duration	T0	Depth	SNR	SDE
1.0	12.9937	0.11320	2	222.17	1935.98	0.935	49.48	10.18

FAP	Border_score	Planet radius	R_p/R_s	Semi-major axis	Habitability zone
0.000080	1.00	2.61298	0.02993	0.10502	I

Table 3.3: TIC 347332255 candidate parameters.

We decided to investigate further this candidate because of the high SNR, the convincing shape of the stacked transit and the subharmonics visible in the SDE plot (figure 3.3). In addition, the border score is good and the same period is retrieved in 9 of the 10 detrendings.

From the transit depth plot in the vetting report 3.6, we can see that the depths of the two transits are not consistent. The folded curve indicates that the period proposed seems correct. From the individual transit plots, we can see that the two transits have different shapes. Furthermore, the first one does not have the shape expected for a real transit, and a momentum dump is visible just after the event. However, the second transit seems very clear and the vetting plots do not reveal any anomaly (figure 3.5).

From the validation we obtained the values listed in table 3.4, with the three most probable scenarios. Based on those values, this candidate is thus statistically validated. The value of the NFPP can be explained by the fact that this star is very isolated. The values obtained corresponds to the dark blue point in figure 3.1.

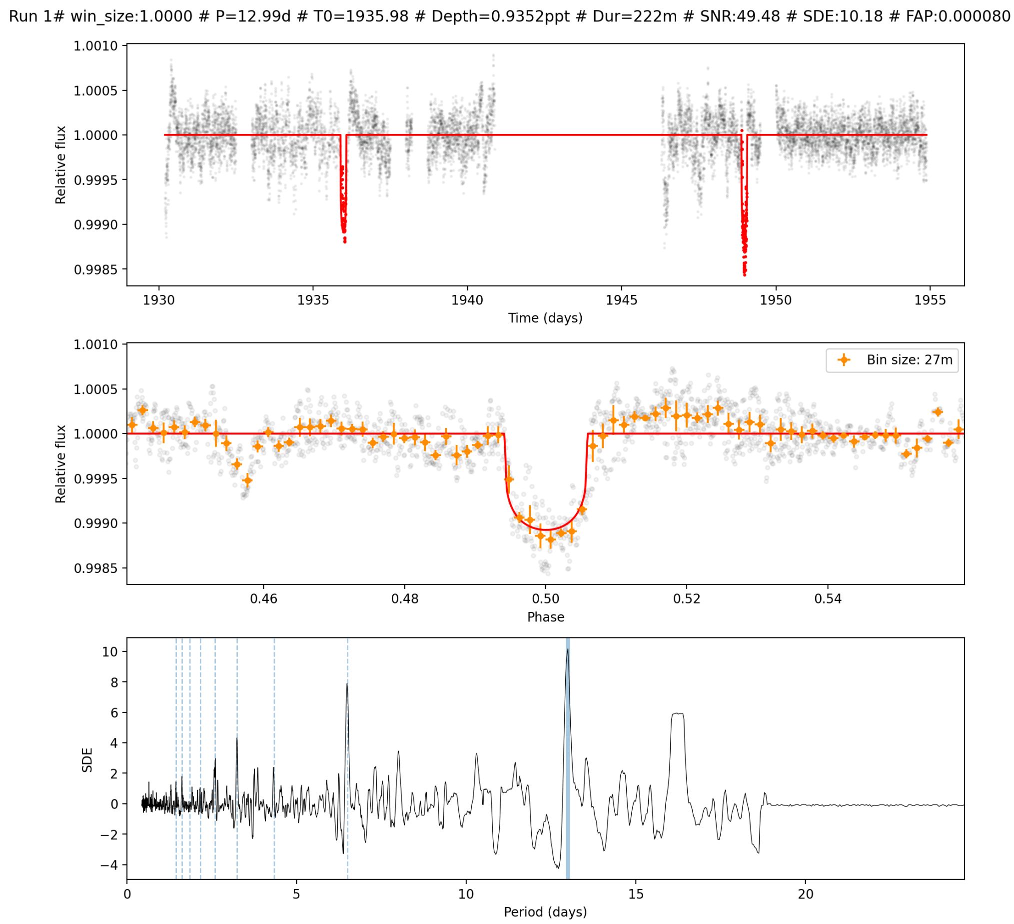

Figure 3.3: TIC 347332255 run 1 win_size 1.0

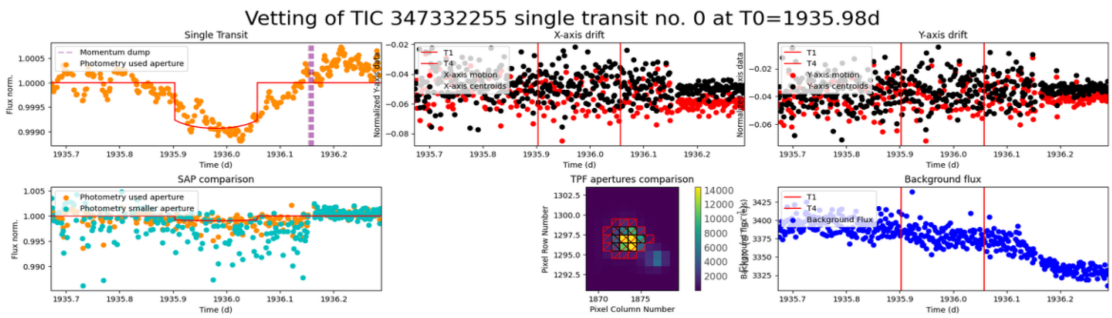

Figure 3.4: TIC 347332255 vetting plots of the first transit.

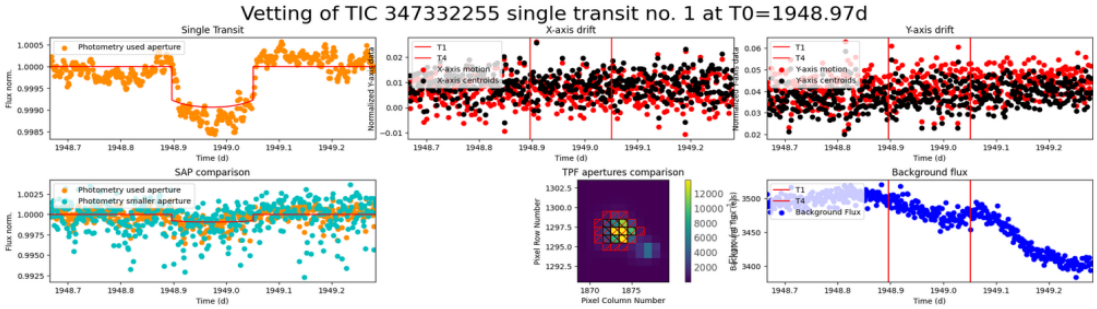

Figure 3.5: TIC 347332255 vetting plots of the second transit.

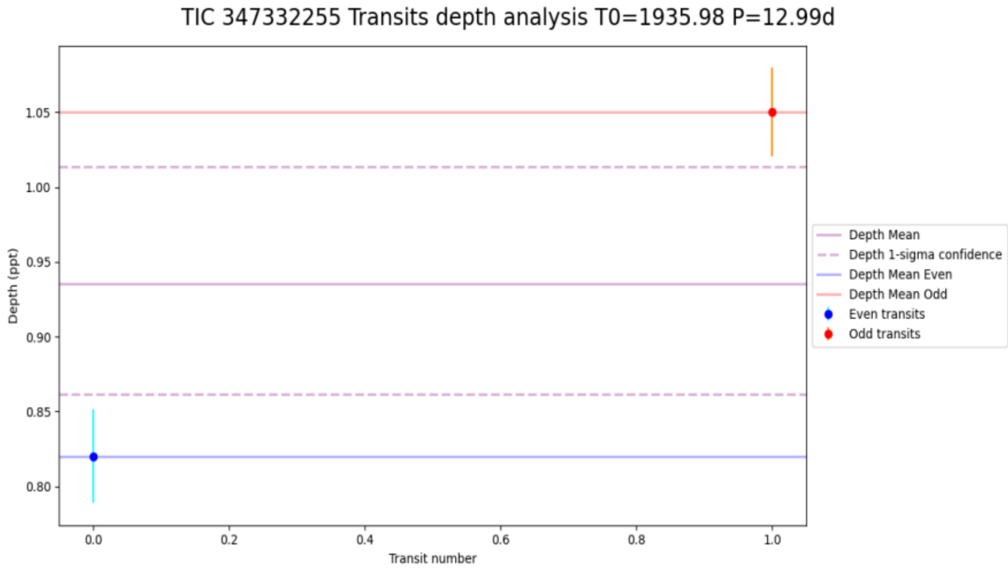

Figure 3.6: TIC 347332255 single-transits depths plot.

Scenario	FPP	NFPP	TP	PTP	DTP
Probability	0.01408	0.0	0.77587	0.12203	0.08803

Table 3.4: TIC 347332255 FPP, NFPP and three most probable scenarios.

In conclusion, the first transit can be ruled out but the second one seems real. Our period of 12.99d is therefore inaccurate and this event could be a single-transit detection.

When we analysed this candidate, only the data from sector 23 were available, but the target has also been recently re-observed by TESS in sector 49 (from 2022-Feb-26 to 2022-Mar-26). These data were released early May 2022 and a quick analysis by some members of the CHEOPS team (private communication with Hugh Osborn) revealed another single transit in this sector, whose depth and duration matched those of the single transit event detected in sector 23 (that they had also detected independently). Follow-up observations with CHEOPS in the following weeks in

May then allowed to recover an orbital period of 20.5 days for the third transiting object in this system. The single transit event that we detected completely independently in sector 23 was thus a real transit detection.

3.2.2 TIC 180695581

TIC 180695581 has one confirmed planet: TOI-1807 b [11]. In addition to sectors 22 and 23, this star has been observed in sector 49. However, the data from this last sector were not part of our analysis since they were only released at the beginning of May.

TIC ID	Sector(s)	Mass (M_Sun)	Rad (R_Sun)	Teff (K)	Lum (L_Sun)	Log(g)
180695581	22,23	0.73	0.741	4612	0.224	4.562

Existing TOI(s)	Period (days)	Radius (R_Earth)
TOI-1807 b	0.549	1.258

Table 3.5: TIC 180695581 stellar and TOI parameters.

For this target, the preparation stage revealed a strong periodic variability. Its period has been estimated to 4.3265d, using a Lomb-Scargle periodogram. An auto-detrend was then applied with the corresponding period to remove this variability. This is likely due to star spots, which are characteristic of young stars such as TIC 180695581 (180 $\pm$ 40 Myr) [11].

TOI-1807 b has a period P = 0.54934 $\pm$ 0.00004 d and was successfully retrieved and masked in the first run.

The candidate that we investigate was selected in the second run, with the parameters in table 3.6.

Win_size.	Period	Per_err	N.Tran	Duration	T0	Depth	SNR	SDE
0.4	21.8844	0.04641	2	166.29	1906.02	0.460	15.55	44.09

FAP	Border_score	Planet radius	R_p/R_s	Semi-major axis	Habitability zone
0.000080	1.00	1.73642	0.01980	0.13813	I

Table 3.6: TIC 180695581 candidate parameters.

This signal is retrieved in 8 of the 10 detrendings. It has a high SDE and SNR and a good border score. Note that the reason for which the SDE plot looks "empty" in figure 3.7 is because the period of the confirmed planet is very short, meaning that we removed a lot of segments from the lightcurve. This is also partly responsible for the very high value of the SDE. We see in figure 3.7 that the transits are not very deep, but they still stand out of the local variability in the graph of the stacked transit fluxes.

The transits depth plot from the vetting shows that the depths are consistent, with transit depths values: 0.44 ± 0.04 ppt and 0.48 ± 0.03 ppt. However, the first transit matches a momentum dump, there is another momentum dump right after the second transit, and their individual shape is not clear. We also see some scattering of the points in the graph of the position of the centroid, showing that the momentum dumps probably affected the observed lightcurve.

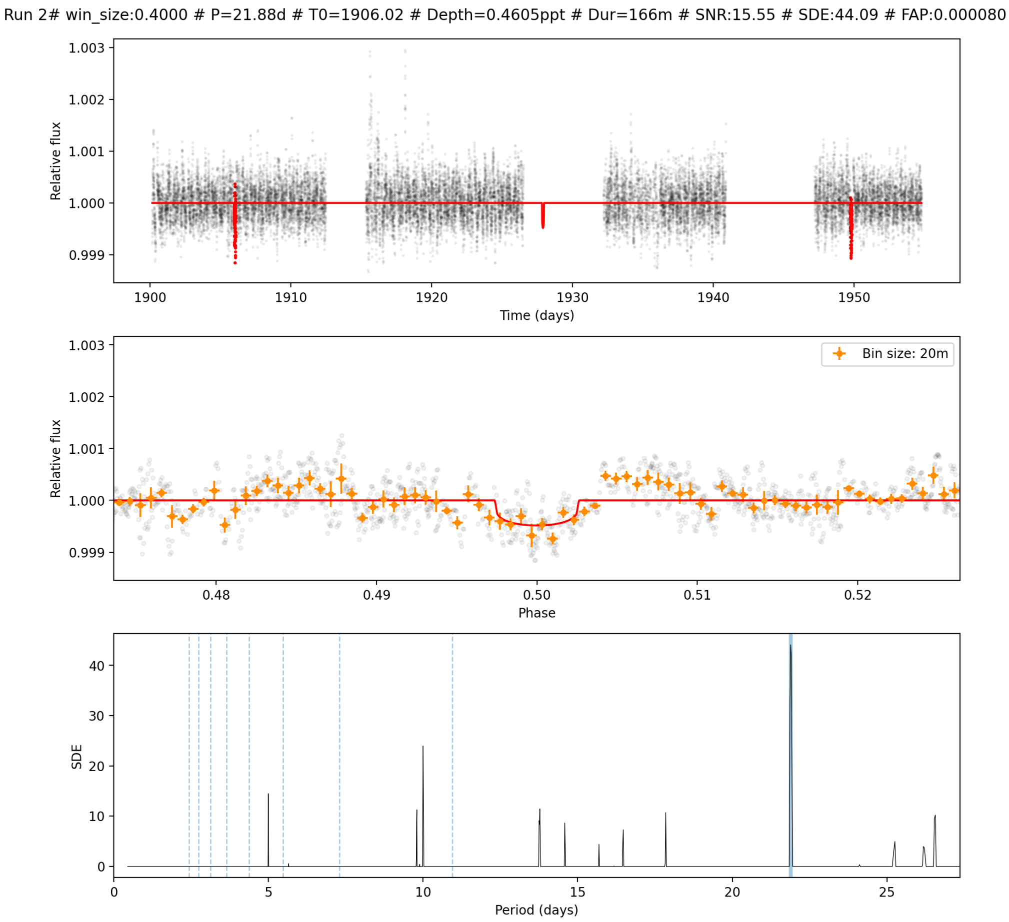

Figure 3.7: TIC 180695581 run 2 win_size 0.4

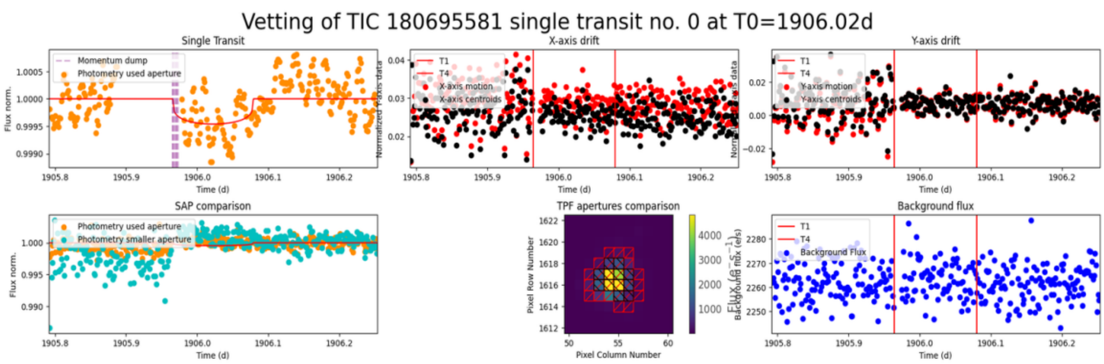

Figure 3.8: TIC 180695581 vetting plots of the first transit.

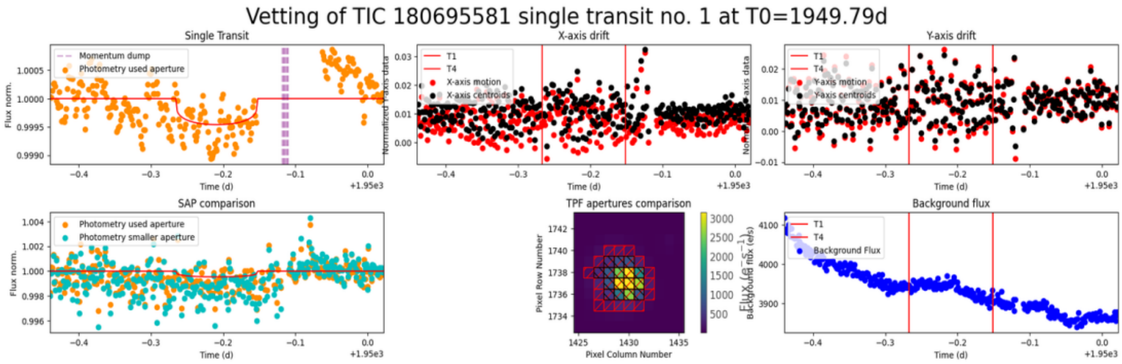

Figure 3.9: TIC 180695581 vetting plots of the second transit.

With the validation stage, we obtained the FPP and NFPP values listed in table 3.7, which places our candidate at the upper border of the "likely planet zone" in figure 3.1 (purple point). Note that the FPP value can be improved since one planet is already confirmed in the system. As explained at the end of section 2.3, we can then use the FPP2 value instead of the FPP one, with FPP2=0.00329. Since we then have FPP < 0.015 and NFPP $< 10^{-3}$, this candidate is statistically validated.

Scenario	FPP	FPP2	NFPP	TP	PTP	STP
Probability	0.07617	0.00329	0.00092	0.75392	0.12675	0.05570

Table 3.7: TIC 180695581 FPP, NFPP and three most probable scenarios.

In conclusion, for this candidate, we do not completely rule it out regarding the statistical validation based on the TRICERATOPS criteria, but it is not a priority target for further observations since some elements of the vetting are not in favor of a real detection. Moreover, the TESS sector 49 data will help to investigate further this possible candidate, and they should be analysed first before planning any other follow-up observations.

3.2.3 TIC 381714186

TIC 381714186 has one candidate planet: TOI 1839.01 which has not been confirmed yet. This candidate was correctly retrieved in the first run, and its period is P = 1.42482 ± 0.00023 d.

TIC ID	Sector(s)	Mass (M_Sun)	Rad (R_Sun)	Teff (K)	Lum (L_Sun)	Log(g)
381714186	23,46	0.93	0.848	5382	0.544	4.551

Existing TOI(s)	Period (days)	Radius (R_Earth)
TOI 1839.01	1.425	2.470

Table 3.8: TIC 381714186 stellar and TOI parameters.

The signal that we retained is the one selected in the second run (table 3.9). The same period is retrieved in all of the 10 detrendings with both good SNR and SDE. The stacked transit fluxes (figure 3.10) show that there can be some variability. However, the presence of some harmonics and subharmonics in the SDE plot encourages us to continue with vetting and validation steps.

Win_size.	Period	Per_err	N.Tran	Duration	T0	Depth	SNR	SDE
0.2	4.0240	0.00032	10	80.09	1933.73	0.400	14.08	22.49

FAP	Border_score	Planet radius	R_p/R_s	Semi-major axis	Habitability zone
0.000080	1.00	1.85129	0.01564	0.04849	I

Table 3.9: TIC 381714186 candidate parameters.

The depths of the ten transits are consistent, with the exception of one outlier (figure 3.11) but it has a large error bar. The third transit (T0=1949.83 BTJD) is the only one matching a momentum dump. For all the other transits, the background, the position of the centroid, and the individual lightcurves in the target pixel file reveal nothing worth mentioning. However, the shapes of the single transits look more like variability than real transit events (see for example figure 3.12 for the second transit).

In order to clarify the ambiguous results for this candidate, we decided to analyse separately the two sectors available (sectors 23 and 46). In this way, if we retrieve the same candidate with a period P = 4.0240d for both sectors independently, it will be an additional hint in favor of a real transiting planet. Note that this can be done because of the small period of the candidate, implying that we can observe several transits in only one sector.

The periods selected for each sectors are listed in table 3.10. The period selected in the first run for both sectors corresponds to the candidate planet TOI 1839.01. However, we see that the 4.02d-period of our second candidate is retrieved in sector 46 but is not present in sector 23. However, we notice that the period of 16.10d in run 4 of sector 23 could be an harmonic of the candidate (P*4). After checking the epochs of the transits, we can say that the two transits with the 16.10d-period are indeed matching transits of our candidate.

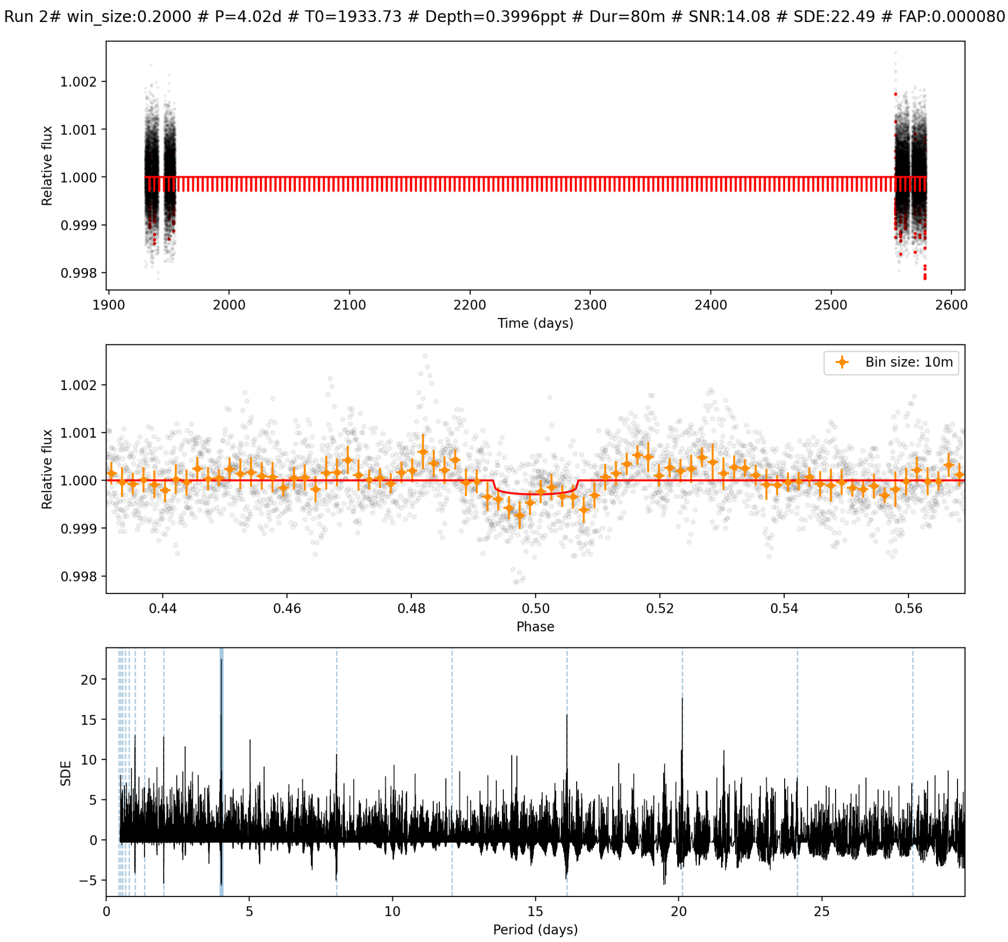

Figure 3.10: TIC 381714186 run 2 win_size 0.2

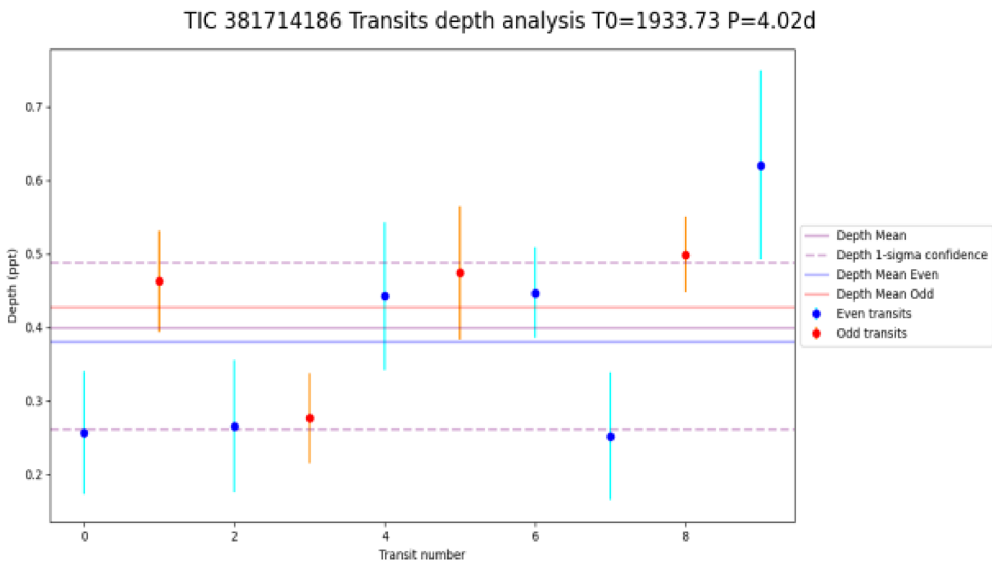

Figure 3.11: TIC 381714186 single-transits depths plot.

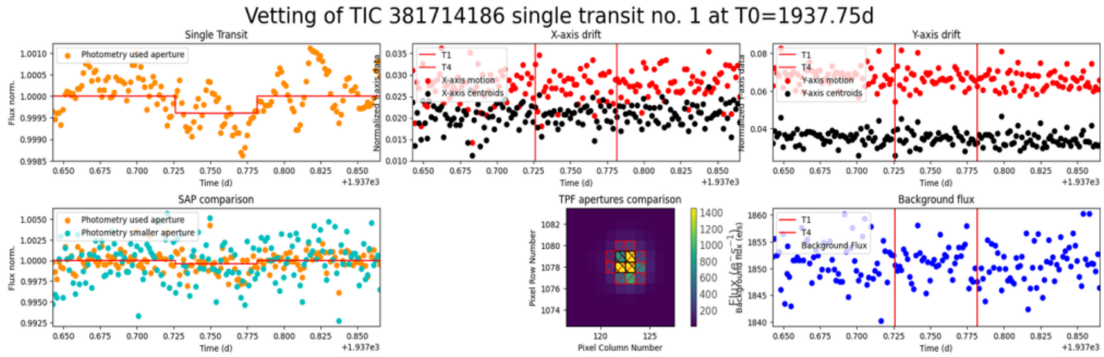

Figure 3.12: TIC 381714186 vetting plots of the second transit.

Run	Period	
	Sector 23	Sector 46
1	1.4244	1.4245
2	9.3418	4.0219
3	2.5040	14.1792
4	16.1056	3.8504
5	7.9338	19.6005

Table 3.10: Comparison of sectors 23 and 46 run independently.

Even if some elements previously discussed are in disfavor of the reliability of this candidate, we obtained good results for the statistical validation (table 3.11). This candidate is then classified as "likely planet" regarding those values (red point in figure 3.1).

Scenario	FPP	NFPP	TP	PTP	STP
Probability	0.21133	0.0	0.59716	0.13568	0.08453

Table 3.11: TIC 381714186 FPP, NFPP and three most probable scenarios.

The results obtained for the two sectors run separately are a hint toward a real detection, but the period is still to determine. This star has been further observed by TESS in sector 50 (from 2022-Mar-26 to 2022-Apr-22). The analysis of these additional data, which have just been released at the time of writing these lines (end of May 2022), will help us to confirm, or not, that this candidate is real.

3.2.4 TIC 16884216

TIC 16884216 has one not yet confirmed planet candidate: TOI 2023.01, with a period P = 11.19005 ± 0.00496d. This candidate is retrieved within the first run of the search stage.

TIC ID	Sector(s)	Mass (M_Sun)	Rad (R_Sun)	Teff (K)	Lum (L_Sun)	Log(g)
16884216	24	0.82	0.696	4958	0.264	4.667

Existing TOI(s)	Period (days)	Radius (R_Earth)
TOI 2023.01	11.190	1.661

Table 3.12: TIC 16884216 stellar and TOI parameters.

We focus on the signal selected in the second run. Its parameters are listed in table 3.13. The period associated with this candidate appears in 6 of the 10 detrendings. We have a good SNR, the SDE is a bit lower but can still hint at a detection. The shape of the stacked transits in figure 3.13 seems convincing at first sight.

Win_size.	Period	Per_err	N.Tran	Duration	T0	Depth	SNR	SDE
0.5	15.7784	0.07010	2	219.19	1965.98	0.277	15.50	10.77

FAP	Border_score	Planet radius	R_p/R_s	Semi-major axis	Habitability zone
0.000080	1.00	1.26497	0.01802	0.11545	I

Table 3.13: TIC 16884216 candidate parameters.

From the vetting report, the two transits have consistent depths with large error bars (see figure 3.14). The shape of the first transit does not look too bad, even if there is some variability (figure 3.15). However, we see big variations in the background flux, that could cause the transit-like event. For the second transit, we see from the photometry that the event is more likely due to variability than to a transiting planet (figure 3.16). The background flux looks better than for the first transit but there is some scattering in the x-position of the centroid, which is not encouraging. Overall, the first transit is the most promising of the two, but it should be considered carefully because of the background flux variations.

For the statistical validation, we obtained the FPP and NFPP values listed in figure 3.14, corresponding to the pink point in figure 3.1. Based on these values, the signal is classified as a likely planet.

With the good values obtained for the statistical validation, it would be interesting to analyse the upcoming data (sectors 50 and 51), to see if the first transit at T0=1965.98 could be associated with other transit-like events, with another period.

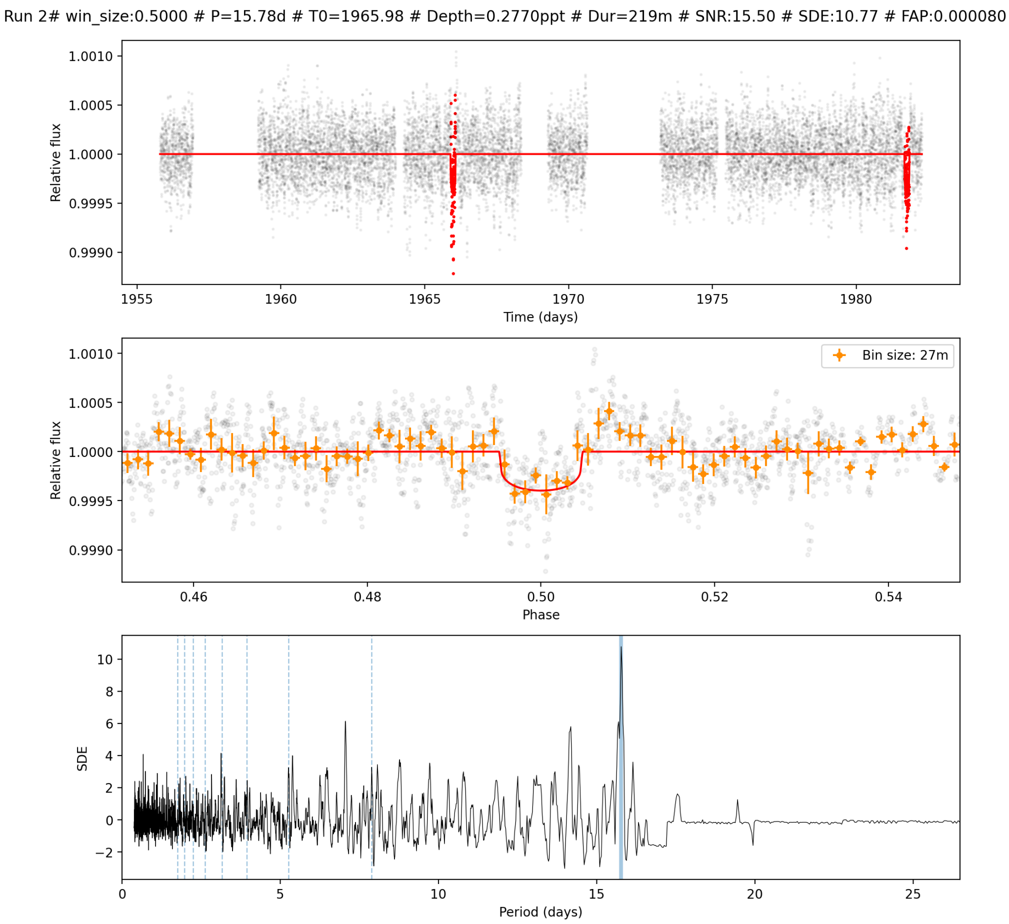

Figure 3.13: TIC 16884216 run 2 win_size 0.5

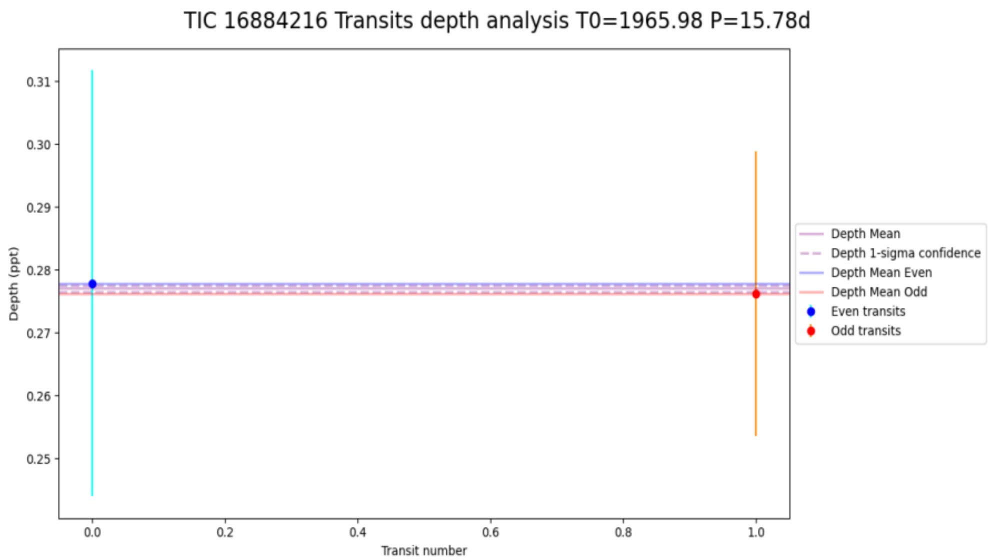

Figure 3.14: TIC 16884216 single-transits depths plot.

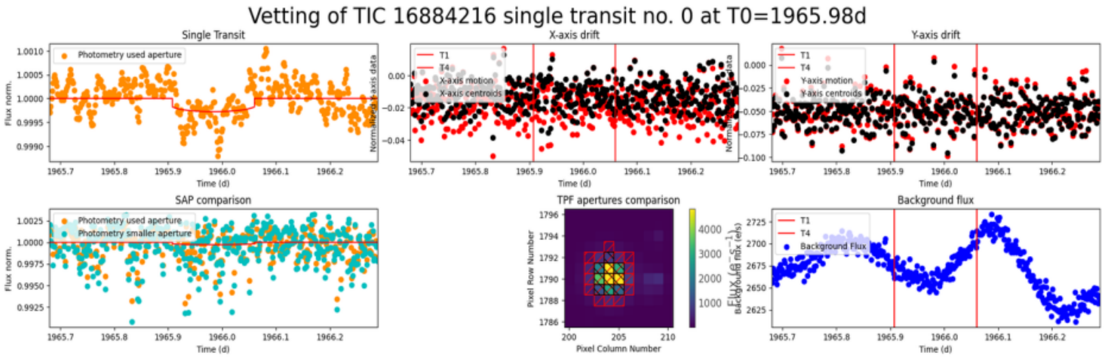

Figure 3.15: TIC 16884216 vetting plots of the first transit.

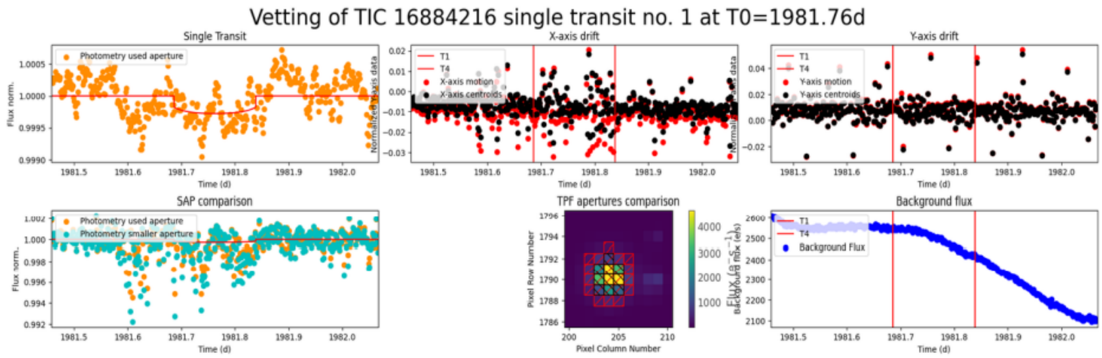

Figure 3.16: TIC 16884216 vetting plots of the second transit.

Scenario	FPP	NFPP	TP	PTP	STP
Probability	0.11494	0.0	0.70628	0.11799	0.07405

Table 3.14: TIC 16884216 FPP, NFPP and three most probable scenarios.

3.2.5 TIC 10837041

TIC 10837041 has one confirmed planet: TOI-2411 b [8].

TIC ID	Sector(s)	Mass (M_Sun)	Rad (R_Sun)	Teff (K)	Lum (L_Sun)	Log(g)
10837041	30	0.64	0.728	4099	0.135	4.520

Existing TOI(s)	Period (days)	Radius (R_Earth)
TOI-2411 b	0.783	1.68

Table 3.15: TIC 10837041 stellar and TOI parameters.

This planet has a period P = 0.78276 ± 0.00012d and is retrieved in the second run of the search stage.

Our candidate of interest for this star was selected in the first run and is found in 7 of the 10 detrendings. Note that, since our candidate is found in the first run, we carefully checked that the proposed transits are not matching the ones of the confirmed planet, which is not the case. The proposed parameters are listed in table 3.16.

Win_size.	Period	Per_err	N.Tran	Duration	T0	Depth	SNR
PDCSAP_FLUX	18.7561	0.08192	2	208.65	2122.57	1.391	31.54

SDE	FAP	Border_score	Planet radius	R_p/R_s	Semi-major axis	Habit. zone
15.27	0.000080	1.00	2.96368	0.03713	0.11928	I

Table 3.16: TIC 10837041 candidate parameters.

This candidate looks particularly convincing, with high SNR and SDE, good border score, clear shape of the transits and several subharmonics visible in figure 3.17.

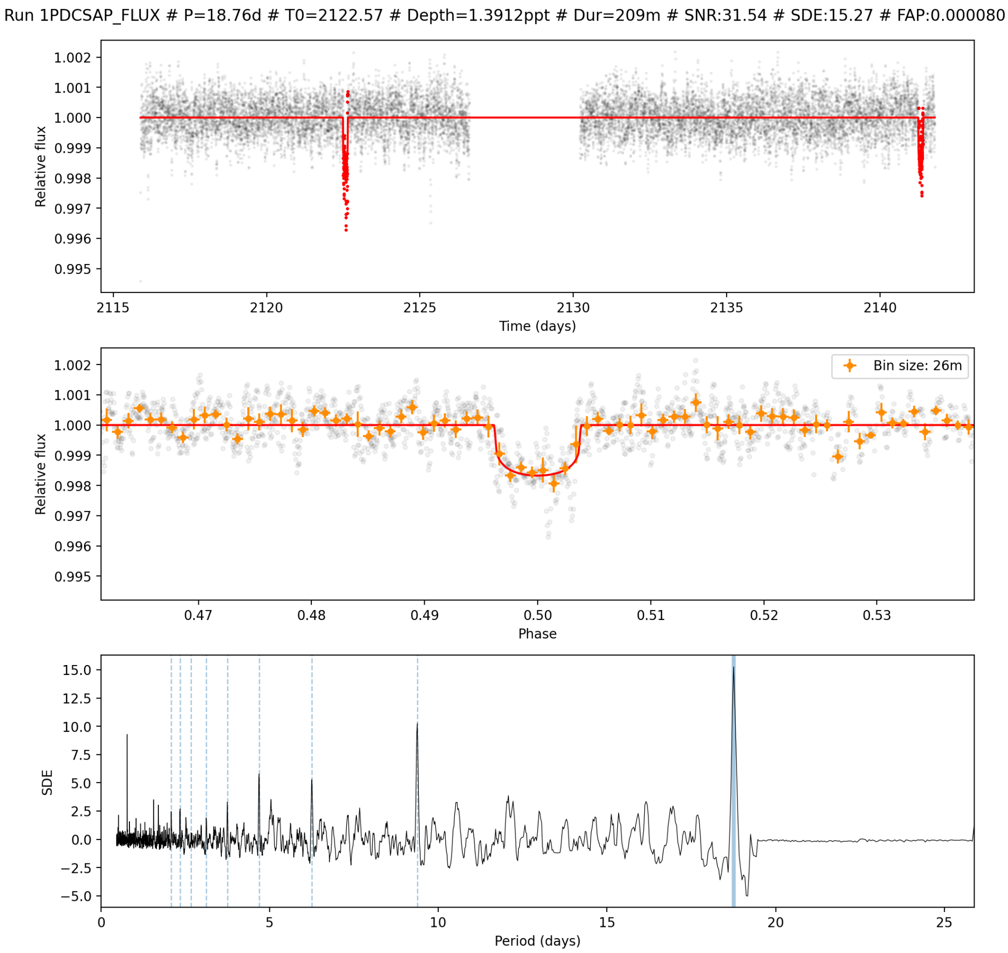

Figure 3.17: TIC 10837041 run 1 PDCSAP_FLUX.

From the folded curve of the vetting report, we can say that the proposed period is correct. The first transit matches a momentum dump but, given its convincing shape, it can simply be an unfortunate coincidence (figure 3.18). The other plots reveal nothing that could produce the transit, which is also true for the second transit. The only plot of the vetting report that is in disfavor of a real detection is the transits depth plot (figure 3.19). Indeed, the two transits have quite different depths (1.68 $\pm$ 0.08 ppt and 1.11 $\pm$ 0.06 ppt), which could mean that they are not produced by the same object.

From the validation stage, we obtained the values listed in table 3.17, which places this candidate inside the "likely planet zone" in figure 3.1, and at the border of the "validated planet zone". As explained in section 2.3, being classified as a validated planet requires: FPP < 0.015 and NFPP $< 10^{-3}$.

However, since TOI-2411 b is a confirmed planet, we can use the FPP2 value instead of the FPP one. This new value pushes our candidate inside the validated planet zone.

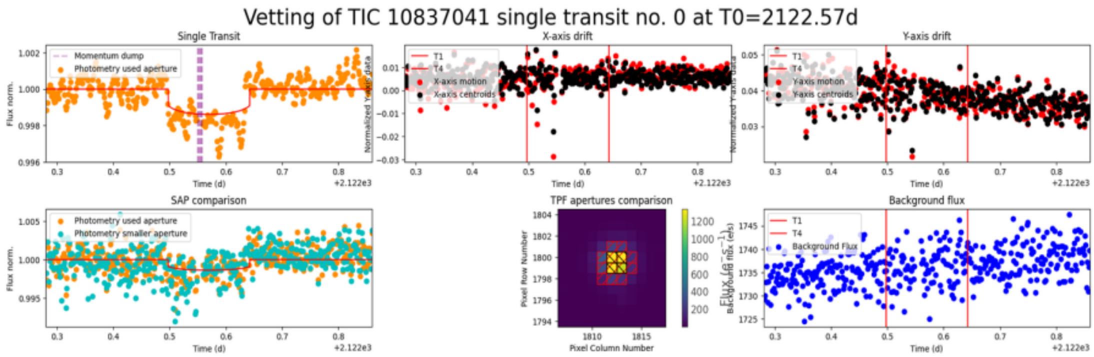

Figure 3.18: TIC 10837041 vetting plots of the first transit.

In conclusion, this candidate looks really promising, even if the two transit events are maybe not associated to the same planet. Further analyses are thus needed. We could perform a fit of each transit to check how different (or not) their depth and duration are. This target has also been observed in sector 3, but there is no short-cadence (2 min) light curve available for this sector. We could still use the long-cadence (30 min) data and see if there are some transit-like events that could be associated with the two transits proposed for our candidate.

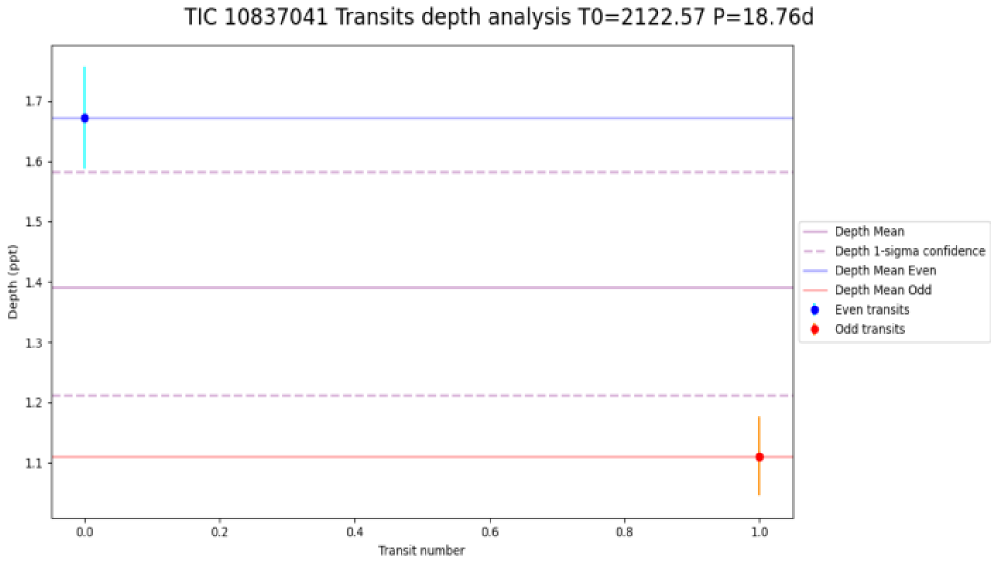

Figure 1: The candidate single-transits depths plot.

Figure 3.19: TIC 10837041 single-transits depths plot.

Scenario	FPP	FPP2	NFPP	TP	PTP	DTP
Probability	0.01673	0.00068	0.0	0.78268	0.11130	0.08928

Table 3.17: TIC 10837041 FPP, NFPP and three most probable scenarios.

3.2.6 TIC 146523262

TIC 146523262 has one candidate planet: TOI 2465.01, which has not been confirmed yet. This candidate was recovered in the first run and has a period P = 3.75921 $\pm$ 0.00074d.

TIC ID	Sector(s)	Mass (M_Sun)	Rad (R_Sun)	Teff (K)	Lum (L_Sun)	Log(g)
146523262	32	1.46	1.015	6808	1.995	4.591

Existing TOI(s)	Period (days)	Radius (R_Earth)
TOI 2465.01	3.759	3.156

Table 3.18: TIC 146523262 stellar and TOI parameters.

The candidate that we present for this star was selected in the second run, with the parameters in table 3.19. Figure 3.21 indicates that the candidate is interesting, by looking at the shape of the transits, even if they are very shallow, and at the harmonics visible in SDE plot. However, the period of this candidate appears in only 2 of the 10 detrendings and we have a border score lower than 1.

Win_size.	Period	Per_err	N.Tran	Duration	T0	Depth	SNR
PDCSAP_FLUX	4.4346	0.03509	6	185.81	2176.86	0.384	14.90

SDE	FAP	Border_score	Planet radius	R_p/R_s	Semi-major axis	Habit. zone
9.79	0.000080	0.83	2.17332	0.01877	0.06012	I

Table 3.19: TIC 146523262 candidate parameters.

Concerning the vetting report, the depths of the transits are not very consistent (see figure 3.20). The individual transit plots show no momentum dump, background variations, centroid shift or contamination by pixels not centered on the target star. However, the individual photometry of the transits shows lots of variability and no clear transit shape. The best looking photometry plot would be the one of the last transit (figure 3.22), but even for this one, we see that the lightcurve shows some variability with an amplitude comparable to (or even larger than) the actual transit-like event.

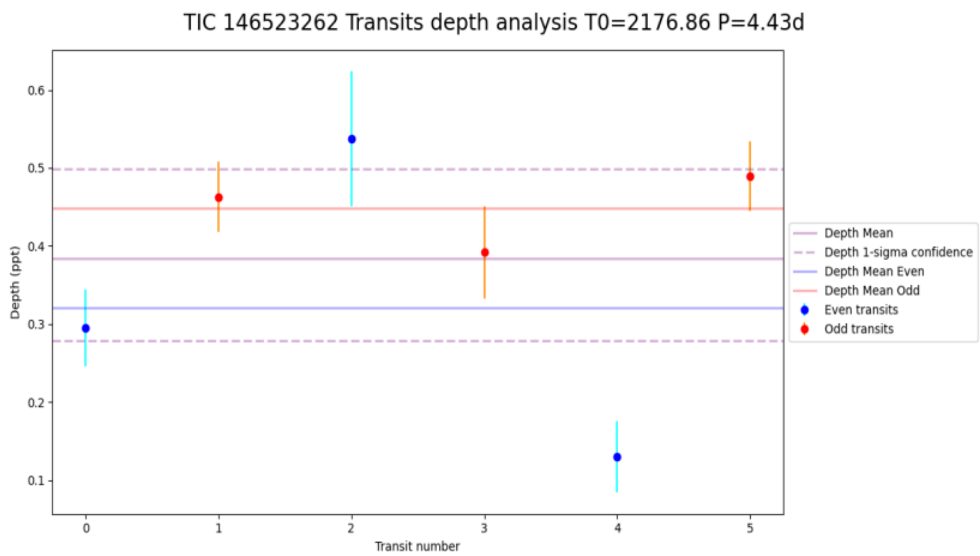

Figure 3.20: TIC 146523262 single-transits depths plot.

By running the validation step, we obtained the values of FPP and NFPP listed in table 3.20, corresponding to the brown point in figure 3.1. The three most probable scenarios computed during the statistical validation are listed in the same table.

In conclusion for this candidate, even if it is classified as a "likely planet", we are not confident in this detection. The main reason we are not in this candidate is because the photometry shows some variability and the signal is only found in 2 of the 10 detrendings, which could indicate that it is actually related to some residual variability that is not entirely removed by these two detrendings (but well in the others). This hypothesis is supported by the fact that the two detrendings in which the signal is found have similar window sizes (1.0 d and 1.1 d).

This target has only been observed in sector 32 and no further observation of this star with TESS is planned.

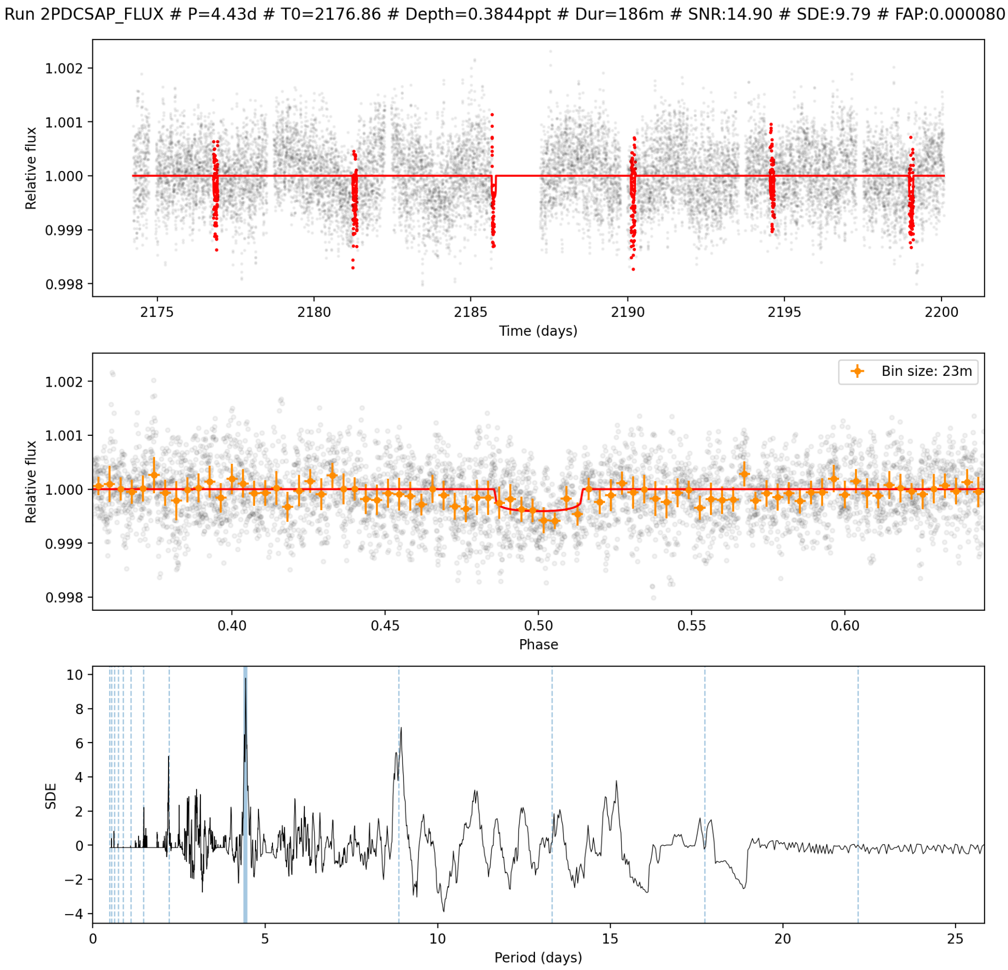

Figure 3.21: TIC 146523262 run 2 PDCSAP_FLUX.

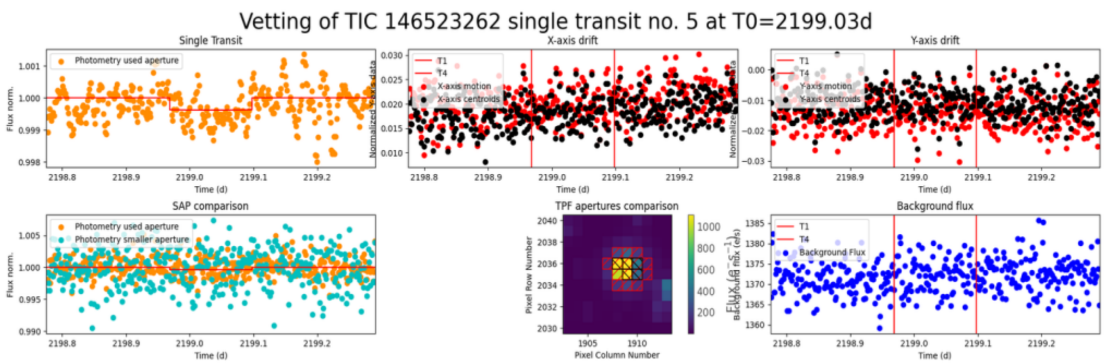

Figure 3.22: TIC 146523262 vetting plots of the last transit.

Scenario	FPP	NFPP	TP	PTP	STP
Probability	0.28858	0.00047	0.55167	0.12069	0.09514

Table 3.20: TIC 146523262 FPP, NFPP and three most probable scenarios.

3.2.7 TIC 37749396

TIC 37749396 has one, not yet confirmed, candidate planet: TOI 260.01 with a period P = 13.47002 ± 0.00324d.

TIC ID	Sector(s)	Mass (M_Sun)	Rad (R_Sun)	Teff (K)	Lum (L_Sun)	Log(g)
37749396	3,42	0.63	0.618	4049	0.093	4.655

Existing TOI(s)	Period (days)	Radius (R_Earth)
TOI 260.01	13.476	1.680

Table 3.21: TIC 37749396 stellar and TOI parameters.

This candidate was not selected as the most promising signal in the first run, and some of its transits were associated with other transit-like events by SHERLOCK. We thus made a second attempt, this time masking manually the transits corresponding to TOI 260.01. We can see the ranges of time initially masked in figure 3.23.

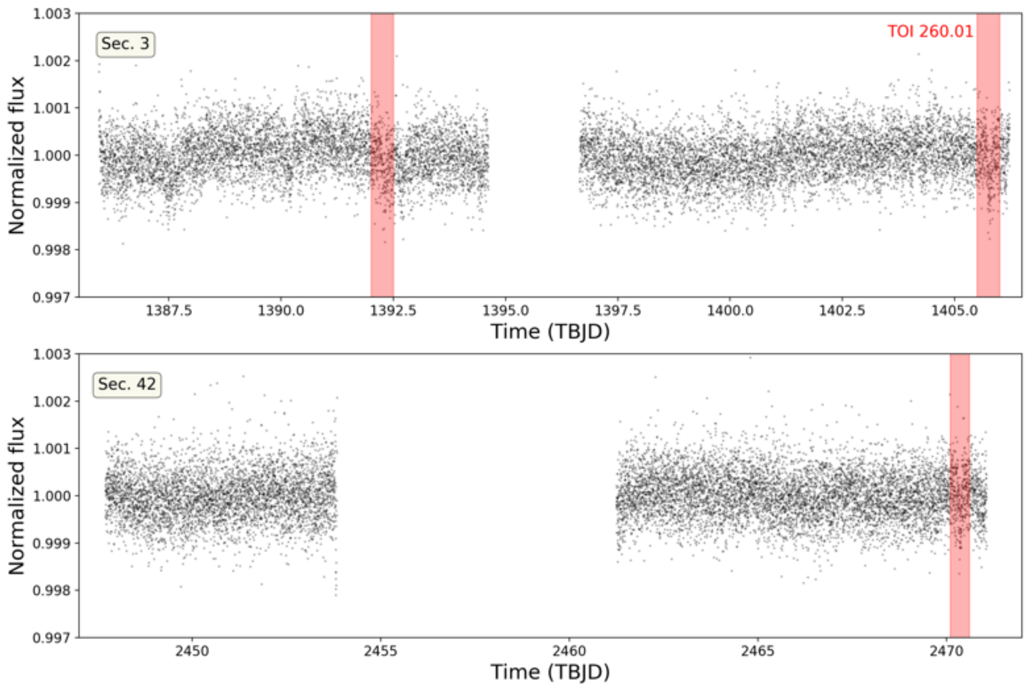

Figure 3.23: TIC 37749396 initial masks.

The signal in table 3.22 is retrieved in 9 of the 10 detrendings in the run 4. The values of SNR and SDE are a bit low but still acceptable. The stacked transit fluxes in figure 3.24 shows an asymmetric shape, with an ingress but no clear egress. We can also see from the SDE panel of this figure the absolute absence of harmonics.

Win_size.	Period	Per_err	N.Tran	Duration	T0	Depth	SNR	SDE
0.5	2.3087	0.00008	15	53.86	1386.55	0.132	12.01	12.81

FAP	Border_score	Planet radius	R_p/R_s	Semi-major axis	Habitability zone
0.000080	1.00	0.77568	0.01072	0.02936	I

Table 3.22: TIC 37749396 candidate parameters.

The vetting report indicates that not all of the transit depths are consistent (see figure 3.25). For several transits, we see a scattering of the points in the centroid position plot (see for example figure 3.26). One of the transits is also matching a momentum dump. Overall, the transit-like events have the same depth as local variability and none of them has a convincing shape.

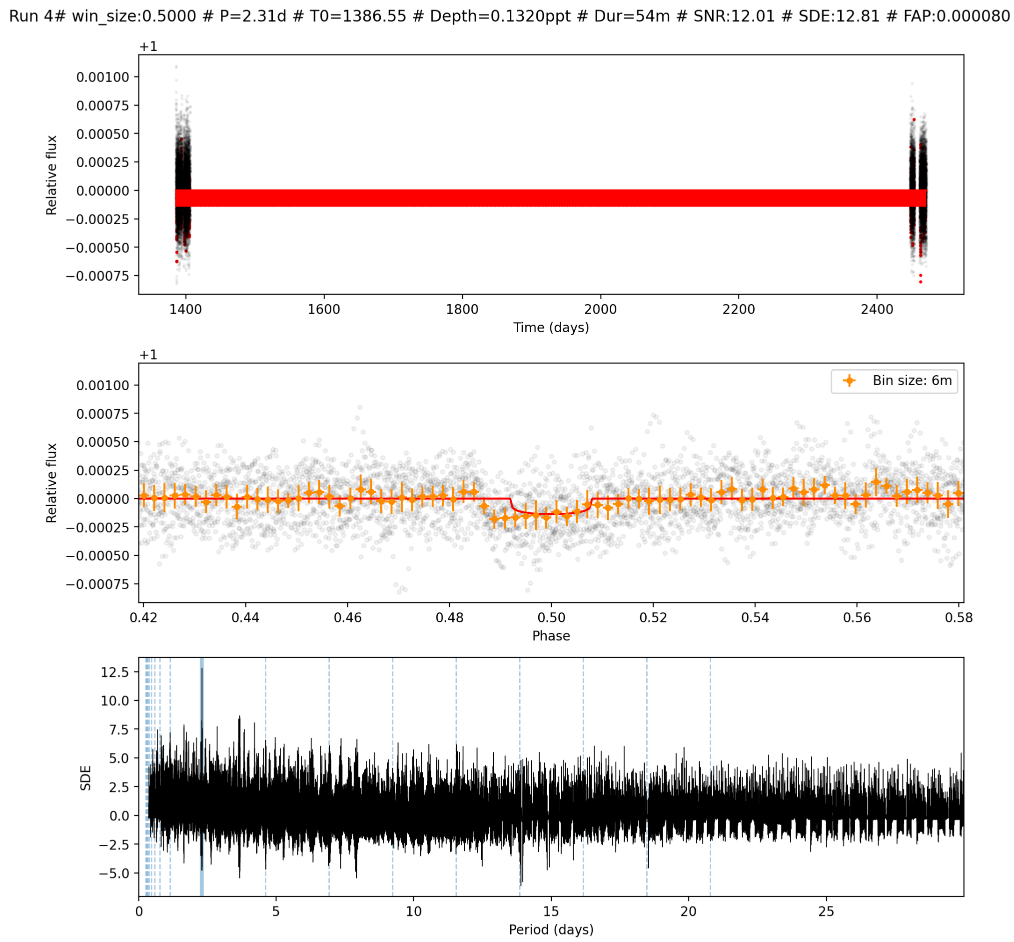

Figure 3.24: TIC 37749396 run 4 win_size 0.5

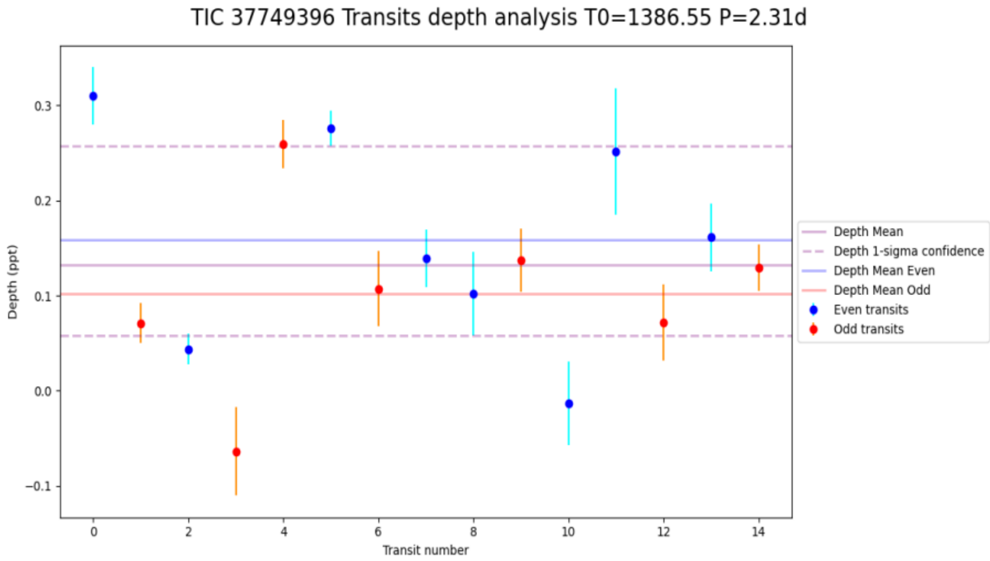

Figure 3.25: TIC 37749396 single-transits depths plot.

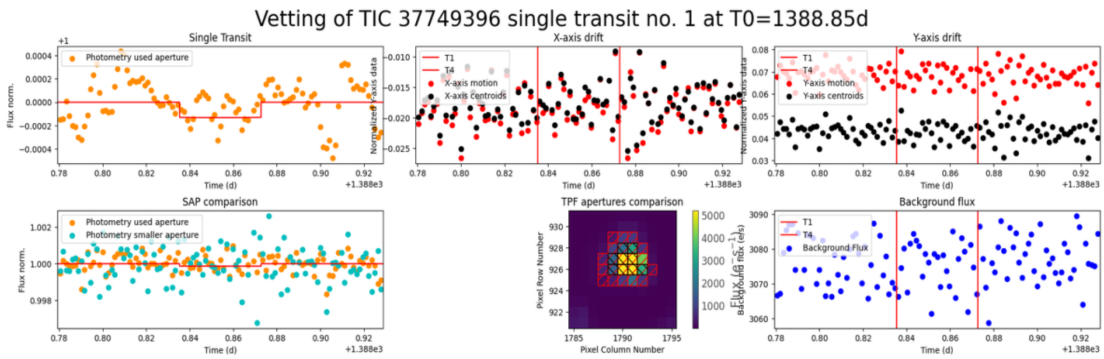

Figure 3.26: TIC 37749396 vetting plots of the second transit.

For the statistical validation, the FPP and NFPP values are listed in table 3.23 along with the three most probable scenarios. The FPP and NFPP obtained correspond to the orange point in figure 3.1.

Scenario	FPP	NFPP	TP	BEB	STP
Probability	0.38951	0.00076	0.50636	0.16841	0.07231

Table 3.23: TIC 37749396 FPP, NFPP and three most probable scenarios.

To conclude, even if this signal is classified as a likely planet, it does not look very promising. It is most probably due to some periodicity in the variability, and this target won't be re-observed by TESS.

3.2.8 TIC 357501308

TIC 357501308 has one candidate planet: TOI 2018.01. It has a period P = 7.43712 ± 0.00115d and we retrieved this candidate with SHERLOCK in the first run of the search stage.

TIC ID	Sector(s)	Mass (M_Sun)	Rad (R_Sun)	Teff (K)	Lum (L_Sun)	Log(g)
357501308	24	0.66	0.622	4218	0.111	4.669

Existing TOI(s)	Period (days)	Radius (R_Earth)
TOI 2018.01	7.435	2.451

Table 3.24: TIC 357501308 stellar and TOI parameters.

The signal in which we are interested is selected in the second run and is presented in table 3.25.

Win_size.	Period	Per_err	N.Tran	Duration	T0	Depth	SNR	SDE
0.9	11.2420	0.10240	2	241.52	1964.11	0.506	21.63	9.80

FAP	Border_score	Planet radius	R_p/R_s	Semi-major axis	Habitability zone
0.000080	1.00	1.52933	0.02228	0.08567	I

Table 3.25: TIC 357501308 candidate parameters.

The period of this candidate is retrieved in 7 of the 10 detrendings in run 2. We have a high SNR and a good border score. The proposed transits look convincing on both the first and second panels in figure 3.27. Some subharmonics are also visible in the SDE plot (third panel).

The vetting report shows that the two transits are similar in depth, and based on the folded curve, the period selected seems correct. For both transits, we see some X-axis data drift and variation in the background flux, but the photometry still shows a transit-like event which differs from the local variations (figure 3.28).

The validation provides us with the values listed in table 3.26, which do not allow this candidate to be classified as a likely planet, even if the FPP is low enough.

Since this candidate seemed promising to us, we checked on the TESS Wiki (used to coordinate the preparation of TESS publications) if there was any upcoming article about this target, and there is indeed a discovery paper in preparation led by the TESS-Keck-Survey team. Besides the confirmation of TOI 2018.01, their abstract also mentions the detection of a previously unknown transiting planet at 11-day orbit in a 3:2 mean-motion resonance with TOI 2018.01. We therefore achieved to detect this previously unknown transiting planet completely independently using SHERLOCK.

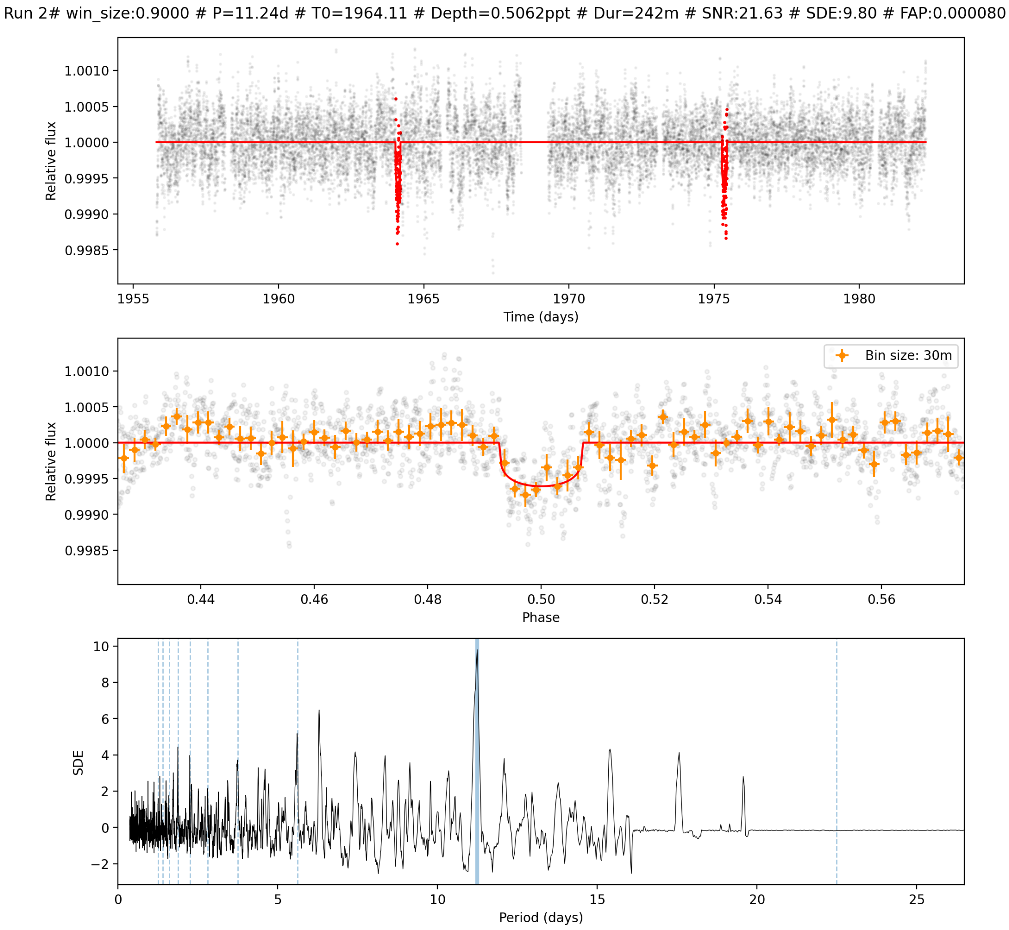

Figure 3.27: TIC 357501308 run 2 win_size 0.9

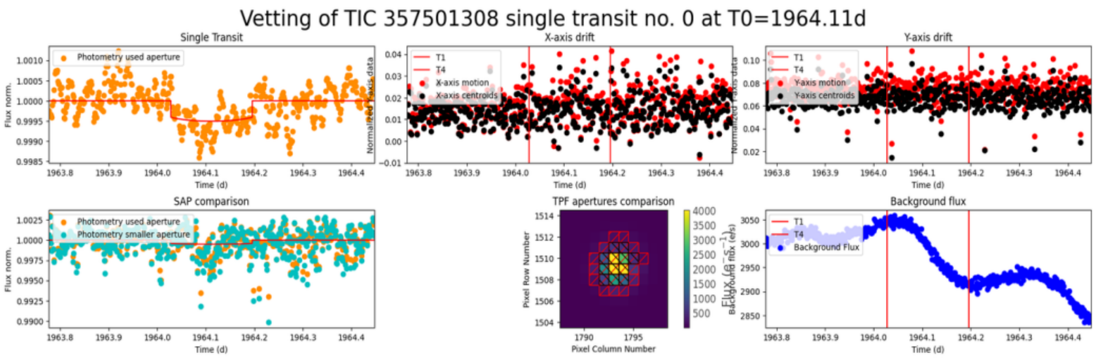

Figure 3.28: TIC 357501308 vetting plots of the first transit.

Scenario	FPP	NFPP	TP	PTP	STP
Probability	0.06771	0.01396	0.77971	0.11151	0.04295

Table 3.26: TIC 357501308 FPP, NFPP and three most probable scenarios.

3.2.9 TIC 368435330

TIC 368435330 has one candidate planet (TOI 1797.01) with a period P=3.64516 ± 0.00001d, which was successfully retrieved by SHERLOCK in the first run. The candidate that we present is selected in the second run with the parameters listed in table 3.27 and is found in all the detrendings.

Win_size.	Period	Per_err	N.Tran	Duration	T0	Depth	SNR	SDE
0.2	1.0391	0.00006	43	64.74	1900.24	0.098	14.77	93.08

FAP	Border_score	Planet radius	R_p/R_s	Semi-major axis	Habitability zone
0.000080	0.98	1.13238	0.00878	0.02064	I

Table 3.27: TIC 368435330 candidate parameters.

This signal looks like an actual transiting planet because of the good SNR, very high SDE and harmonics visible in figure 3.29. Also, even if shallow, we see a convincing shape for the stacked transits. The large number of transit events increases even more our confidence in the detection.

The transits depth plot from the vetting shows consistent depths with only a few outliers among the 43 transits (figure 3.30). The individual graphs reveal nothing particular, except for some scattering in the centroid position plots for a few transits.

Since this candidate seemed very promising, we looked if there was any upcoming article about this target, and indeed there is a paper in preparation with follow-up observations by CHEOPS (Serrano et al., submitted). Some people from the CHEOPS team had indeed also found this candidate by analysing independently the TESS data and scheduled some follow-up observations with CHEOPS to confirm it. A few months after our analysis of this target, it was classified as a TOI (TOI-1797.02) with a period P = 1.0389231 ± 0.0001573d, matching the period that we found independently using SHERLOCK.

TIC ID	Sector(s)	Mass (M_Sun)	Rad (R_Sun)	Teff (K)	Lum (L_Sun)	Log(g)
368435330	22,48	1.08	1.049	5922	1.219	4.429

Existing TOI(s)	Period (days)	Radius (R_Earth)
TOI 1797.01	3.645	2.993
TOI 1797.02	1.038	1.537

Table 3.28: TIC 368435330 stellar and TOI parameters.

From the statistical validation, we obtained the values for FPP and NFPP listed in table 3.29. We can note that in this case we have high FPP and NFPP values, and the planet is not located in the likely-planet zone, while the candidate appears to be real. The most probable scenario computed with the statistical validation is an unresolved background eclipsing binary, and not a transiting planet.

The team leading the upcoming paper was able to validate and confirm the two planets (thus including the new one) using higher-precision CHEOPS photometry, multi-color ground-based photometry, radial velocities and high-resolution imaging (private communication with Luisa Maria Serrano).

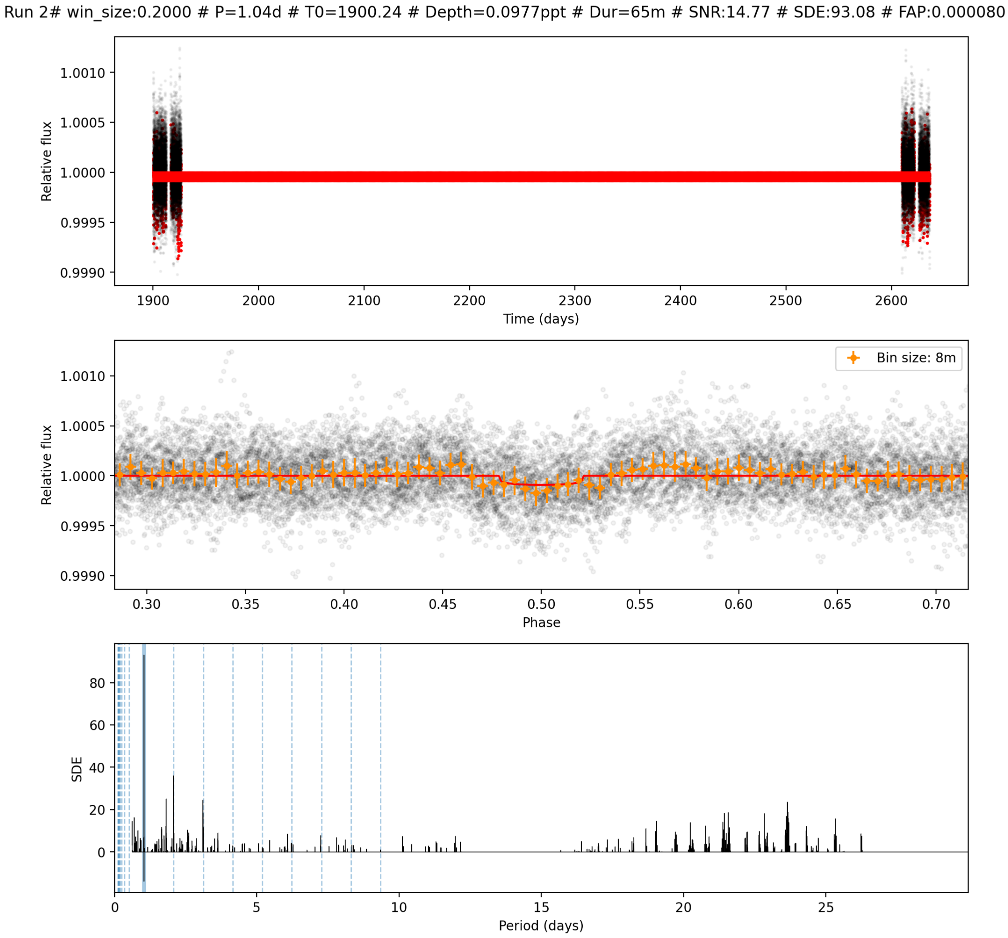

Figure 3.29: TIC 368435330 run 2 win_size 0.2

Scenario	FPP	NFPP	BEB	TP	BEBx2P
Probability	0.68497	0.00577	0.36867	0.21997	0.10015

Table 3.29: TIC 368435330 FPP, NFPP and three most probable scenarios.

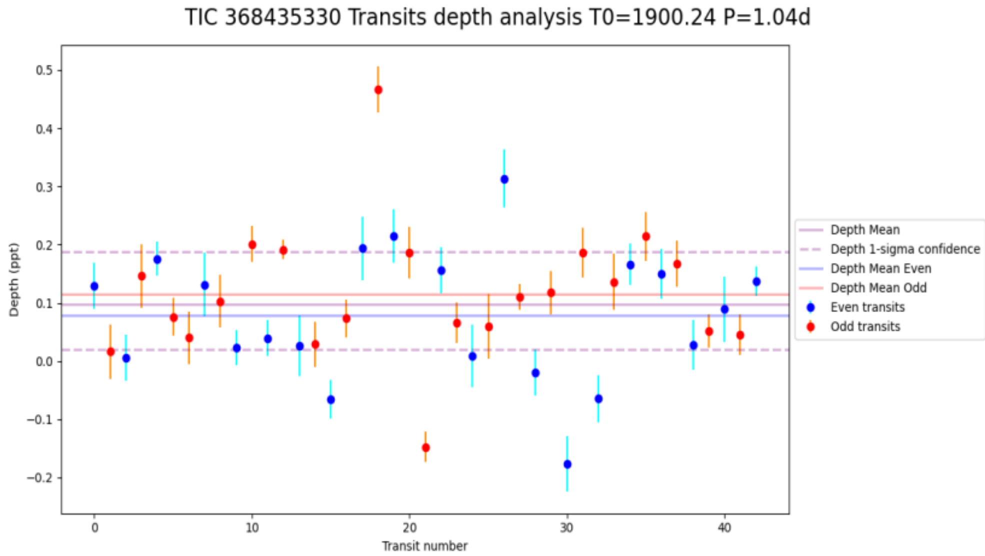

Figure 3.30: TIC 368435330 single-transits depths plot.

3.2.10 TIC 144401492

TIC 144401492 has two planetary candidates which have not been confirmed yet : TOI 1803.01 and TOI 1803.02 with respective periods P = 12.89115±0.00266d and 6.29439±0.00138d. These two candidates are well recovered in the first two runs.

TIC ID	Sector(s)	Mass (M_Sun)	Rad (R_Sun)	Teff (K)	Lum (L_Sun)	Log(g)
144401492	22	0.79	0.689	4868	0.241	4.660

Existing TOI(s)	Period (days)	Radius (R_Earth)
TOI 1803.01	12.891	4.027
TOI 1803.02	6.294	3.132

Table 3.30: TIC 144401492 stellar and TOI parameters.

The candidate presented in table 3.31 is selected as the most promising signal in the third run, and is detected in 9 of the 10 detrendings. The value of the SNR is satisfactory, and the SDE is a bit low, but let us remind that we are searching for candidates potentially missed by TESS detection pipeline. The selected signal is displayed in figure 3.31.

Win_size.	Period	Per_err	N.Tran	Duration	T0	Depth	SNR	SDE
1.1	7.9671	0.01702	4	126.63	1900.24	0.573	10.22	7.51

FAP	Border_score	Planet radius	R_p/R_s	Semi-major axis	Habitability zone
0.004002	1.00	1.80179	0.02498	0.07240	I

Table 3.31: TIC 144401492 candidate parameters.

The plots produced during the vetting stage reveal nothing problematic enough to rule out this candidate, even if there is some variability in the lightcurve of the star (see for example figure 3.33). There are differences between the transit depths, but this is not very significant considering the error bars, as shown in figure 3.32.

From the validation step, we obtained the values in table 3.32.

Scenario	FPP	NFPP	TP	PTP	STP
Probability	0.20051	0.00623	0.63130	0.13515	0.09424

Table 3.32: TIC 14440192 FPP, NFPP and three most probable scenarios.

Thus, this candidate is not classified as a likely planet. Since there were some contrast curves available, we wanted to test and show an example of how these can be included in the validation step.

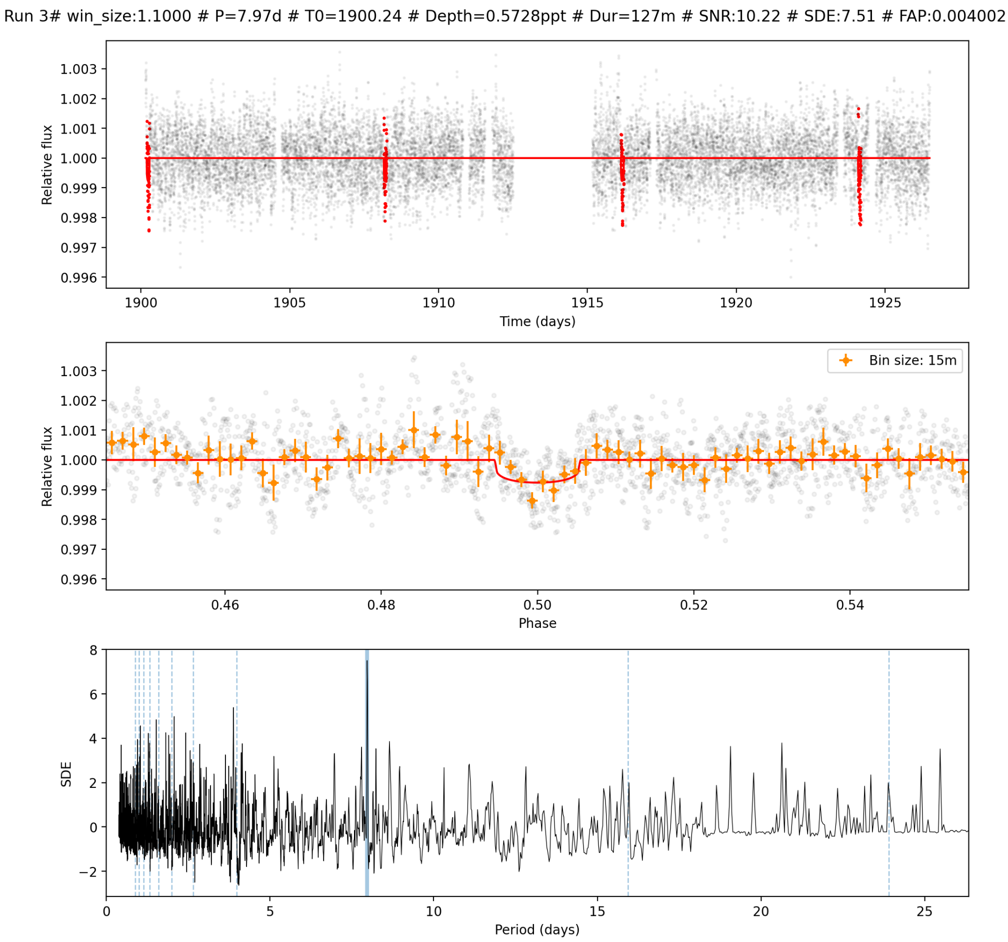

Figure 3.31: TIC 14440192 run 3 win_size 1.1

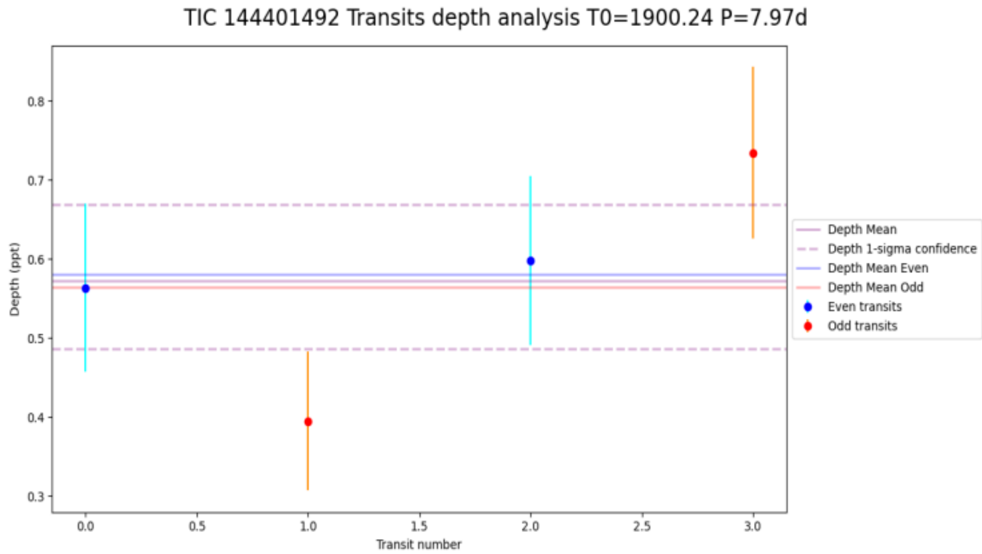

Figure 3.32: TIC 144401492 single-transits depths plot.

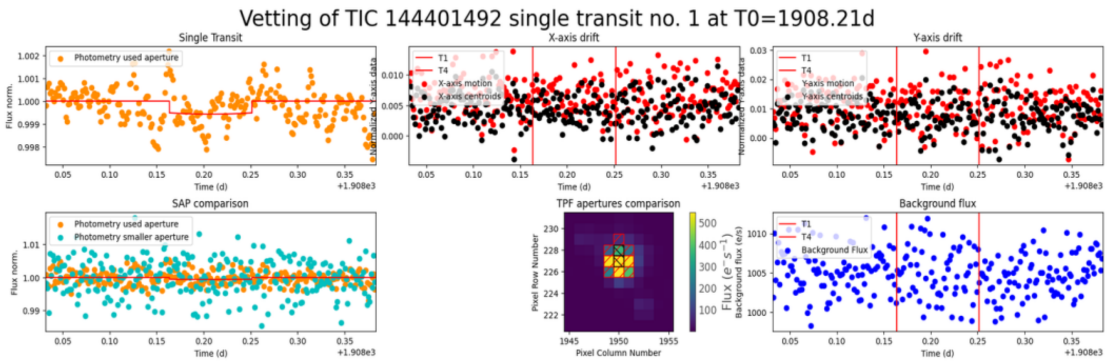

Figure 3.33: TIC 144401492 vetting plots of the second transit.

The calculation from which we obtained those FPP and NFPP values was done assuming that unresolved companions beyond 2.2 arcseconds around the target can be ruled out (default assumption in TRICERATOPS). Therefore, if we are able to decrease this separation, we can further constrain the probabilities of scenarios involving unresolved companions. This is done by using high-resolution images of the target, that produce a contrast curve which can then be used in the validation stage [9]. Basically, a contrast curve is a plot showing the difference in magnitude that could exist between the host star and a detectable companion, as a function of the angular separation.

We were able to obtain such contrast curves (via TESS Follow-up Observing Program), for two different wavelengths, from high resolution images of the target obtained with the Gemini-North/'Alopeke instrument. Those two contrast curves are shown in figure 3.34.

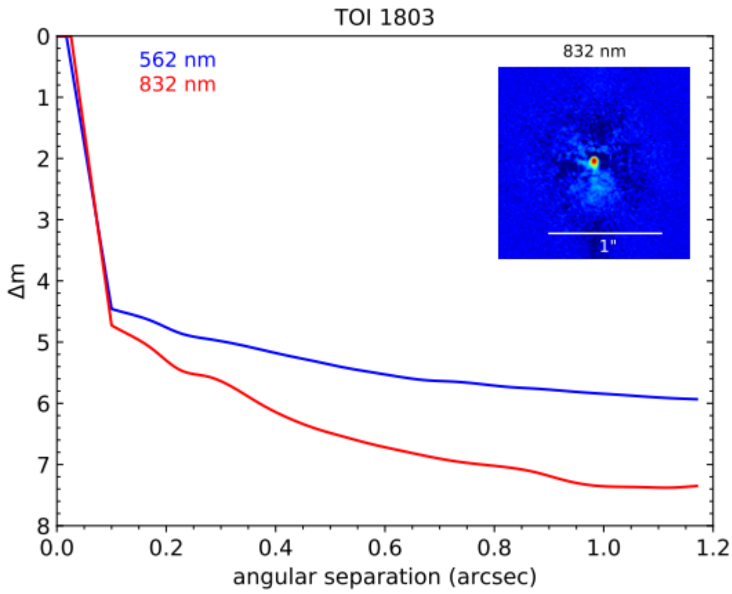

Figure 3.34: Contrast curves for TIC 14440192 at 562 nm and 832 nm.

The values of the validation step obtained without any contrast curve and with the contrast curves at 562 nm and 832 nm, are compared in table 3.33, along with the evolution of the probabilities for the three most probable scenarios. As expected, the probabilities of scenarios involving unresolved companions decrease when including the contrast curves. The corresponding points are placed on figure 3.35 and we see that the FPP value was improved.

	FPP	NFPP	TP	PTP	STP
Without cc	0.20051	0.00623	0.63130	0.13515	0.09424
With cc at 562 nm	0.11012	0.00806	0.82081	0.04847	0.02729
With cc at 832 nm	0.10323	0.00822	0.83558	0.04119	0.02415

Table 3.33: FPP and NFPP values with and without contrast curve and evolution of the probabilities for the three most probable scenarios.

In conclusion, for this candidate, it is a result worth presenting since we showed how we can use contrast curves to improve the validation, even if it did not allow us to classify the signal as a likely planet in this case. Indeed, the FPP criterion is fulfilled but not the NFPP criterion. The NFPP is related to scenarios where the transit is produced by a resolved nearby star rather than the target star. Contrast curves allow to reduce the probabilities of scenarios involving unresolved companions. These scenarios are included in the FPP but not in the NFPP. Including contrast curves in the analyses can reduce the FPP but should not have any significant impact on the NFPP. One way to decrease the NFPP is to obtain ground-based photometry (with a higher angular resolution than TESS) and show that the transit event is well on the target, and not on the resoled nearby stars. The candidate could still be real and it will be interesting to further investigate it by analysing the recently-released data of sector 49 (that were not part of the analysis presented here).

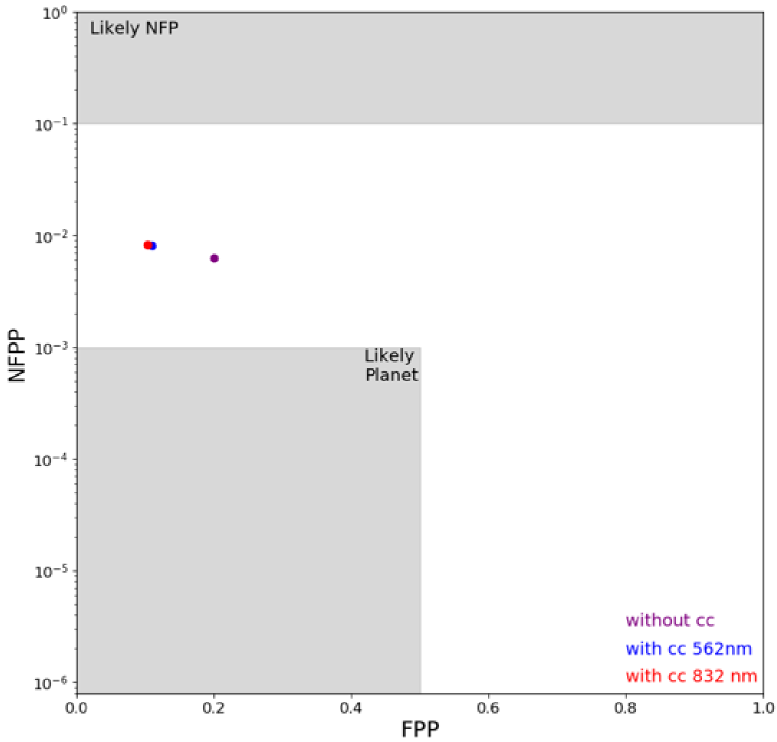

Figure 3.35: FPP and NFPP values with and without contrast curve.

3.2.11 TIC 306263608

At the time we started the analysis of TIC 306263608, this star only had one candidate planet with a period P = 20.77297 ± 0.00008d: TOI 1471.01. The candidate presented in this section was categorized as TOI 1472.02 in the meantime.

TIC ID	Sector(s)	Mass (M_Sun)	Rad (R_Sun)	Teff (K)	Lum (L_Sun)	Log(g)
306263608	17,42,43	1	0.966	5625	0.842	4.468

Existing TOI(s)	Period (days)	Radius (R_Earth)
TOI 1471.01	20.773	3.918
TOI 1471.02	683.328	3.432

Table 3.34: TIC 306263608 stellar and TOI parameters.

On our first attempt to run the search stage, SHERLOCK was matching the three transits of TOI 1471.01 together with the two transits of our candidate, with a period of about 10 days. By looking at the depth and shape of the transits, it appeared clearly that they belonged to two distinct candidates. We thus masked the transits of TOI 1471.01, as illustrated in figure 3.36, in order to investigate further our candidate. The parameters finally obtained are listed in table 3.35.

The vetting plots show two clear transits similar in depth and in shape, with no momentum dumps, no background variation, no flux variation in other pixels and no centroid shift (see figure 3.38).

The main difficulty with this candidate is to estimate its period. Only two transits were observed, and they are in sectors separated by more than 600 days. For the moment, the period attributed to this planetary candidate in the ExoFOP data base is thus the time difference between the two transits: 683.32817 ± 00042d, corresponding to the maximum possible period.

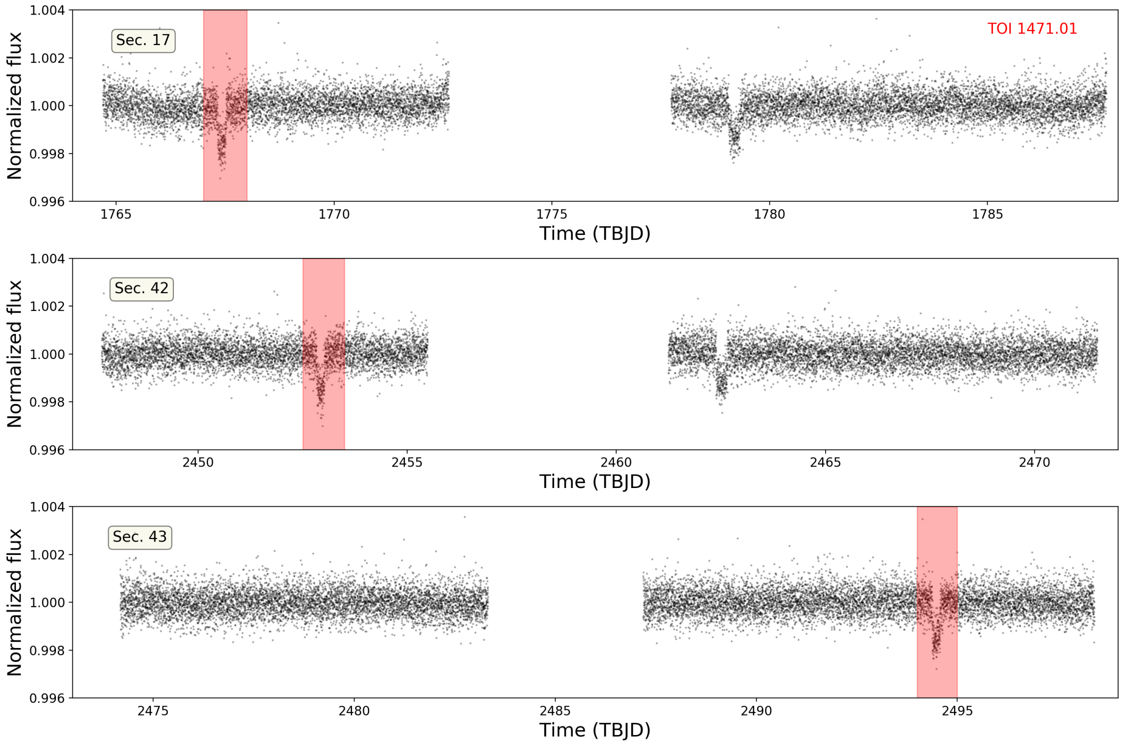

Figure 3.36: TIC 306263608 initial masks.

Win_size.	Period	Per_err	N.Tran	Duration	T0	Depth	SNR	SDE
0.5	22.0425	0.00410	2	162.70	1779.20	0.658	34.70	15.14

FAP	Border_score	Planet radius	R_p/R_s	Semi-major axis	Habitability zone
0.000080	1.00	2.70600	0.02279	0.15415	I

Table 3.35: TIC 306263608 candidate parameters.

By looking at the lightcurve in figure 3.36, we can roughly constrain the minimum period possible for the candidate. Using sector 42 and sector 43 which follow each other, we can say that the minimum period possible is about 21 days, corresponding to the case where a transit occurs in the middle of sector 43, where there is no data available. If the period was shorter than this limit, we would see at least one additional transit in the lightcurve.

However, with only two transits separated by such a long duration, there are several potential period aliases close to this minimum possible period. This can be seen in the SDE plot of figure 3.37 where we see other high peaks close to the blue line (selected period), corresponding to these potential period aliases.

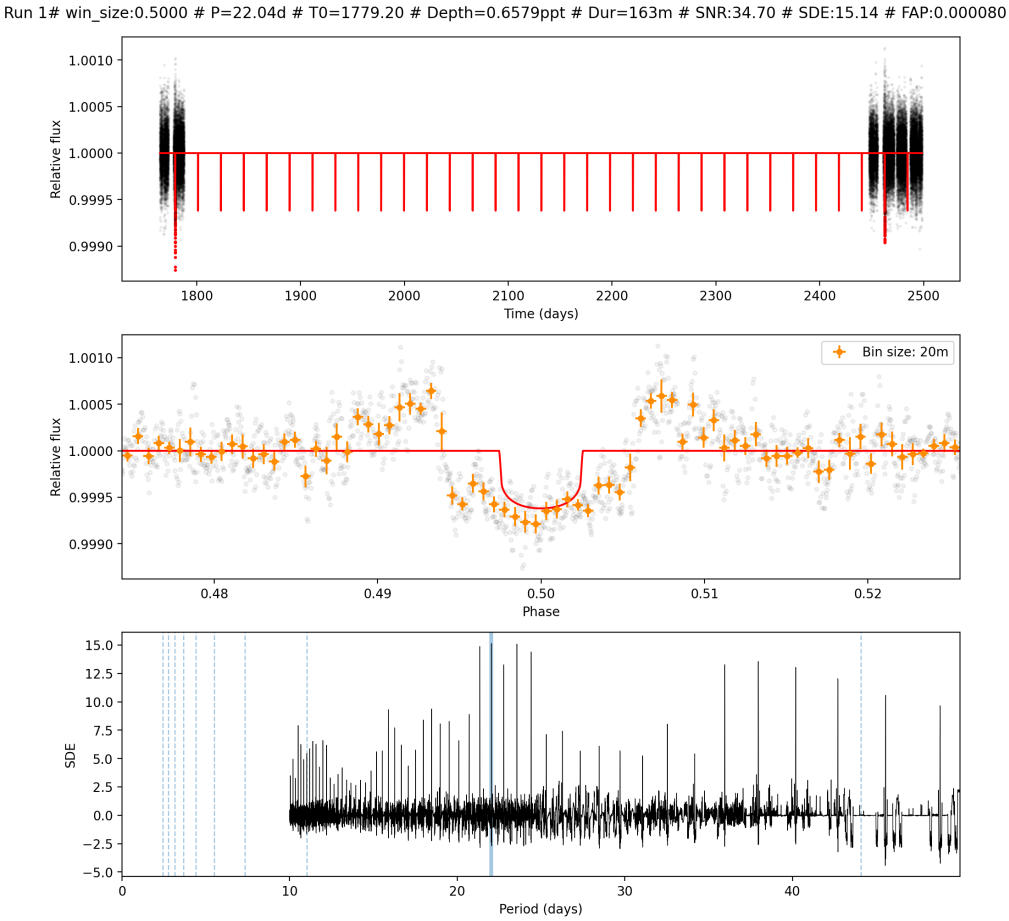

Figure 3.37: TIC 306263608 run 1 win_size 0.5

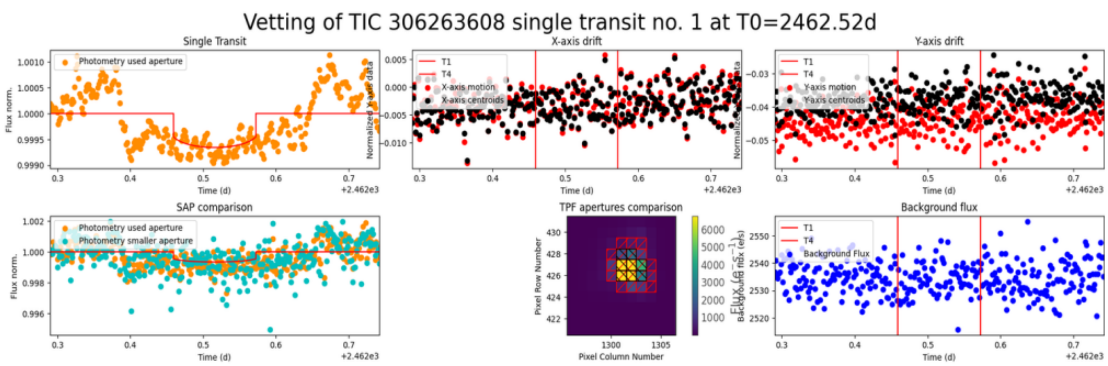

Figure 3.38: TIC 30626308 vetting plots of the second transit.

Following the same logic than previously, the next possible range of period starts at about 37 days, corresponding to the situation where a transit occurs just after the end of sector 43.

The results of the statistical validation are listed in table 3.36. We have a good FPP value but a NFPP that is a bit too high to place the candidate in the "likely planet zone". However, with the previous results and the fact that this candidate is now a TOI, there is not much doubt that it is a real detection.

Scenario	FPP	NFPP	TP	PTP	DTP
Probability	0.03326	0.00374	0.71439	0.14553	0.10682

Table 3.36: TIC 306263608 FPP, NFPP and three most probable scenarios.

To solve the true period of this candidate among the possible aliases, we would need further observations to get at least a third transit. This star is not planned to be reobserved with TESS. However, a third transit could be recovered by observing the target with CHEOPS during specific transit windows corresponding to the period aliases.

Discussing this possibility with some members of the CHEOPS team, we found out that they had actually also detected this planet candidate independently in the TESS data. Targeted follow-up observations of some of the possible period aliases with CHEOPS then revealed an orbital period of more than 50 days (private communication with Hugh Osborn), making this planet a very interesting one (Osborn et al. in prep.). The planet candidate that we detected completely independently with SHERLOCK was thus a real transit detection.

Chapter 4

Conclusion

During this work, we searched in TESS data for new transit-like signals in systems with already at least one transiting planet candidate. This goal was successfully achieved using SHERLOCK. Indeed, we were able to retrieve the already known TOI(s), identify new interesting signals in some systems, and perform a vetting and a statistical validation when the signal looked promising enough. Out of the target list of 100 candidates that we established, 20 looked promising enough after the search stage to perform a vetting and a statistical validation. Finally, 11 candidates were presented in this master thesis.

For 7 of them, the values obtained from the statistical validation fulfill the requirements to be in the "likely planet zone" (FPP < 0.5 and NFPP $< 10^{-3}$). We were able to improve the FPP value for 3 candidates, using the fact that if one planet in the system is already confirmed we can use the FPP2 value instead of the FPP (which was the case for TIC 180695581 and TIC 10837041), and using contrast curves for TIC 14440192. In this conclusion, we can thus present the final validation graph (figure 4.1), taking into account those improvements. With these refined values, we find that 3 candidates are statistically validated (FPP < 0.015 and NFPP $< 10^{-3}$).

For 4 targets, the proposed candidate turned out to be a real detection, also found by other teams, that we recovered independently with about the same period. This is a great result, showing that SHERLOCK is working as expected and is a convenient and reliable tool to find new planets. Note that 3 of the real detections (TIC 357501308, TIC 368435330 and TIC 306263608) do not meet the conditions to be in the "likely planet zone". It is therefore important to not only rely on this criterion, but to consider it together with the results of the search stage and of the vetting, in order to have a global overview of the candidate. Conversely, the statistical validation can tag a candidate as a validated planet when in fact, it is due to systematics, variability non well corrected, etc. Therefore, the community has to be careful when using the statistical validation, which can be very useful combined with more methods, but is risky when used alone.

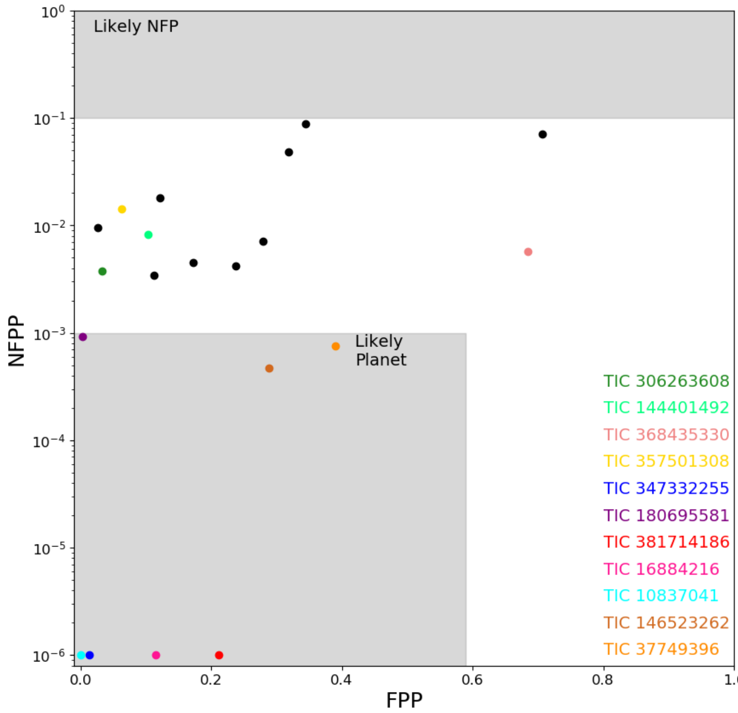

Figure 4.1: Improved FPP and NFPP values of the 20 most promising candidates

The fact that 4 of our candidates are indeed real detections is encouraging for the other promising candidates presented in this work. The 2 most promising candidates to us from the 11 presented are the following:

- TIC 10837041. With a confirmed planet that allowed us to statistically validate this candidate, this is one of the most promising candidate presented. Both transits look convincing, but the main question still to address for this candidate is to determine if the two transit-like events are produced by the same planet or not.
- TIC 16884216. For this candidate, the first transit looks real. But the second transit is less promising. We thus need to see if the first transit could be associated with another transit-like event.

Defining the goals of this work in the introduction, we wrote that we wanted to perform follow-up observations with CHEOPS for the most promising candidates, which was not done. The candidates that were the most suitable for follow-up observations with CHEOPS turned out to be found by other teams, and observations with CHEOPS are already scheduled for them. For our two most promising candidates (TIC 10837041 and TIC 16884216), we can not provide ephemerides precise enough to schedule an observation, since for the first one it could be two different planets, and for the other one, only one transit is really convincing. Thus, we can not determine precisely the period to use. The other candidates did not look promising enough to us to perform such follow-up observations and it would be better to wait for new TESS data release to confirm, or not, the relevance of these candidates.

The upcoming and recently released data from TESS are thus of particular interest for us, to pursue the work undertaken in this master thesis.

Bibliography

[1] Alibert, Y., Mousis, O., Mordasini, C., Benz, W., 2005. New Jupiter and Saturn formation models meet observations. ApJ 626, L57–L60. https://doi.org/10.1086/431325

[2] Becker, J.C., Vanderburg, A., Adams, F.C., Rappaport, S.A., Schwengeler, H.M., 2015. WASP-47: A Hot Jupiter System with Two Additional Planets Discovered by K2. ApJ 812, L18. https://doi.org/10.1088/2041-8205/812/2/L18

[3] Benz, W., Broeg, C., Fortier, A., Rando, N., Beck, T., Beck, M., Queloz, D., Ehrenreich, D., Maxted, P.F.L., Isaak, K.G., Billot, N., Alibert, Y., Alonso, R., António, C., Asquier, J., Bandy, T., Bárczy, T., Barrado, D., Barros, S.C.C., Baumjohann, W., ... Wolter, D., 2021. The CHEOPS mission. Exp Astron 51, 109–151. https://doi.org/10.1007/s10686-020-09679-4

[4] Cameron, A.C., 2016. Extrasolar Planetary Transits, in: Bozza, V., Mancini, L., Sozzetti, A. (Eds.), Methods of Detecting Exoplanets, Astrophysics and Space Science Library. Springer International Publishing, Cham, pp. 89–131. https://doi.org/10.1007/978-3-319-27458-4_2

[5] Delrez, L., Ehrenreich, D., Alibert, Y., Bonfanti, A., Borsato, L., Fossati, L., Hooton, M.J., Hoyer, S., Pozuelos, F.J., Salmon, S., Sulis, S., Wilson, T.G., Adibekyan, V., Bourrier, V., Brandeker, A., Charnoz, S., Deline, A., Guterman, P., Haldemann, J., ... Walton, N.A., 2021. Transit detection of the long-period volatile-rich super-Earth ν^2 Lupi d with $CHEOPS$. Nat Astron 5, 775–787. https://doi.org/10.1038/s41550-021-01381-5

[6] Dorn, C., Mosegaard, K., Grimm, S.L., Alibert, Y., 2018. Interior characterization in multi-planetary systems: TRAPPIST-1. ApJ 865, 20. https://doi.org/10.3847/1538-4357/aad95d

[7] Dumusque, X., Turner, O., Dorn, C., Eastman, J.D., Allart, R., Adibekyan, V., Sousa, S., Santos, N.C., Mordasini, C., Bourrier, V., Bouchy, F., Coffinet, A., Davies, M.D., Diaz, R.F., Fausnaugh, M.M., Glidden, A., Guerrero, N., Henze, C.E., Jenkins, J.M., ... Winn, J.N., 2019. Hot, rocky and warm, puffy super-Earths orbiting TOI-402 (HD 15337). A&A 627, A43. https://doi.org/10.1051/0004-6361/201935457

[8] Giacalone, S., Dressing, C.D., Hedges, C., Kostov, V.B., Collins, K.A., Jensen, E.L.N., Yahalomi, D.A., Bieryla, A., Ciardi, D.R., Howell, S.B., Lillo-Box, J., Barkaoui, K.,

Winters, J.G., Matthews, E., Livingston, J.H., Quinn, S.N., Safonov, B.S., Cadieux, C., Furlan, E., ... Zou, Y., 2022. Validation of 13 Hot and Potentially Terrestrial TESS Planets. arXiv:2201.12661 [astro-ph]. https://doi.org/10.3847/1538-3881/ac4334

[9] Giacalone, S., Dressing, C.D., Jensen, E.L.N., Collins, K.A., Ricker, G.R., Vanderspek, R., Seager, S., Winn, J.N., Jenkins, J.M., Barclay, T., Barkaoui, K., Cadieux, C., Charbonneau, D., Collins, K.I., Conti, D.M., Doyon, R., Evans, P., Ghachoui, M., Gillon, M., ... Waite, I.A., 2021. Vetting of 384 TESS Objects of Interest with TRICERATOPS and Statistical Validation of 12 Planet Candidates. AJ 161, 24. https://doi.org/10.3847/1538-3881/abc6af

[10] Günther, M.N., Zhan, Z., Seager, S., Rimmer, P.B., Ranjan, S., Stassun, K.G., Oelkers, R.J., Daylan, T., Newton, E., Kristiansen, M.H., Olah, K., Gillen, E., Rappaport, S., Ricker, G.R., Latham, D.W., Winn, J.N., Jenkins, J.M., Glidden, A., Fausnaugh, M., ... Ting, E.B., 2020. Stellar Flares from the First Tess Data Release: Exploring a New Sample of M-dwarfs. AJ 159, 60. https://doi.org/10.3847/1538-3881/ab5d3a

[11] Hedges, C., Hughes, A., Giacalone, S., Zhou, G., David, T.J., Becker, J., Vanderburg, A., Rodriguez, J.E., Atherton, S., Quinn, S., Dressing, C.D., Bieryla, A., Fetherolf, T., Price-whelan, A., Bedell, M., Latham, D.W., Ricker, G., Vanderspek, R.K., Seager, S., ... Stassun, K.G., 2021. TOI-2076 and TOI-1807: Two young, comoving planetary systems within 50 pc identified by TESS that are ideal candidates for further follow-up. AJ 162, 54. https://doi.org/10.3847/1538-3881/ac06cd

[12] Hippke, M., David, T.J., Mulders, G.D., Heller, R., 2019. Wotan: Comprehensive time-series de-trending in Python. AJ 158, 143. https://doi.org/10.3847/1538-3881/ab3984

[13] Hippke, M., Heller, R., 2019. Transit Least Squares: Optimized transit detection algorithm to search for periodic transits of small planets. A&A 623, A39. https://doi.org/10.1051/0004-6361/201834672

[14] Hord, B.J., Colón, K.D., Kostov, V., Galgano, B., Ricker, G.R., Vanderspek, R., Seager, S., Winn, J.N., Jenkins, J.M., Barclay, T., Caldwell, D.A., Essack, Z., Fausnaugh, M., Guerrero, N.M., Wohler, B., 2021. A Uniform Search for Nearby Planetary Companions to Hot Jupiters in TESS Data Reveals Hot Jupiters are Still Lonely. AJ 162, 263. https://doi.org/10.3847/1538-3881/ac2602

[15] Huang, C.X., Burt, J., Vanderburg, A., Günther, M.N., Shporer, A., Dittmann, J.A., Winn, J.N., Wittenmyer, R., Sha, L., Kane, S.R., Ricker, G.R., Vanderspek, R.K., Latham, D.W., Seager, S., Jenkins, J.M., Caldwell, D.A., Collins, K.A., Guerrero, N., Smith, J.C., ... Rodriguez, J.E., 2018. TESS Discovery of a Transiting Super-Earth in the π Mensae System. ApJ 868, L39. https://doi.org/10.3847/2041-8213/aaef91

[16] Jenkins, J.M., Twicken, J.D., McCauliff, S., Campbell, J., Sanderfer, D., Lung, D., Mansouri-Samani, M., Girouard, F., Tenenbaum, P., Klaus, T., Smith, J.C., Caldwell, D.A.,

Chacon, A.D., Henze, C., Heiges, C., Latham, D.W., Morgan, E., Swade, D., Rinehart, S., Vanderspek, R., 2016. The TESS science processing operations center, in: Chiozzi, G., Guzman, J.C. (Eds.), . Presented at the SPIE Astronomical Telescopes + Instrumentation, Edinburgh, United Kingdom, p. 99133E. https://doi.org/10.1117/12.2233418

[17] Kopparapu, R. kumar, Ramirez, R., Kasting, J.F., Eymet, V., Robinson, T.D., Mahadevan, S., Terrien, R.C., Domagal-Goldman, S., Meadows, V., Deshpande, R., 2013. Habitable Zones Around Main-Sequence Stars: New Estimates. ApJ 765, 131. https://doi.org/10.1088/0004-637X/765/2/131

[18] Kostov, V.B., Schlieder, J.E., Barclay, T., Quintana, E.V., Colon, K.D., Brande, J., Collins, K.A., Feinstein, A.D., Hadden, S., Kane, S.R., Kreidberg, L., Kruse, E., Lam, C., Matthews, E., Montet, B.T., Pozuelos, F.J., Stassun, K.G., Winters, J.G., Ricker, G., ... Youngblood, A., 2019. The L 98-59 System: Three Transiting, Terrestrial-Sized Planets Orbiting a Nearby M-dwarf. AJ 158, 32. https://doi.org/10.3847/1538-3881/ab2459

[19] Leleu, A., Alibert, Y., Hara, N.C., Hooton, M.J., Wilson, T.G., Robutel, P., Delisle, J.-B., Laskar, J., Hoyer, S., Lovis, C., Bryant, E.M., Ducrot, E., Cabrera, J., Delrez, L., Acton, J.S., Adibekyan, V., Allart, R., Prieto, C.A., Alonso, R., ... Osorio, M.R.Z., 2021. Six transiting planets and a chain of Laplace resonances in TOI-178. A&A 649, A26. https://doi.org/10.1051/0004-6361/202039767

[20] Lendl, M., Csizmadia, S., Deline, A., Fossati, L., Kitzmann, D., Heng, K., Hoyer, S., Salmon, S., Benz, W., Broeg, C., Ehrenreich, D., Fortier, A., Queloz, D., Bonfanti, A., Brandeker, A., Cameron, A.C., Delrez, L., Muñoz, A.G., Hooton, M.J., ... Wolter, D., 2020. The hot dayside and asymmetric transit of WASP-189b seen by CHEOPS. A&A 643, A94. https://doi.org/10.1051/0004-6361/202038677

[21] Lissauer, J.J., Marcy, G.W., Rowe, J.F., Bryson, S.T., Adams, E., Buchhave, L.A., Ciardi, D.R., Cochran, W.D., Fabrycky, D.C., Ford, E.B., Fressin, F., Geary, J., Gilliland, R.L., Holman, M.J., Howell, S.B., Jenkins, J.M., Kinemuchi, K., Koch, D.G., Morehead, R.C., ... Twicken, J.D., 2012. Almost All of Kepler's Multiple Planet Candidates are Planets. https://doi.org/10.1088/0004-637X/750/2/112

[22] Mustill, A.J., Davies, M.B., Johansen, A., 2015. The destruction of inner planetary systems during high-eccentricity migration of gas giants. ApJ 808, 14. https://doi.org/10.1088/0004-637X/808/1/14

[23] Pedersen, M.G., Chowdhury, S., Johnston, C., Bowman, D., Aerts, C., Handler, G., De Cat, P., Neiner, C., David-Uraz, A., Buzasi, D., Tkachenko, A., Simon-Diaz, S., Moravveji, E., Sikora, J., Mirouh, G.M., Lovekin, C.C., Cantiello, M., Daszynska-Daszkiewicz, J., Pigulski, A., ... Ricker, G.R., 2019. Diverse Variability of O and B Stars Revealed from 2-minute Cadence Light Curves in Sectors 1 and 2 of the TESS Mission: Selection of an Asteroseismic Sample. ApJ 872, L9. https://doi.org/10.3847/2041-8213/ab01e1

[24] Pozuelos, F.J., Suárez, J.C., de Elía, G.C., Berdiñas, Z.M., Bonfanti, A., Dugaro, A., Gillon, M., Jehin, E., Günther, M.N., Van Grootel, V., Garcia, L.J., Thuillier, A., Delrez, L., Rodón, J.R., 2020. GJ 273: on the formation, dynamical evolution, and habitability of a planetary system hosted by an M dwarf at 3.75 parsec. A&A 641, A23. https://doi.org/10.1051/0004-6361/202038047

[25] Ricker, G.R., Winn, J.N., Vanderspek, R., Latham, D.W., Bakos, G.Á., Bean, J.L., Berta-Thompson, Z.K., Brown, T.M., Buchhave, L., Butler, N.R., Butler, R.P., Chaplin, W.J., Charbonneau, D., Christensen-Dalsgaard, J., Clampin, M., Deming, D., Doty, J., De Lee, N., Dressing, C., ... Villasenor, J., 2014. Transiting Exoplanet Survey Satellite. J. Astron. Telesc. Instrum. Syst 1. https://doi.org/10.1117/1.JATIS.1.1.014003

[26] Savitzky, Abraham., Golay, M.J.E., 1964. Smoothing and Differentiation of Data by Simplified Least Squares Procedures. Anal. Chem. 36, 1627–1639. https://doi.org/10.1021/ac60214a047

[27] Stassun, K.G., Oelkers, R.J., Paegert, M., Torres, G., Pepper, J., De Lee, N., Collins, K., Latham, D.W., Muirhead, P.S., Chittidi, J., Rojas-Ayala, B., Fleming, S.W., Rose, M.E., Tenenbaum, P., Ting, E.B., Kane, S.R., Barclay, T., Bean, J.L., Brassuer, C.E., ... Winn, J.N., 2019. The Revised TESS Input Catalog and Candidate Target List. https://doi.org/10.3847/1538-3881/ab3467

[28] Twicken, J.D., Catanzarite, J.H., Clarke, B.D., Girouard, F., Jenkins, J.M., Klaus, T.C., Li, J., McCauliff, S.D., Seader, S.E., Tenenbaum, P., Wohler, B., Bryson, S.T., Burke, C.J., Caldwell, D.A., Haas, M.R., Henze, C.E., Sanderfer, D.T., 2018. Kepler Data Validation I – Architecture, Diagnostic Tests, and Data Products for Vetting Transiting Planet Candidates. https://doi.org/10.1088/1538-3873/aab694

[29] Vanderspek, R., Huang, C.X., Vanderburg, A., Ricker, G.R., Latham, D.W., Seager, S., Winn, J.N., Jenkins, J.M., Burt, J., Dittmann, J., Newton, E., Quinn, S.N., Shporer, A., Charbonneau, D., Irwin, J., Ment, K., Winters, J.G., Collins, K.A., Evans, P., ... Villaseñor, J.N.S., 2019. TESS Discovery of an ultra-short-period planet around the nearby M dwarf LHS 3844. ApJ 871, L24. https://doi.org/10.3847/2041-8213/aafb7a

[30] Winn, J.N., 2014. Transits and Occultations. arXiv: Earth and Planetary Astrophysics.

[31] Mikulski Archive for Space Telescopes (MAST) Portal [WWW Document], n.d. URL https://mast.stsci.edu/portal/Mashup/Clients/Mast/Portal.html (accessed 5.30.22).

[32] NASA Exoplanet Archive [WWW Document], n.d. URL https://exoplanetarchive.ipac.caltech.edu/index.html (accessed 5.1.22).

[33] TESS Observations [WWW Document], n.d. URL https://tess.mit.edu/observations/ (accessed 5.3.22).

[34] NExScI, 2022. Exoplanet Follow-up Observing Program Web Service. https://doi.org/10.26134/EXOFOP5

[35] URL https://github.com/franpoz/SHERLOCK (accessed 5.30.22)

Appendix A

Target list

1	TIC 352413427	26	TIC 27491137	51	TIC 4897275	76	TIC 10837041
2	TIC 58542531	27	TIC 31374837	52	TIC 368435330	77	TIC 248387177
3	TIC 29054413	28	TIC 119292328	53	TIC 8967242	78	TIC 251094370
4	TIC 62483237	29	TIC 34077285	54	TIC 180695581	79	TIC 274194927
5	TIC 357501308	30	TIC 356158613	55	TIC 27194429	80	TIC 318753380
6	TIC 23814735	31	TIC 251848941	56	TIC 381714186	81	TIC 142868621
7	TIC 21832928	32	TIC 63898957	57	TIC 63698669	82	TIC 154618248
8	TIC 91555165	33	TIC 178155732	58	TIC 183985250	83	TIC 311271011
9	TIC 420051632	34	TIC 122617317	59	TIC 242083025	84	TIC 146523262
10	TIC 117799904	35	TIC 377064495	60	TIC 47617161	85	TIC 71013298
11	TIC 449197831	36	TIC 178819686	61	TIC 142378043	86	TIC 262435954
12	TIC 192790476	37	TIC 164767175	62	TIC 243187830	87	TIC 167661160
13	TIC 149845414	38	TIC 101011575	63	TIC 16884216	88	TIC 369376388
14	TIC 421951960	39	TIC 257605131	64	TIC 105840719	89	TIC 179985715
15	TIC 65416038	40	TIC 349488688	65	TIC 39200363	90	TIC 123664207
16	TIC 422914082	41	TIC 138126035	66	TIC 75878355	91	TIC 263179590
17	TIC 334632624	42	TIC 114018671	67	TIC 287256467	92	TIC 224225541
18	TIC 178170828	43	TIC 23434737	68	TIC 271478281	93	TIC 37749396
19	TIC 50618703	44	TIC 406672232	69	TIC 212253390	94	TIC 42054565
20	TIC 77253676	45	TIC 13499636	70	TIC 425561347	95	TIC 203377303
21	TIC 453211454	46	TIC 119700084	71	TIC 310231275	96	TIC 443666343
22	TIC 306263608	47	TIC 418959198	72	TIC 20203297	97	TIC 152563846
23	TIC 130181866	48	TIC 16920150	73	TIC 82452140	98	TIC 300579472
24	TIC 144401492	49	TIC 67418624	74	TIC 70420766	99	TIC 176780257
25	TIC 347332255	50	TIC 257241363	75	TIC 9006668	100	TIC 117979455

Table A.1: Target list in order of their analysis.

Appendix B

Additional plots and tables

B.1 TIC 347332255

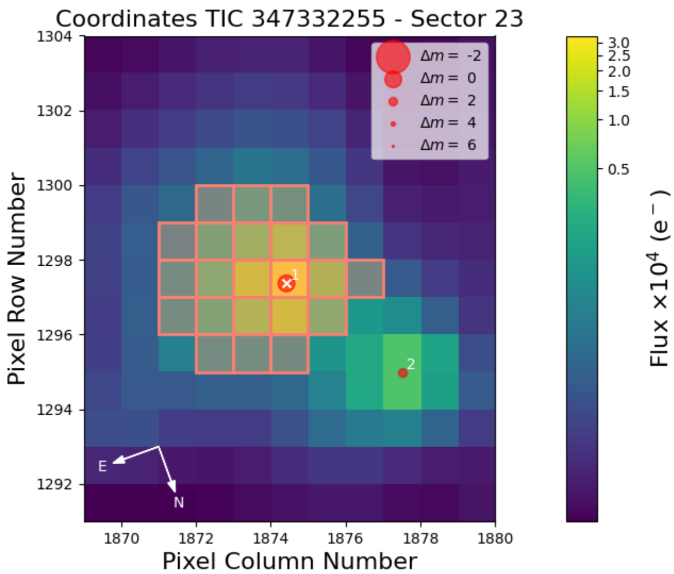

Figure B.1: TIC 347332255 Field of view plot sector 23.

Win_size	Period	P_err	N.Tra	Depth	T. dur	T0	SNR	SDE	FAP	Border	Match. OI	Harm.	Plan. rad	Rp/Rs	*a*	Habit.
PDCSAP	21.88439	0.069612	2	0.661	221.7	1906.0044	23.547	10.032	8.0032e-05	1.00	nan	-	2.08108	0.02429	0.13813	I
0.2000	nan	-13.455983	nan	nan	nan	0.0000	nan	0.000	nan	0.00	nan	-	nan	nan	nan	-
0.3000	10.00026	0.012257	4	0.297	177.9	1906.0436	13.442	45.869	8.0032e-05	1.00	nan	-	1.39438	0.01532	0.08195	I
0.4000	21.88439	0.046408	2	0.460	166.3	1906.0223	15.549	44.093	8.0032e-05	1.00	nan	-	1.73642	0.01980	0.13813	I
0.5000	21.88439	0.058051	2	0.542	201.4	1906.0111	19.305	22.435	8.0032e-05	1.00	nan	-	1.88371	0.02144	0.13813	I
0.6000	21.88439	0.069612	2	0.612	201.4	1906.0111	21.593	14.685	8.0032e-05	1.00	nan	-	2.00186	0.02314	0.13813	I
0.7000	21.88439	0.069612	2	0.663	201.4	1906.0111	23.051	13.104	8.0032e-05	1.00	nan	-	2.08375	0.02414	0.13813	I
0.8000	21.88439	0.069612	2	0.688	201.4	1906.0111	23.684	12.468	8.0032e-05	1.00	nan	-	2.12216	0.02470	0.13813	I
0.9000	21.88439	0.069612	2	0.668	221.7	1906.0044	23.694	12.005	8.0032e-05	1.00	nan	-	2.09074	0.02444	0.13813	I
1.0000	21.88439	0.069612	2	0.677	221.7	1906.0044	23.954	11.681	8.0032e-05	1.00	nan	-	2.10587	0.02471	0.13813	I
1.1000	21.88439	0.069612	2	0.698	221.7	1906.0044	24.631	10.887	8.0032e-05	1.00	nan	-	2.13858	0.02512	0.13813	I

Elected signal with QUORUM algorithm from 9 VOTES –> NAME: 2 Period:21.8843862502699 CORR_SDE: 82.57338386717291 SNR: 15.548749340974062 SDE: 44.092583618393306 FAP: 8.0032e-05 BORDER_SCORE: 1.0 Proposed selection with BASIC algorithm was –> NAME: 1 Period:10.000260063509034 SNR: 13.442209225257285 New best signal is good enough to keep searching. Going to the next run.

Table B.1: TIC 347332255 report log run 1.

Detrend no.	Period	Per_err	Duration	T0	Depth	SNR	SDE	FAP	Border_score	Matching OI	Harmonic	Plan. rad	Rp/Rs	*a*	Habit.
9	12.9937	0.11320	222.17	1935.98	0.935	49.48	10.18	0.000080	1.00	nan	4*this(0)	2.61298	0.02993	0.10502	I
0	5.4806	0.07130	146.84	1935.46	0.445	19.95	7.41	0.004482	1.00	TOI 1835.01	-	1.80168	0.02222	0.05907	I
0	7.4533	0.01803	233.36	1937.56	0.408	15.43	41.99	0.000080	0.50	nan	-	1.72523	0.02056	0.07250	I
2	7.8639	0.06447	142.80	1932.69	0.314	18.82	7.87	0.002081	1.00	nan	-	1.51440	0.01648	0.07514	I
2	13.9998	0.05550	174.62	1933.54	0.167	11.59	6.71	0.015286	1.00	nan	-	1.10560	0.01578	0.11037	I

Table B.2: TIC 347332255 candidates report log.

B.2 TIC 180695581

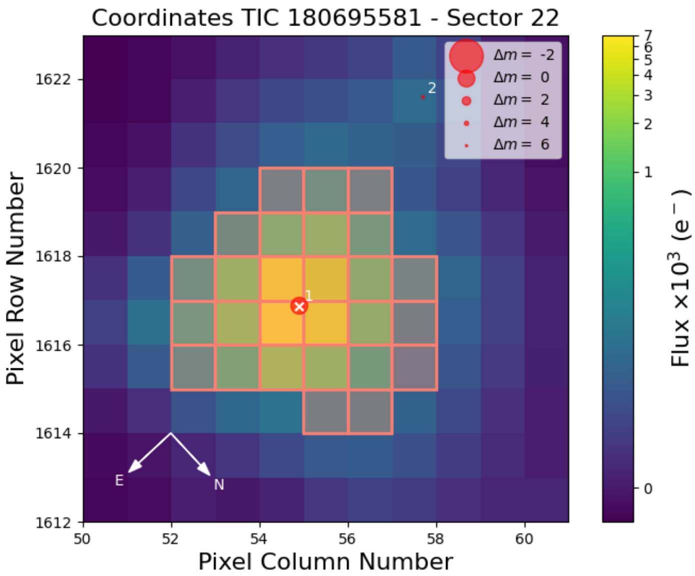

Figure B.2: TIC 180695581 Field of view plot sector 22.

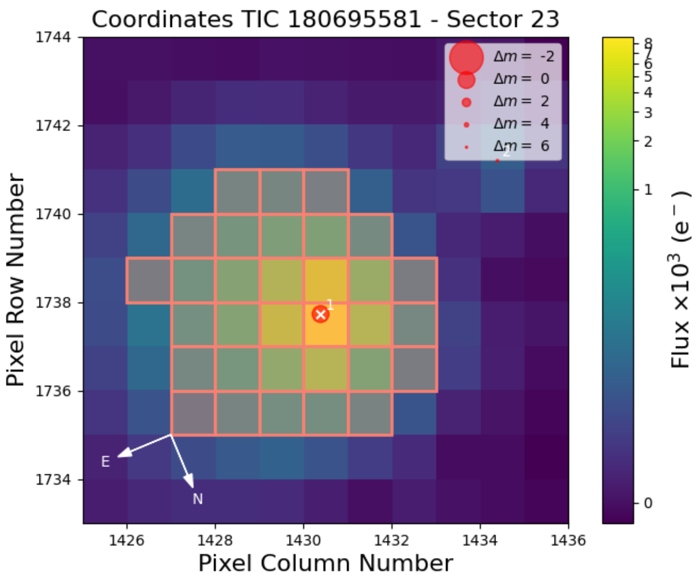

Figure B.3: TIC 180695581 Field of view plot sector 23.

Win_size	Period	P_err	N.Tra	Depth	T. dur	T0	SNR	SDE	FAP	Border	Match. OI	Harm.	Plan. rad	Rp/Rs	*a*	Habit.
PDCSAP	3.24865	0.027726	4	0.583	76.9	1932.7566	18.778	8.762	0.000240096	1.00	nan	-	2.06237	0.02188	0.04168	I
0.2000	6.99302	0.027538	4	0.154	122.2	1933.5493	12.250	5.817	0.076990796	1.00	nan	-	1.06084	0.01342	0.06948	I
0.3000	12.96852	0.100235	2	0.516	183.2	1936.0166	31.142	7.214	0.006562625	1.00	nan	4*this(0)	1.94053	0.02285	0.10488	I
0.4000	12.96852	0.087819	2	0.719	202.5	1936.0154	42.755	8.277	0.001040416	1.00	nan	4*this(0)	2.29131	0.02692	0.10488	I
0.5000	12.96852	0.100495	2	0.866	202.5	1936.0154	48.497	8.708	0.000240096	1.00	nan	4*this(0)	2.51390	0.02961	0.10488	I
0.6000	12.96852	0.100495	2	0.928	202.5	1936.0064	49.767	9.111	8.0032e-05	1.00	nan	4*this(0)	2.60242	0.03040	0.10488	I
0.7000	12.96852	0.100495	2	0.916	221.7	1936.0087	50.494	9.543	8.0032e-05	1.00	nan	4*this(0)	2.58665	0.02971	0.10488	I
0.8000	12.99367	0.100495	2	0.927	222.2	1935.9804	50.269	9.951	8.0032e-05	1.00	nan	4*this(0)	2.60086	0.02987	0.10502	I
0.9000	12.99367	0.100495	2	0.934	222.2	1935.9804	50.052	10.086	8.0032e-05	1.00	nan	4*this(0)	2.61200	0.02993	0.10502	I
1.0000	12.99367	0.113203	2	0.935	222.2	1935.9804	49.478	10.176	8.0032e-05	1.00	nan	4*this(0)	2.61298	0.02993	0.10502	I
1.1000	12.99367	0.113203	2	0.931	222.2	1935.9804	48.699	10.112	8.0032e-05	1.00	nan	4*this(0)	2.60662	0.02988	0.10502	I

Elected signal with QUORUM algorithm from 9 VOTES –> NAME: 8 Period:12.993670772694191 CORR_SDE: 19.056874093170215 SNR: 49.47755847685227 SDE: 10.176000729362736 FAP: 8.0032e-05 BORDER_SCORE: 1.0 Proposed selection with BASIC algorithm was –> NAME: 8 Period:12.993670772694191 SNR: 49.47755847685227 New best signal is good enough to keep searching. Going to the next run.

Table B.3: TIC 180695581 report log run 2.

Detrend no.	Period	Per_err	Duration	T0	Depth	SNR	SDE	FAP	Border_score	Matching OI	Harmonic	Plan. rad	Rp/Rs	*a*	Habit.
1	0.5495	0.00060	64.53	1900.44	0.219	31.72	30.81	0.000080	0.96	TOI 1807.01	-	1.19830	0.01324	0.01184	I
3	21.8844	0.04641	166.29	1906.02	0.460	15.55	44.09	0.000080	1.00	nan	-	1.73642	0.01980	0.13813	I
5	19.4984	0.03984	274.97	1916.52	0.406	14.14	57.24	0.000080	1.00	nan	-	1.63019	0.01876	0.12790	I
0	21.8844	0.08116	181.39	1900.37	0.518	16.93	30.24	0.000080	1.00	nan	1*SOI2	1.84094	0.02105	0.13813	I

Table B.4: TIC 180695581 candidates report log.

B.3 TIC 381714186

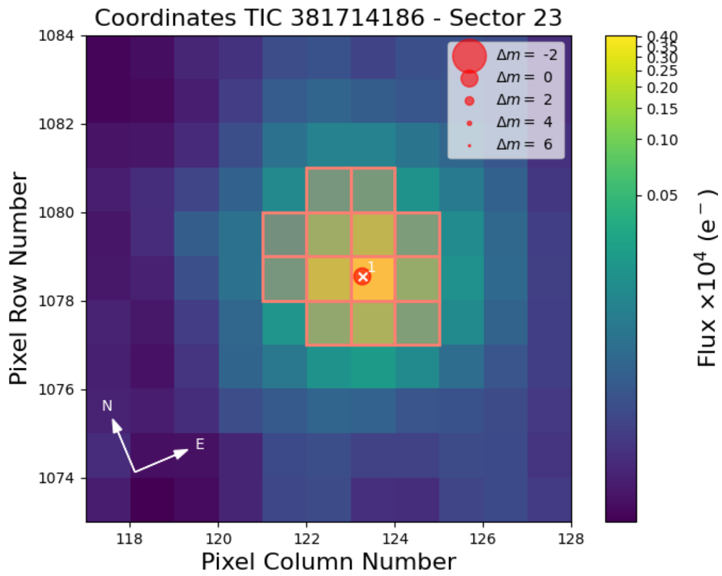

Figure B.4: TIC 381714186 Field of view plot sector 23.

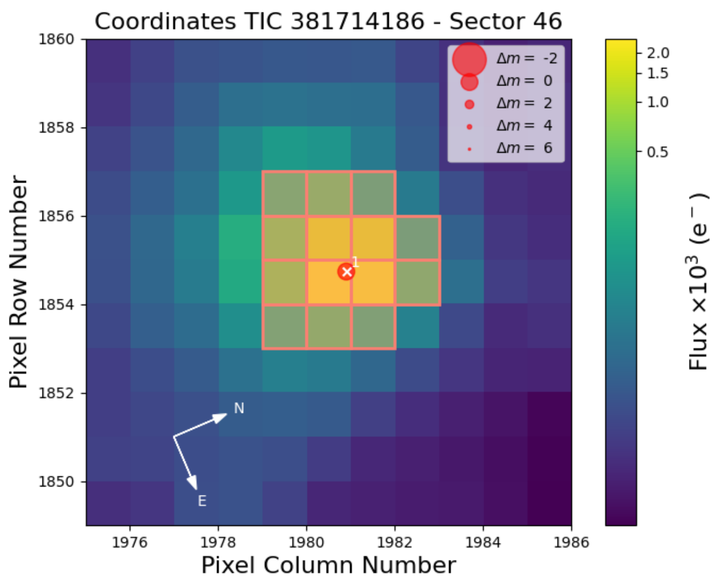

Figure B.5: TIC 381714186 Field of view plot sector 46.

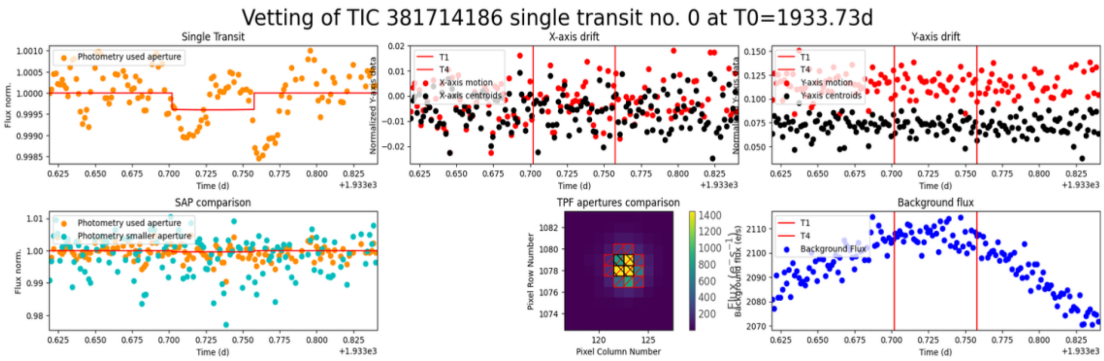

Figure B.6: TIC 381714186 vetting plots of the first transit.

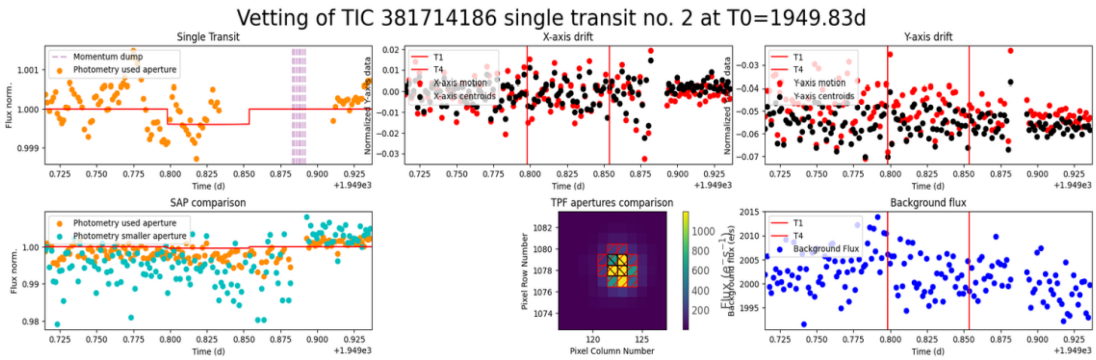

Figure B.7: TIC 381714186 vetting plots of the third transit.

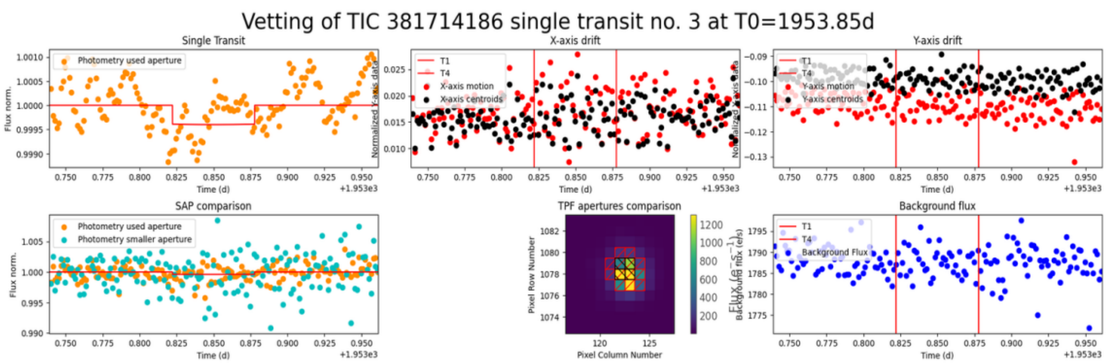

Figure B.8: TIC 381714186 vetting plots of the fourth transit.

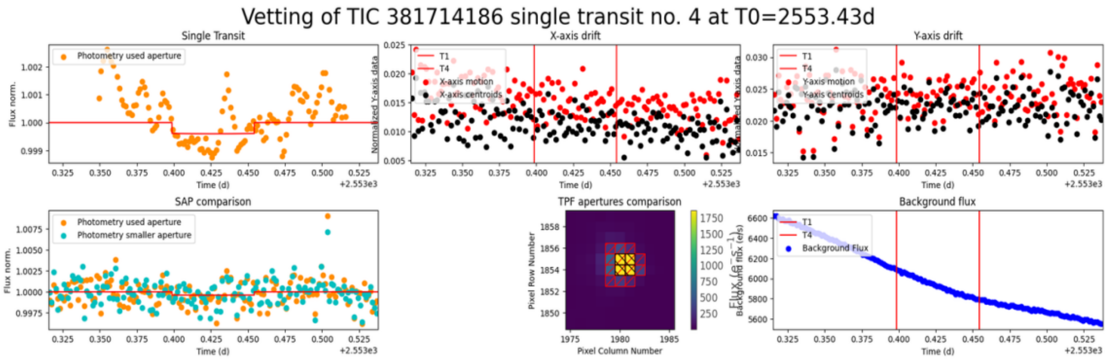

Figure B.9: TIC 381714186 vetting plots of the fifth transit.

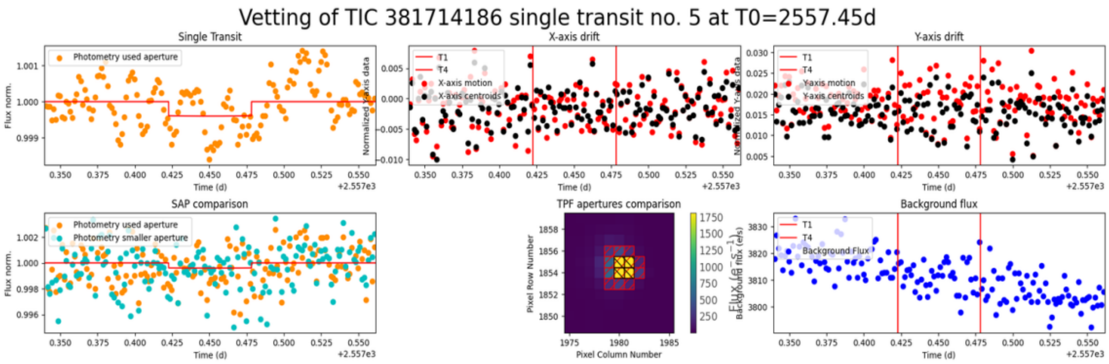

Figure B.10: TIC 381714186 vetting plots of the sixth transit.

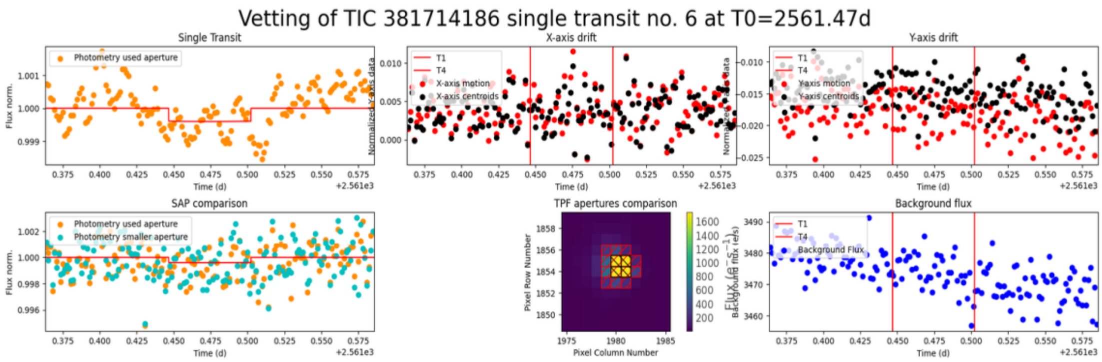

Figure B.11: TIC 381714186 vetting plots of the seventh transit.

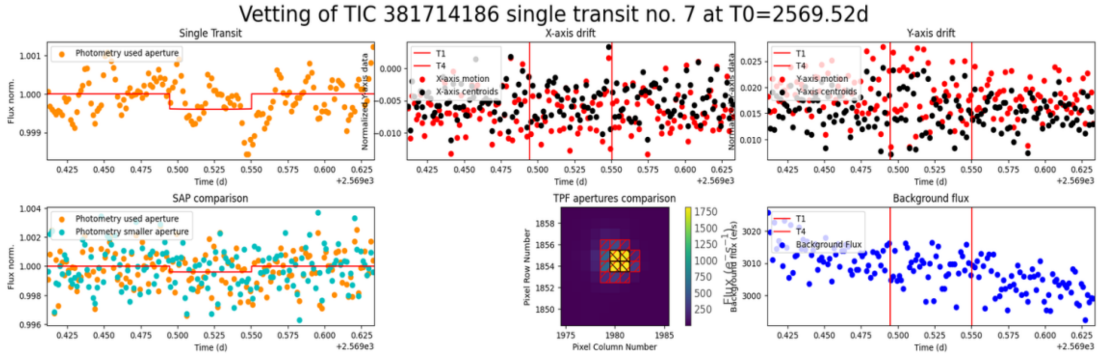

Figure B.12: TIC 381714186 vetting plots of the eight transit.

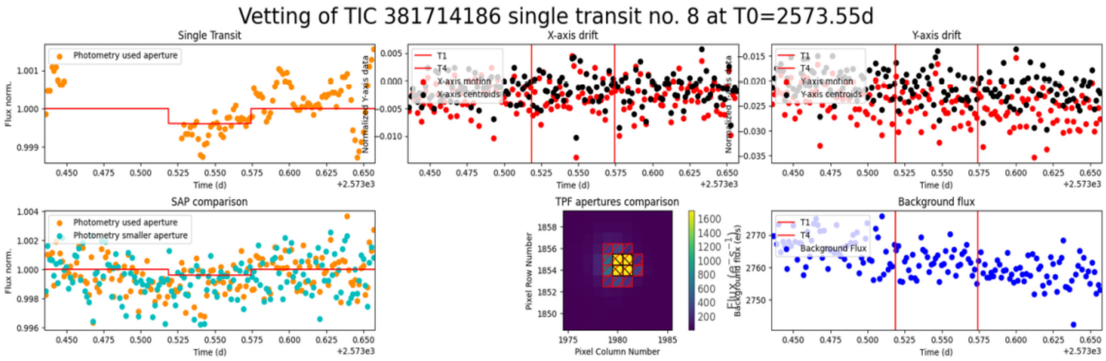

Figure B.13: TIC 381714186 vetting plots of the ninth transit.

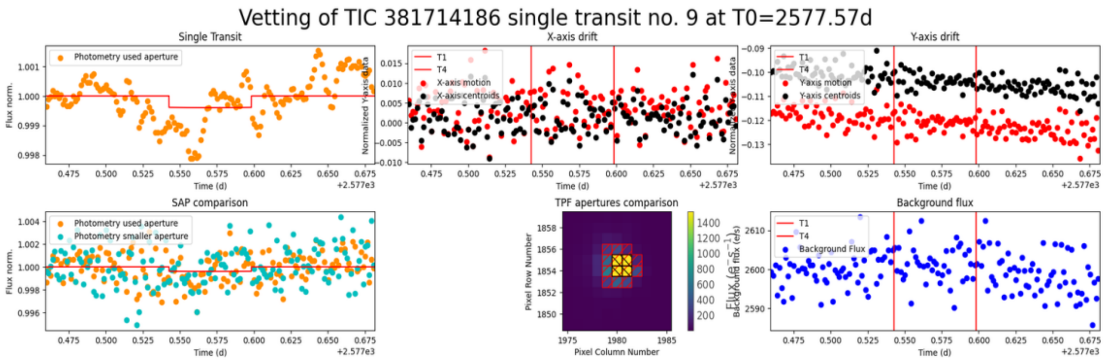

Figure B.14: TIC 381714186 vetting plots of the tenth transit.

Win_size	Period	P_err	N.Tra	Depth	T. dur	T0	SNR	SDE	FAP	Border	Match. OI	Harm.	Plan. rad	Rp/Rs	*a*	Habit.
PDCSAP	25.68501	0.016621	1	2.042	218.0	1955.5760	18.837	13.985	8.0032e-05	1.00	nan	-	4.18480	0.04501	0.16685	I
0.2000	4.02400	0.000324	10	0.400	80.1	1933.7299	14.082	22.489	8.0032e-05	1.00	nan	-	1.85129	0.01564	0.04849	I
0.3000	4.02400	0.000324	10	0.503	80.1	1933.7299	17.369	21.812	8.0032e-05	1.00	nan	-	2.07793	0.01840	0.04849	I
0.4000	4.02400	0.000432	10	0.538	80.1	1933.7299	18.421	21.779	8.0032e-05	1.00	nan	-	2.14828	0.01925	0.04849	I
0.5000	4.02400	0.000432	10	0.547	80.1	1933.7299	18.694	21.283	8.0032e-05	1.00	nan	-	2.16539	0.01957	0.04849	I
0.6000	4.02400	0.000432	10	0.566	80.1	1933.7299	19.283	19.187	8.0032e-05	1.00	nan	-	2.20378	0.01999	0.04849	I
0.7000	4.02400	0.000432	10	0.606	80.1	1933.7352	20.827	17.946	8.0032e-05	1.00	nan	-	2.28030	0.02045	0.04849	I
0.8000	4.02400	0.000432	10	0.600	80.1	1933.7299	20.270	17.709	8.0032e-05	1.00	nan	-	2.26925	0.02085	0.04849	I
0.9000	4.02400	0.000432	10	0.620	80.1	1933.7299	20.878	17.026	8.0032e-05	1.00	nan	-	2.30684	0.02125	0.04849	I
1.0000	4.02400	0.000432	10	0.633	80.1	1933.7299	21.225	16.003	8.0032e-05	1.00	nan	-	2.32937	0.02160	0.04849	I
1.1000	4.02400	0.000432	10	0.665	80.1	1933.7352	22.520	15.661	8.0032e-05	1.00	nan	-	2.38819	0.02185	0.04849	I

Elected signal with QUORUM algorithm from 10 VOTES –> NAME: 0 Period:4.02400358171477 CORR_SDE: 44.56812822731864 SNR: 14.08200346480217 SDE: 22.488505068830506 FAP: 8.0032e-05 BORDER_SCORE: 1.0 Proposed selection with BASIC algorithm was –> NAME: 0 Period:4.02400358171477 SNR: 14.08200346480217 New best signal is good enough to keep searching. Going to the next run.

Table B.5: TIC 381714186 report log run 2.

Detrend no.	Period	Per_err	Duration	T0	Depth	SNR	SDE	FAP	Border_score	Matching OI	Harmonic	Plan. rad	Rp/Rs	*a*	Habit.
1	1.4238	0.00011	55.46	1931.36	0.486	24.11	43.03	0.000080	1.00	TOI 1839.01	-	2.04230	0.01881	0.02426	I
1	4.0240	0.00032	80.09	1933.73	0.400	14.08	22.49	0.000080	1.00	nan	-	1.85129	0.01564	0.04849	I
1	14.1687	0.00116	130.19	1934.64	0.278	7.82	123.26	0.000080	1.00	nan	-	1.54419	0.01765	0.11223	I
6	9.3365	0.00066	125.41	1931.33	0.284	8.39	290.70	0.000080	1.00	nan	-	1.56023	0.01751	0.08498	I

Table B.6: TIC 381714186 candidates report log.

B.4 TIC 16884216

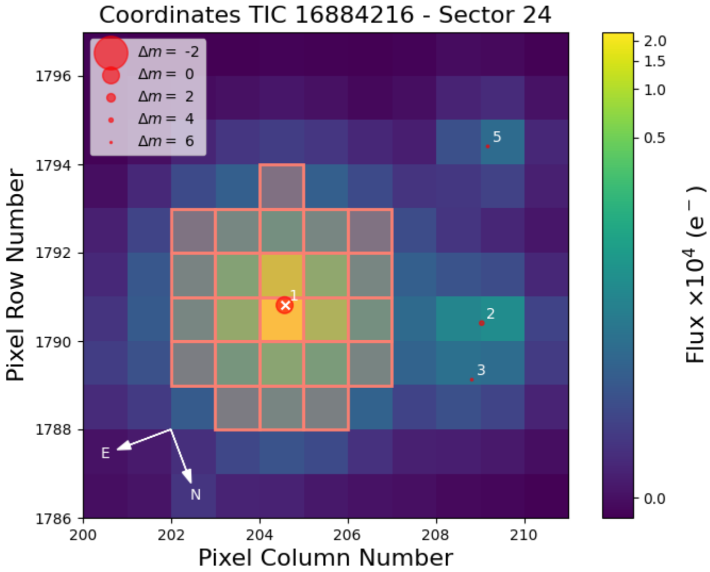

Figure B.15: TIC 16884216 Field of view plot sector 24.

Win_size	Period	P_err	N.Tra	Depth	T. dur	T0	SNR	SDE	FAP	Border	Match. OI	Harm.	Plan. rad	Rp/Rs	*a*	Habit.
PDCSAP	7.37199	0.096729	2	0.512	214.5	1960.6184	22.072	9.294	8.0032e-05	1.00	nan	-	1.71977	0.02176	0.06952	I
0.2000	0.74412	0.001671	28	0.149	8.5	1956.3195	6.411	6.601	0.018807523	1.00	nan	-	0.92615	0.00829	0.01507	I
0.3000	15.80644	0.070264	2	0.255	163.9	1965.9676	12.522	6.184	0.040736295	1.00	nan	-	1.21454	0.01558	0.11559	I
0.4000	15.77840	0.084217	2	0.245	219.2	1965.9840	13.789	8.479	0.000640256	1.00	nan	-	1.18972	0.01707	0.11545	I
0.5000	15.77840	0.070097	2	0.277	219.2	1965.9840	15.500	10.769	8.0032e-05	1.00	nan	-	1.26497	0.01802	0.11545	I
0.6000	15.77840	0.070097	2	0.297	219.2	1965.9840	16.520	9.084	8.0032e-05	1.00	nan	-	1.31069	0.01852	0.11545	I
0.7000	15.77840	0.070097	2	0.310	219.2	1965.9840	17.133	7.403	0.004481793	1.00	nan	-	1.33866	0.01884	0.11545	I
0.8000	8.77638	0.076719	1	0.330	145.8	1964.1575	10.429	6.688	0.015686275	1.00	nan	-	1.38153	0.01752	0.07809	I
0.9000	8.76358	0.083031	1	0.333	146.4	1964.1975	10.545	6.656	0.016566627	1.00	nan	-	1.38708	0.01756	0.07801	I
1.0000	8.76358	0.083031	1	0.342	146.4	1964.1975	10.779	6.688	0.015846339	1.00	nan	-	1.40574	0.01779	0.07801	I
1.1000	15.77840	0.097905	2	0.351	219.2	1965.9840	19.100	6.756	0.014245698	1.00	nan	-	1.42442	0.01985	0.11545	I

Elected signal with QUORUM algorithm from 6 VOTES –> NAME: 3 Period:15.778403879344825 CORR_SDE: 16.643638463960606 SNR: 15.499634073877573 SDE: 10.769413123739215 FAP: 8.0032e-05 BORDER_SCORE: 1.0 Proposed selection with BASIC algorithm was –> NAME: 3 Period:15.778403879344825 SNR: 15.499634073877573 New best signal is good enough to keep searching. Going to the next run.

Table B.7: TIC 16884216 report log run 2.

Detrend no.	Period	Per_err	Duration	T0	Depth	SNR	SDE	FAP	Border_score	Matching OI	Harmonic	Plan. rad	Rp/Rs	*a*	Habit.
3	11.1921	0.06194	201.73	1964.13	0.315	16.76	6.64	0.017367	1.00	TOI 2023.01	-	1.34991	0.01897	0.09183	I
4	15.7784	0.07010	219.19	1965.98	0.277	15.50	10.77	0.000080	1.00	nan	-	1.26497	0.01802	0.11545	I
3	2.8325	0.00993	35.87	1957.76	0.166	6.58	6.13	0.044098	1.00	nan	0.25*SOI1	0.98018	0.01153	0.03674	I
0	7.3720	0.09172	210.56	1960.64	0.481	20.18	8.47	0.000640	1.00	nan	-	1.66613	0.02147	0.06952	I
1	20.4510	0.03958	117.93	1959.70	0.187	8.03	6.38	0.027771	1.00	nan	-	1.04033	0.01532	0.13725	I

Table B.8: TIC 16884216 candidates report log.

B.5 TIC 10837041

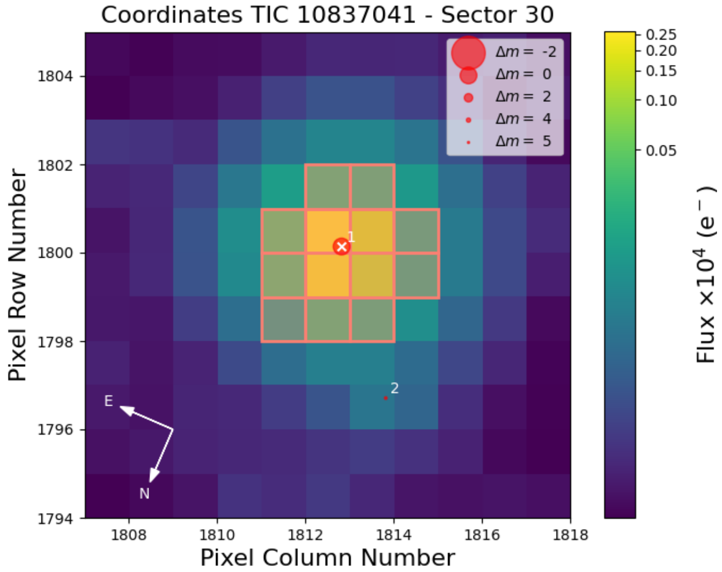

Figure B.16: TIC 10837041 Field of view plot sector 30.

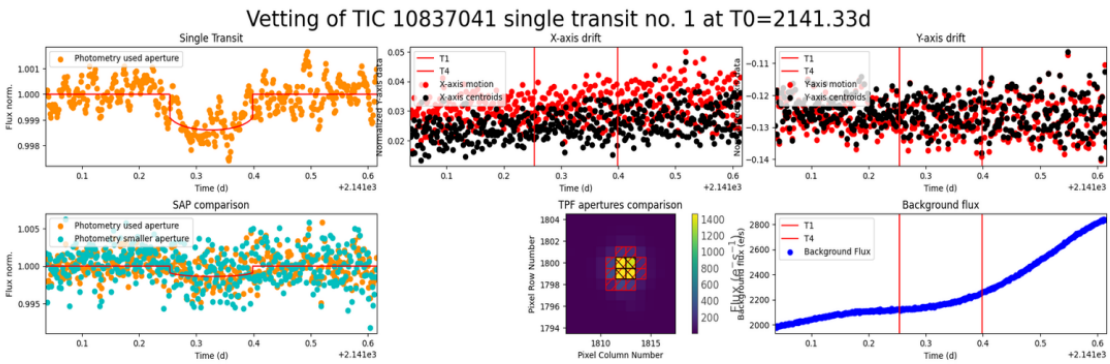

Figure B.17: TIC 10837041 vetting plots of the second transit.

Win_size	Period	P_err	N.Tra	Depth	T. dur	T0	SNR	SDE	FAP	Border	Match. OI	Harm.	Plan. rad	Rp/Rs	*a*	Habit.
PDCSAP	18.75613	0.081920	2	1.391	208.6	2122.5700	31.543	15.269	8.0032e-05	1.00	nan	-	2.96368	0.03713	0.11928	I
0.2000	0.78319	0.001483	28	0.336	78.3	2116.0058	19.298	20.499	8.0032e-05	1.00	TOI 2411.01	-	1.45717	0.01727	0.01436	I
0.3000	0.78319	0.001780	28	0.382	78.3	2116.0058	21.608	15.710	8.0032e-05	1.00	TOI 2411.01	-	1.55294	0.01848	0.01436	I
0.4000	0.78319	0.001780	28	0.522	12.7	2115.9927	11.796	13.217	8.0032e-05	1.00	TOI 2411.01	-	1.81505	0.01902	0.01436	I
0.5000	18.75613	0.081920	2	1.178	208.6	2122.5700	27.157	12.108	8.0032e-05	1.00	nan	-	2.72735	0.03423	0.11928	I
0.6000	18.75613	0.081920	2	1.264	208.6	2122.5700	28.982	12.676	8.0032e-05	1.00	nan	-	2.82437	0.03541	0.11928	I
0.7000	18.75613	0.081920	2	1.313	208.6	2122.5700	30.058	12.771	8.0032e-05	1.00	nan	-	2.87950	0.03609	0.11928	I
0.8000	18.75613	0.081920	2	1.361	208.6	2122.5700	31.066	13.505	8.0032e-05	1.00	nan	-	2.93154	0.03674	0.11928	I
0.9000	18.75613	0.081920	2	1.392	208.6	2122.5700	31.729	13.984	8.0032e-05	1.00	nan	-	2.96484	0.03715	0.11928	I
1.0000	18.75613	0.081920	2	1.400	208.6	2122.5700	31.900	14.165	8.0032e-05	1.00	nan	-	2.97293	0.03726	0.11928	I
1.1000	18.75613	0.081920	2	1.400	208.6	2122.5700	31.929	14.258	8.0032e-05	1.00	nan	-	2.97348	0.03726	0.11928	I

Elected signal with QUORUM algorithm from 8 VOTES –> NAME: PDCSAP_FLUX Period:18.75613453332626 CORR_SDE: 26.929517515217164 SNR: 31.542986523373656 SDE: 15.269314055020043 FAP: 8.0032e-05 BORDER_SCORE: 1.0 Proposed selection with BASIC algorithm was –> NAME: 0 Period:0.7831911951410924 SNR: 19.29841889780203 New best signal is good enough to keep searching. Going to the next run.

Table B.9: TIC 10837041 report log run 1.

Detrend no.	Period	Per_err	Duration	T0	Depth	SNR	SDE	FAP	Border_score	Matching OI	Harmonic	Plan. rad	Rp/Rs	*a*	Habit.
0	18.7561	0.08192	208.65	2122.57	1.391	31.54	15.27	0.000080	1.00	nan	-	2.96368	0.03713	0.11928	I
1	0.7826	0.00148	77.30	2116.01	0.340	19.59	22.66	0.000080	1.00	TOI 2411.01	-	1.46575	0.01720	0.01435	I
10	14.9466	0.09078	212.69	2124.51	0.423	8.35	8.36	0.000800	1.00	nan	2*this(7)	1.63340	0.01970	0.10253	I
9	9.4939	0.04957	212.27	2125.14	0.273	6.84	20.13	0.000080	1.00	nan	0.5*SOI1	1.31209	0.01861	0.07576	I
10	12.2640	0.02325	229.77	2120.84	0.214	5.43	56.85	0.000080	1.00	nan	-	1.16154	0.01750	0.08986	I

Table B.10: TIC 10837041 candidates report log.

B.6 146523262

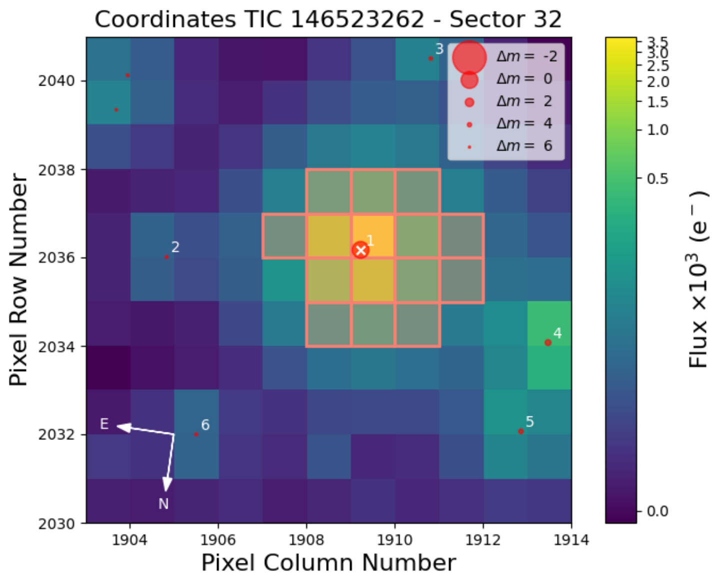

Figure B.18: TIC 146523262 Field of view plot sector 32.

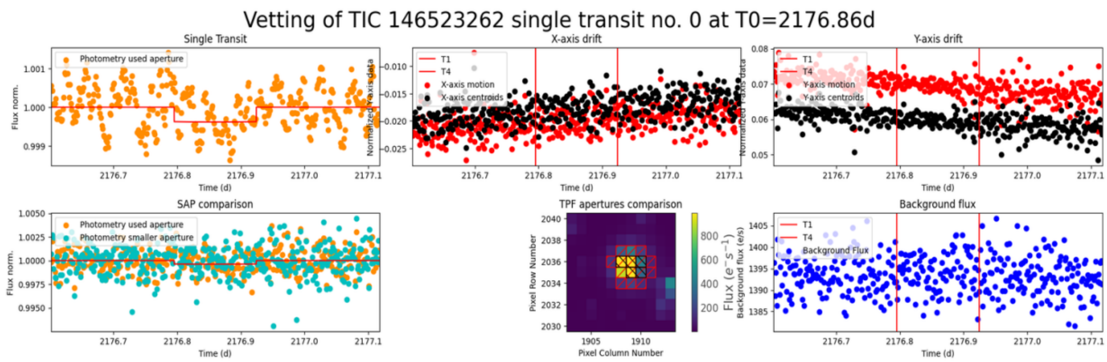

Figure B.19: TIC 146523262 vetting plots of the first transit.

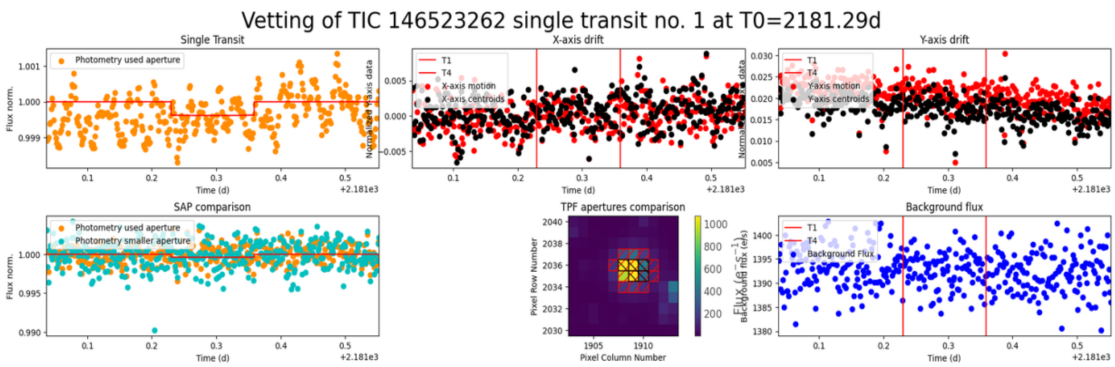

Figure B.20: TIC 146523262 vetting plots of the second transit.

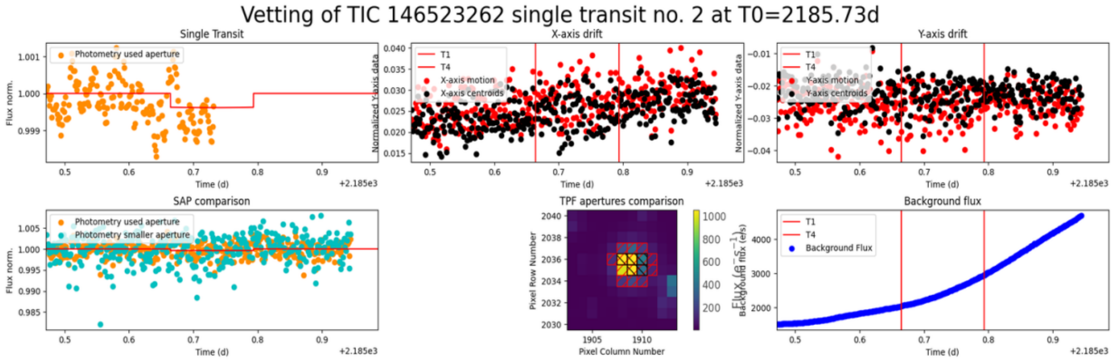

Figure B.21: TIC 146523262 vetting plots of the third transit.

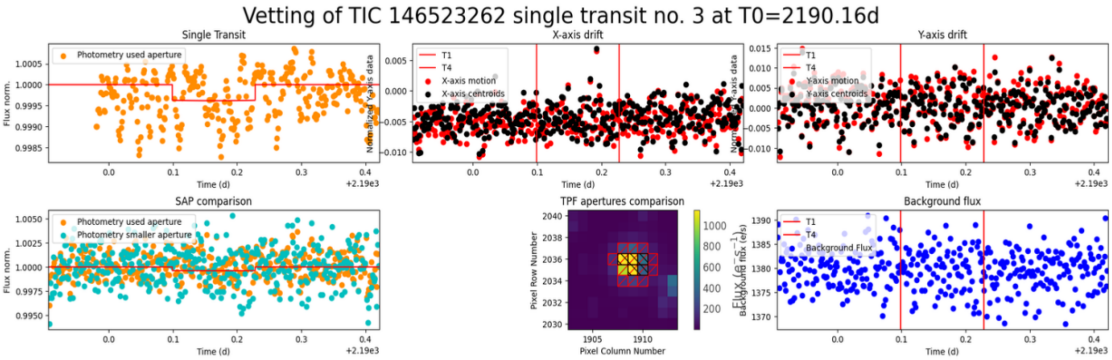

Figure B.22: TIC 146523262 vetting plots of the fourth transit.

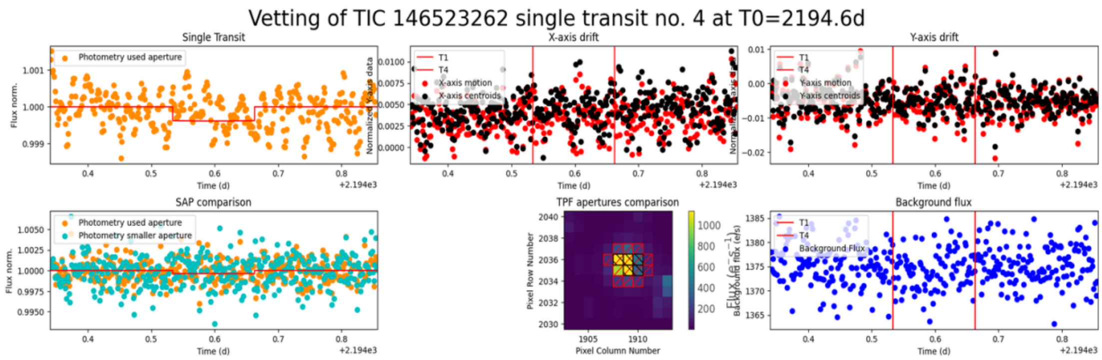

Figure B.23: TIC 146523262 vetting plots of the fifth transit.

Win_size	Period	P_err	N.Tra	Depth	T. dur	T0	SNR	SDE	FAP	Border	Match. OI	Harm.	Plan. rad	Rp/Rs	*a*	Habit.
PDCSAP	4.43465	0.035089	6	0.384	185.8	2176.8598	14.903	9.787	8.0032e-05	0.83	nan	-	2.17332	0.01877	0.06012	I
0.2000	0.77777	0.001247	31	0.163	43.6	2174.3812	8.086	5.153	nan	0.97	nan	-	1.41477	0.00954	0.01884	I
0.3000	0.52023	0.001638	45	0.232	12.5	2174.5560	7.373	4.882	nan	1.00	nan	-	1.68742	0.00922	0.01441	I
0.4000	0.61994	0.002076	37	0.115	29.2	2174.2708	5.145	4.613	nan	0.97	nan	-	1.18733	0.00932	0.01619	I
0.5000	2.93520	0.009163	7	0.201	153.3	2176.8653	8.666	5.675	0.096278511	0.86	nan	-	1.57028	0.01335	0.04566	I
0.6000	2.93520	0.011005	7	0.210	153.3	2176.8653	9.069	6.210	0.038895558	0.86	nan	-	1.60756	0.01373	0.04566	I
0.7000	2.93520	0.011005	7	0.238	71.2	2176.8975	7.030	5.857	0.071628651	0.86	nan	-	1.70951	0.01370	0.04566	I
0.8000	2.19886	0.009967	10	0.249	51.8	2176.3474	7.382	5.845	0.073469388	1.00	nan	0.5*this(0)	1.74766	0.01271	0.03767	I
0.9000	2.19886	0.009967	10	0.256	51.8	2176.3474	7.597	5.996	0.057543017	1.00	nan	0.5*this(0)	1.77468	0.01309	0.03767	I
1.0000	4.43465	0.028709	6	0.287	168.9	2176.8603	10.271	6.538	0.021048419	0.83	nan	-	1.87815	0.01592	0.06012	I
1.1000	4.43465	0.028709	6	0.266	185.8	2176.8598	10.294	7.391	0.004561825	0.83	nan	-	1.80791	0.01514	0.06012	I

Elected signal with QUORUM algorithm from 5 VOTES –> NAME: PDCSAP_FLUX Period:4.43464926512103 CORR_SDE: 11.714434735169966 SNR: 14.90251640826056 SDE: 9.786742943306555 FAP: 8.0032e-05 BORDER_SCORE: 0.8333333333333334 Proposed selection with BASIC algorithm was –> NAME: PDCSAP_FLUX Period:4.43464926512103 SNR: 14.90251640826056 New best signal is good enough to keep searching. Going to the next run.

Table B.11: TIC 146523262 report log run 2.

Detrend no.	Period	Per_err	Duration	T0	Depth	SNR	SDE	FAP	Border_score	Matching OI	Harmonic	Plan. rad	Rp/Rs	*a*	Habit.
2	3.7574	0.01783	148.19	2174.85	0.564	22.06	17.61	0.000080	1.00	TOI 2465.01	-	2.63346	0.02257	0.05384	I
0	4.4346	0.03509	185.81	2176.86	0.384	14.90	9.79	0.000080	0.83	nan	-	2.17332	0.01877	0.06012	I
10	3.1222	0.01193	145.43	2174.83	0.214	9.17	10.83	0.000080	1.00	nan	-	1.62116	0.01436	0.04758	I
7	13.2077	0.05426	220.53	2182.92	0.259	7.14	24.96	0.000080	1.00	nan	-	1.78299	0.01754	0.12446	I
5	7.9570	0.01384	145.15	2175.52	0.166	5.28	48.87	0.000080	1.00	nan	-	1.43026	0.01527	0.08878	I

Table B.12: TIC 146523262 candidates report log.

B.7 TIC 37749396

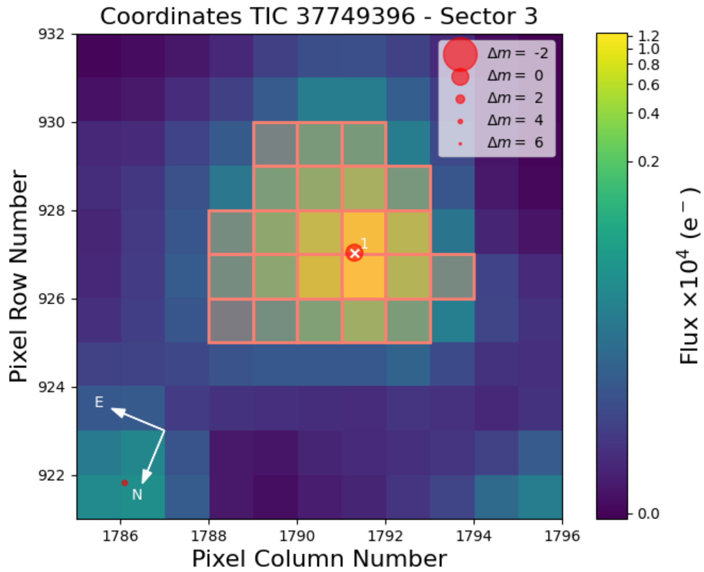

Figure B.24: TIC 37749396 Field of view plot sector 3.

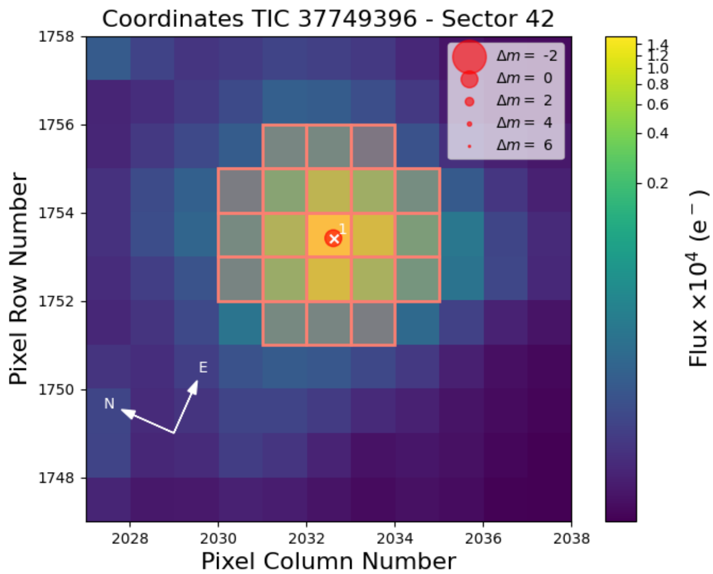

Figure B.25: TIC 37749396 Field of view plot sector 42.

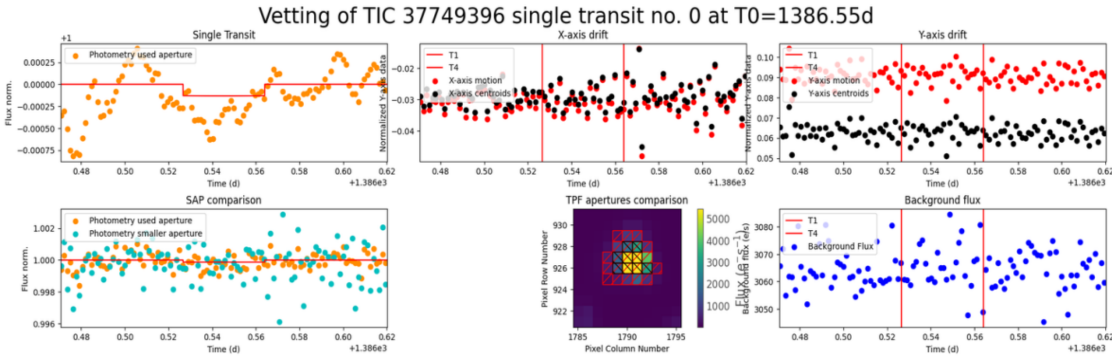

Figure B.26: TIC 37749396 vetting plots of the first transit.

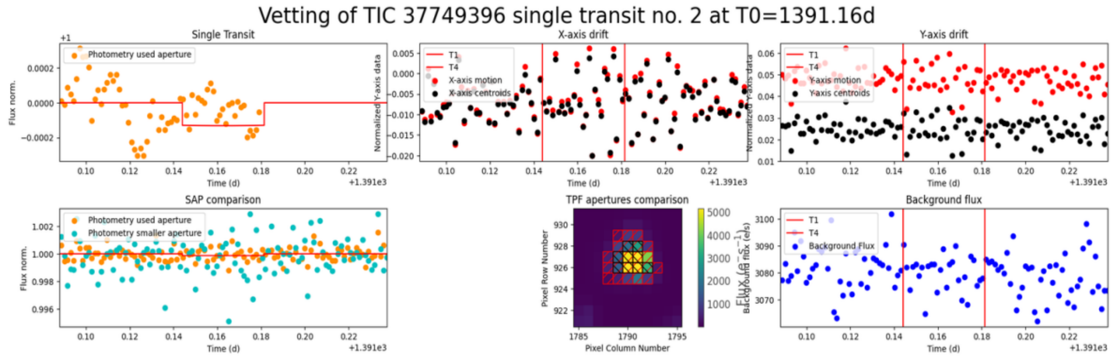

Figure B.27: TIC 37749396 vetting plots of the third transit.

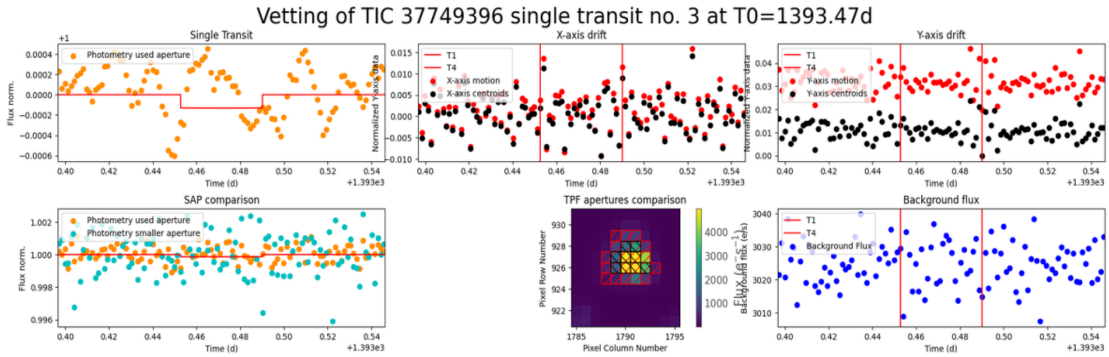

Figure B.28: TIC 37749396 vetting plots of the fourth transit.

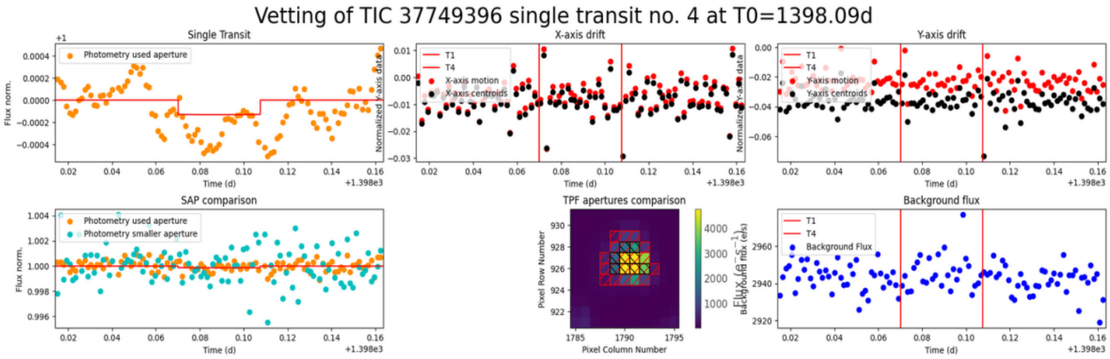

Figure B.29: TIC 37749396 vetting plots of the fifth transit.

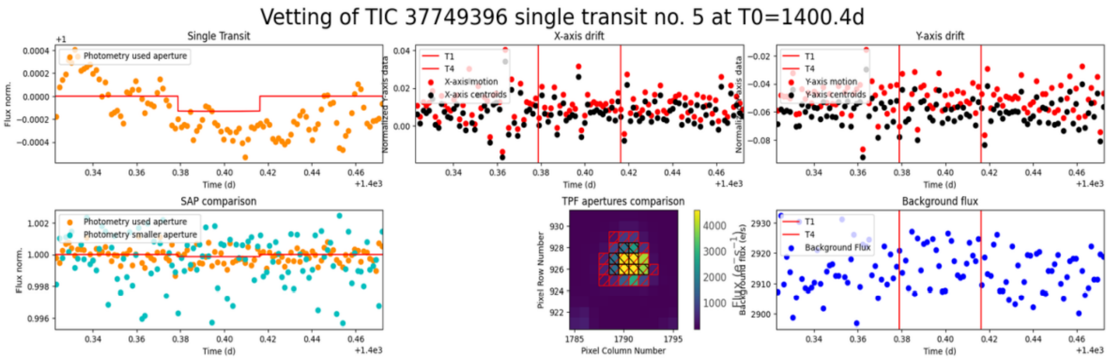

Figure B.30: TIC 37749396 vetting plots of the sixth transit.

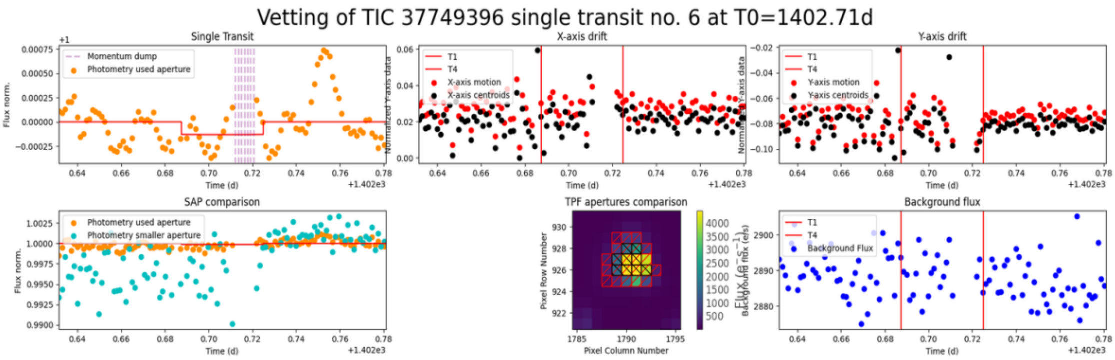

Figure B.31: TIC 37749396 vetting plots of the seventh transit.

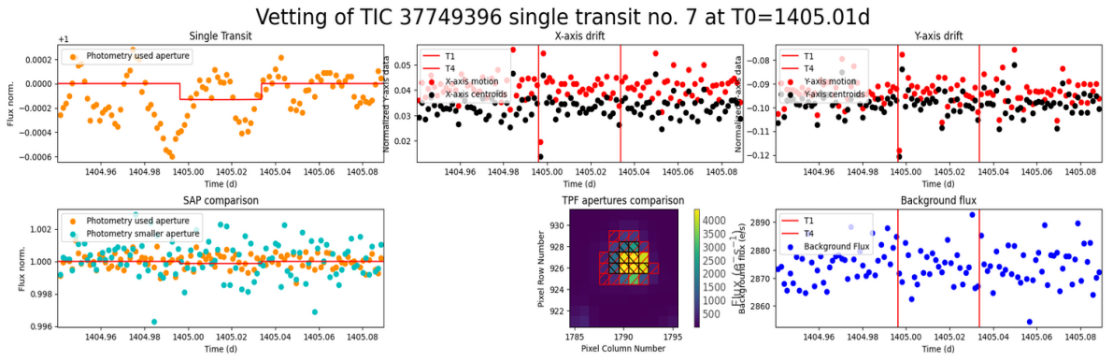

Figure B.32: TIC 37749396 vetting plots of the eighth transit.

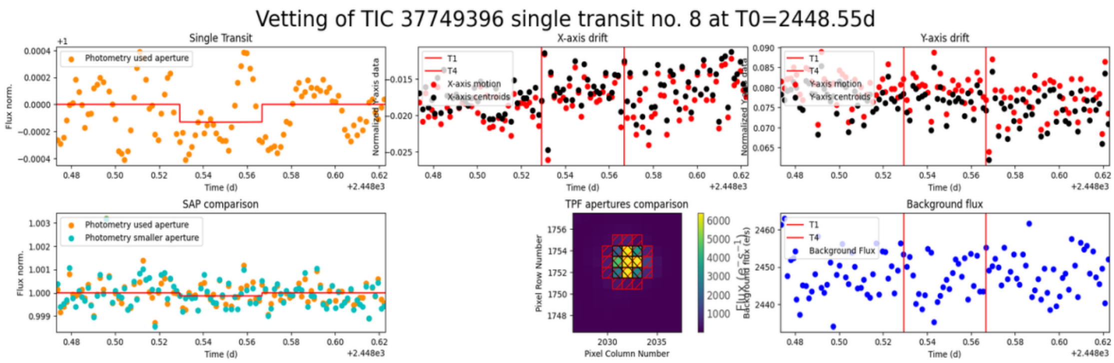

Figure B.33: TIC 37749396 vetting plots of the ninth transit.

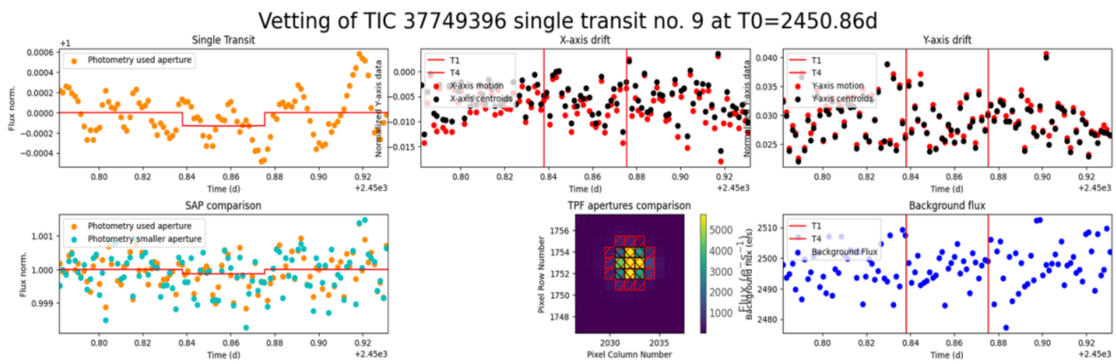

Figure B.34: TIC 37749396 vetting plots of the tenth transit.

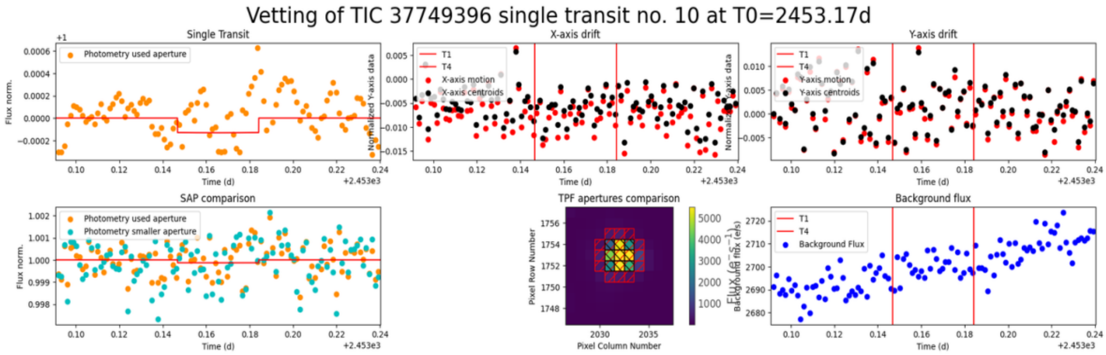

Figure B.35: TIC 37749396 vetting plots of the eleventh transit.

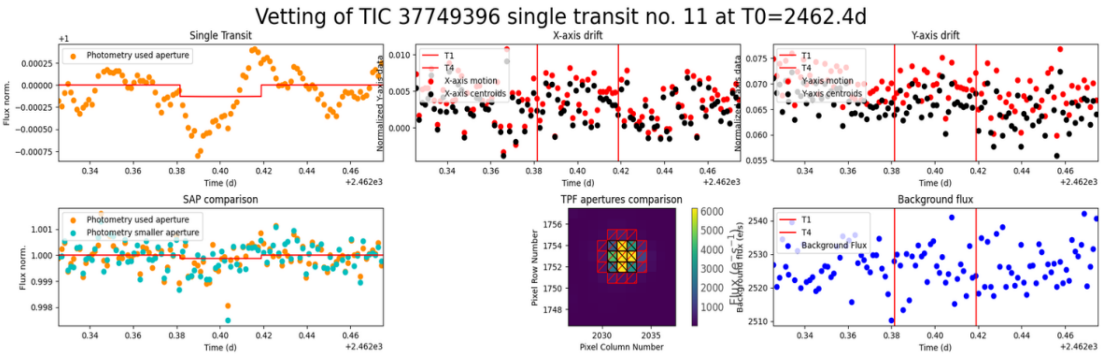

Figure B.36: TIC 37749396 vetting plots of the twelfth transit.

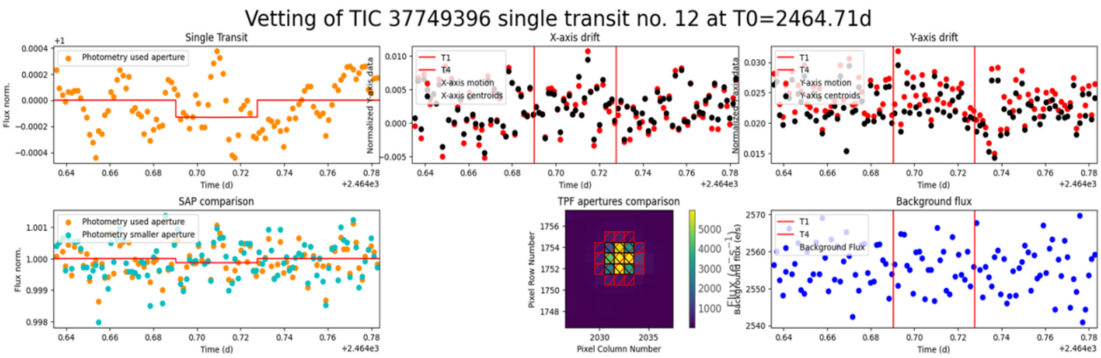

Figure B.37: TIC 37749396 vetting plots of the thirteenth transit.

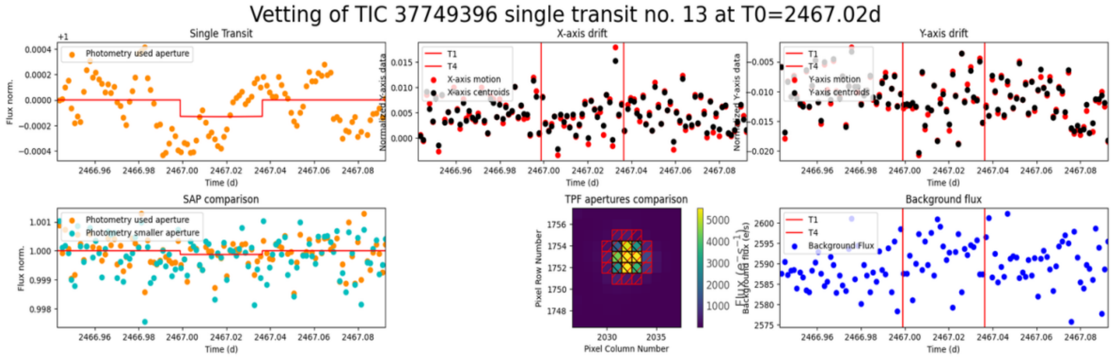

Figure B.38: TIC 37749396 vetting plots of the fourteenth transit.

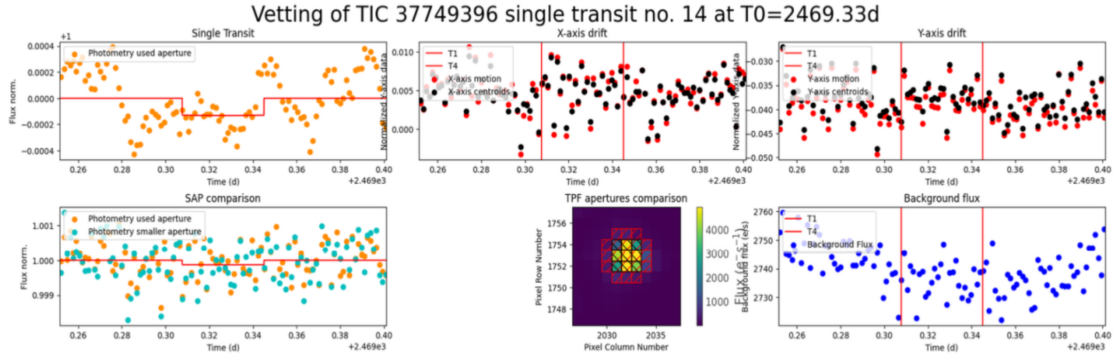

Figure B.39: TIC 37749396 vetting plots of the fifteenth transit.

Win_size	Period	P_err	N.Tra	Depth	T. dur	T0	SNR	SDE	FAP	Border	Match. OI	Harm.	Plan. rad	Rp/Rs	*a*	Habit.
PDCSAP	2.62285	0.000394	9	0.220	28.3	1387.6116	9.348	9.513	8.0032e-05	1.00	nan	0.25*SOI3	1.00106	0.01264	0.03197	I
0.2000	14.29283	0.000581	4	0.162	95.7	1390.4155	10.382	9.929	8.0032e-05	1.00	nan	1*SOI2	0.85990	0.01195	0.09900	I
0.3000	2.30870	0.000077	15	0.113	53.9	1386.5454	10.360	10.294	8.0032e-05	1.00	nan	-	0.71604	0.00988	0.02936	I
0.4000	2.30870	0.000077	15	0.123	53.9	1386.5454	11.211	11.980	8.0032e-05	1.00	nan	-	0.74774	0.01036	0.02936	I
0.5000	2.30870	0.000077	15	0.132	53.9	1386.5454	12.007	12.813	8.0032e-05	1.00	nan	-	0.77568	0.01072	0.02936	I
0.6000	2.30870	0.000102	15	0.129	53.9	1386.5454	11.709	11.208	8.0032e-05	1.00	nan	-	0.76708	0.01063	0.02936	I
0.7000	2.30870	0.000077	15	0.127	53.9	1386.5454	11.464	10.508	8.0032e-05	1.00	nan	-	0.75929	0.01052	0.02936	I
0.8000	2.30870	0.000077	15	0.127	53.9	1386.5454	11.474	10.495	8.0032e-05	1.00	nan	-	0.75941	0.01054	0.02936	I
0.9000	2.30870	0.000077	15	0.129	53.9	1386.5454	11.692	10.752	8.0032e-05	1.00	nan	-	0.76710	0.01066	0.02936	I
1.0000	2.30870	0.000077	15	0.131	53.9	1386.5454	11.904	10.783	8.0032e-05	1.00	nan	-	0.77386	0.01077	0.02936	I
1.1000	2.30870	0.000102	15	0.156	27.5	1386.5315	10.023	10.329	8.0032e-05	1.00	nan	-	0.84437	0.01078	0.02936	I

Elected signal with QUORUM algorithm from 9 VOTES –> NAME: 3 Period:2.3087015472076207 CORR_SDE: 23.99605835233048 SNR: 12.00697702506435 SDE: 12.813429217263849 FAP: 8.0032e-05 BORDER_SCORE: 1.0 Proposed selection with BASIC algorithm was –> NAME: 3 Period:2.3087015472076207 SNR: 12.00697702506435 New best signal is good enough to keep searching. Going to the next run.

Table B.13: TIC 37749396 report log run 4.

Detrend no.	Period	Per_err	Duration	T0	Depth	SNR	SDE	FAP	Border_score	Matching OI	Harmonic	Plan. rad	Rp/Rs	*a*	Habit.
1	1.8642	0.00008	47.92	1387.48	0.138	11.97	11.64	0.000080	0.95	nan	-	0.79187	0.01032	0.02546	I
2	14.1148	0.00086	94.27	1390.21	0.220	13.53	8.94	0.000240	1.00	TOI 260.01	-	1.00102	0.01396	0.09817	I
8	10.5985	0.00097	104.36	1392.72	0.229	13.72	9.68	0.000080	1.00	nan	-	1.02046	0.01456	0.08110	I
4	2.3087	0.00008	53.86	1386.55	0.132	12.01	12.81	0.000080	1.00	nan	-	0.77568	0.01072	0.02936	I
3	3.6742	0.00019	77.53	1387.09	0.109	9.42	23.37	0.000080	0.90	nan	0.25*SOI2	0.70393	0.01013	0.04002	I

Table B.14: TIC 37749396 candidates report log.

B.8 TIC 357501308

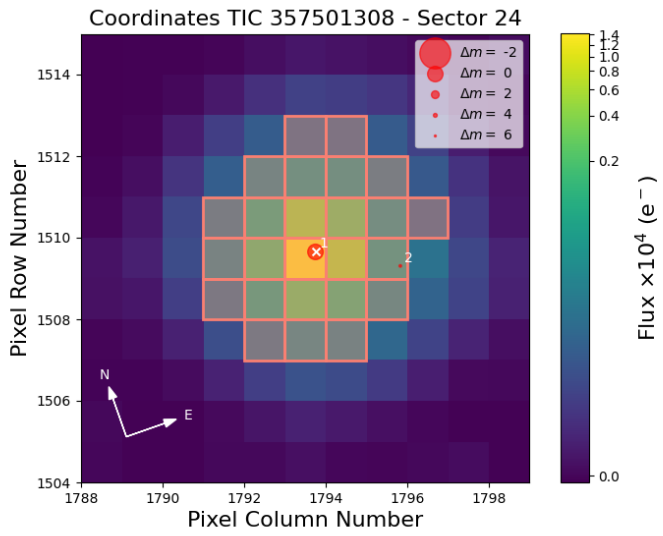

Figure B.40: TIC 357501308 Field of view plot sector 24.

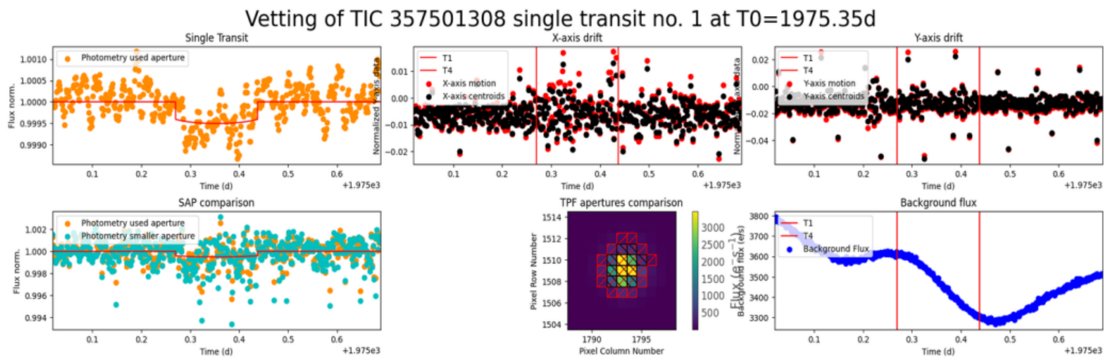

Figure B.41: TIC 357501308 vetting plots of the second transit.

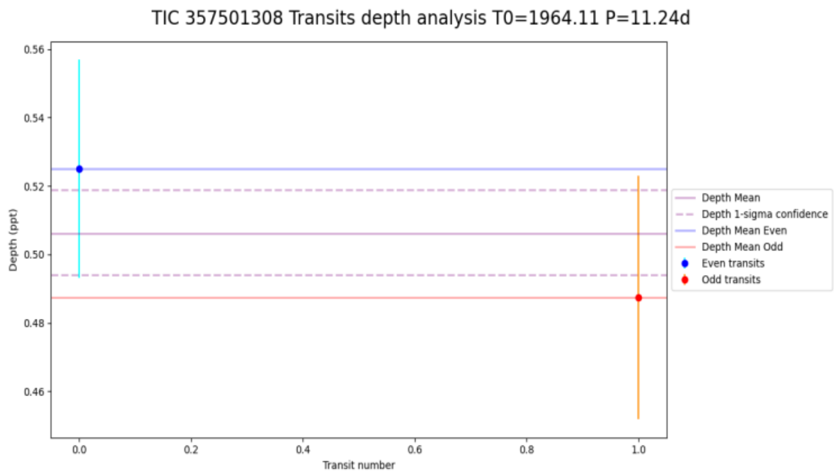

Figure B.42: TIC 357501308 single-transits depths plot.

Win_size	Period	P_err	N.Tra	Depth	T. dur	T0	SNR	SDE	FAP	Border	Match. OI	Harm.	Plan. rad	Rp/Rs	a	Habit.
PDCSAP	26.48465	inf	1	1.059	709.6	1956.1598	35.171	10.189	8.0032e-05	1.00	nan	-	2.21194	0.03255	0.15168	I
0.2000	10.16781	0.044967	3	0.334	132.9	1955.8106	12.190	6.801	0.013445378	0.67	nan	-	1.24201	0.01644	0.08012	I
0.3000	10.16781	0.037509	3	0.422	132.9	1955.8106	15.289	7.483	0.004001601	0.67	nan	-	1.39626	0.01898	0.08012	I
0.4000	2.24499	0.007005	10	0.316	22.6	1957.3551	9.677	6.706	0.015366146	1.00	nan	-	1.20795	0.01420	0.02927	I
0.5000	11.24199	0.068407	2	0.386	241.5	1964.1120	16.998	7.723	0.002480992	1.00	nan	-	1.33570	0.01954	0.08567	I
0.6000	11.24199	0.085336	2	0.429	241.5	1964.1120	18.805	8.710	0.000240096	1.00	nan	-	1.40783	0.02056	0.08567	I
0.7000	11.24199	0.093966	2	0.462	241.5	1964.1120	20.088	9.430	8.0032e-05	1.00	nan	-	1.46034	0.02130	0.08567	I
0.8000	11.24199	0.102405	2	0.486	241.5	1964.1120	20.966	9.678	8.0032e-05	1.00	nan	-	1.49865	0.02185	0.08567	I
0.9000	11.24199	0.102405	2	0.506	241.5	1964.1120	21.633	9.797	8.0032e-05	1.00	nan	-	1.52933	0.02228	0.08567	I
1.0000	11.24199	0.102405	2	0.522	241.5	1964.1120	22.130	9.568	8.0032e-05	1.00	nan	-	1.55264	0.02261	0.08567	I
1.1000	11.24199	0.102405	2	0.534	241.5	1964.1120	22.505	9.408	8.0032e-05	1.00	nan	-	1.57060	0.02286	0.08567	I

Elected signal with QUORUM algorithm from 7 VOTES –> NAME: 7 Period:11.241990704526843 CORR_SDE: 16.20904520633399 SNR: 21.63310279618836 SDE: 9.796675674157907 FAP: 8.0032e-05 BORDER_SCORE: 1.0 Proposed selection with BASIC algorithm was –> NAME: PDCSAP_FLUX Period:26.484653470798303 SNR: 35.171458186210764 New best signal is good enough to keep searching. Going to the next run.

Table B.15: TIC 357501308 report log run 2.

Detrend no.	Period	Per_err	Duration	T0	Depth	SNR	SDE	FAP	Border_score	Matching OI	Harmonic	Plan. rad	Rp/Rs	a	Habit.
2	7.4332	0.02961	134.98	1958.26	0.834	38.65	21.09	0.000080	1.00	TOI 2018.01	-	1.96364	0.02835	0.06502	I
8	11.2420	0.10240	241.52	1964.11	0.506	21.63	9.80	0.000080	1.00	nan	-	1.52933	0.02228	0.08567	I
0	26.4310	inf	698.99	1956.16	1.062	34.94	8.25	0.001040	1.00	nan	-	2.21492	0.03264	0.15148	I
0	5.5773	0.08051	134.06	1958.52	0.556	14.61	10.74	0.000080	1.00	nan	0.5*SOI2	1.60357	0.02270	0.05369	I
0	10.7593	0.08863	243.11	1958.58	0.782	24.38	16.27	0.000080	0.67	nan	-	1.90145	0.02675	0.08320	I

Table B.16: TIC 357501308 candidates report log.

B.9 TIC 368435330

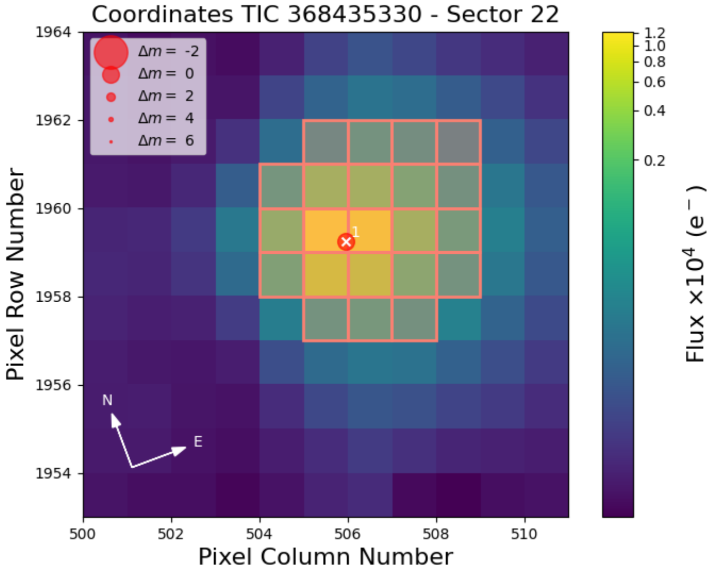

Figure B.43: TIC 368435330 Field of view plot sector 22.

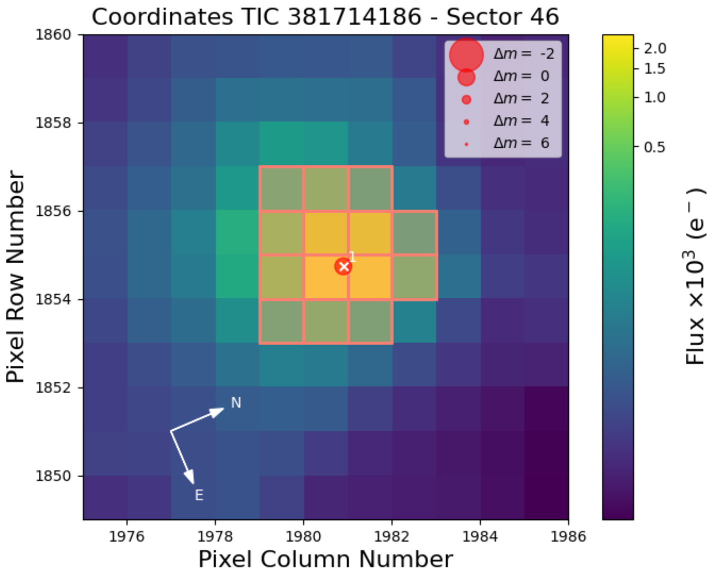

Figure B.44: TIC 368435330 Field of view plot sector 46.

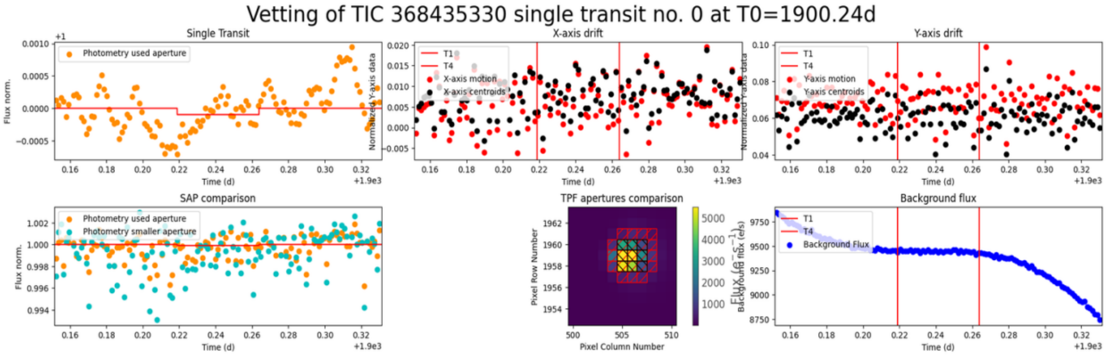

Figure B.45: TIC 368435330 vetting plots of the first transit.

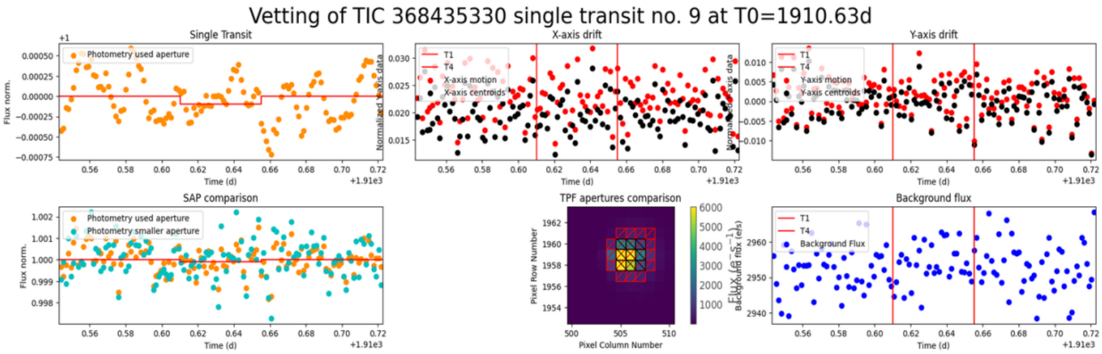

Figure B.46: TIC 368435330 vetting plots of the tenth transit.

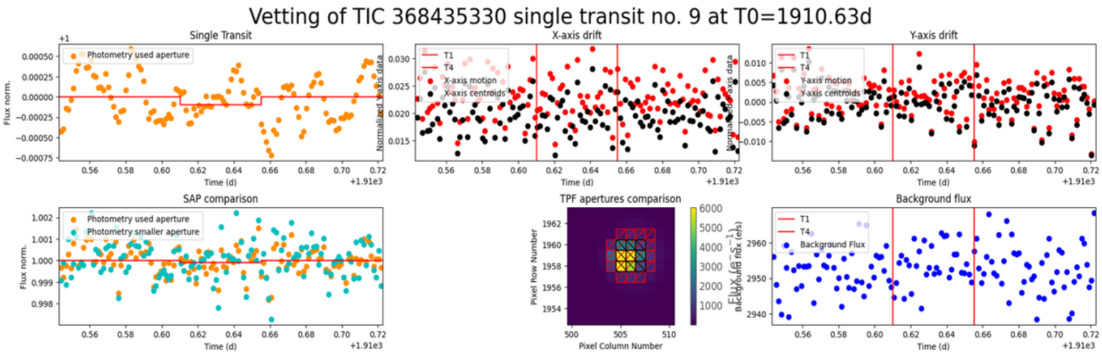

Figure B.47: TIC 368435330 vetting plots of the twentieth transit.

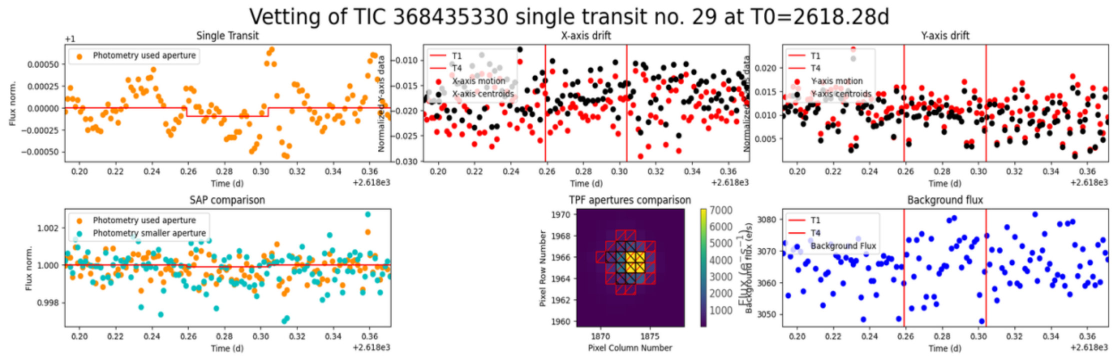

Figure B.48: TIC 368435330 vetting plots of the thirtieth transit.

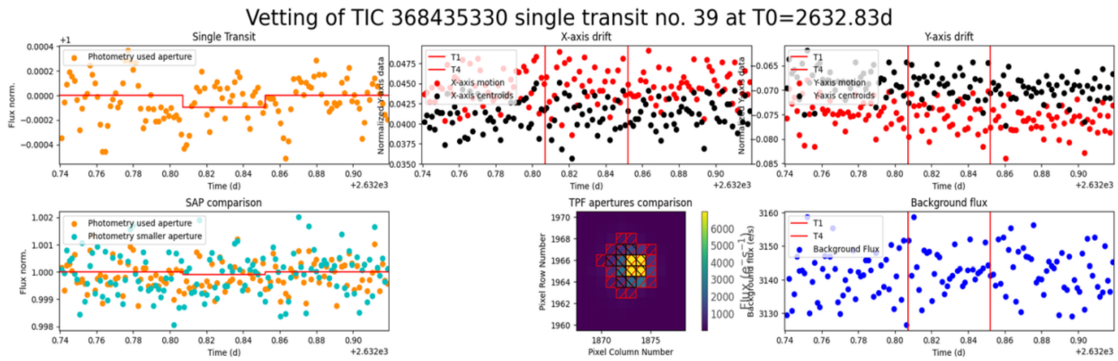

Figure B.49: TIC 368435330 vetting plots of the fortieth transit.

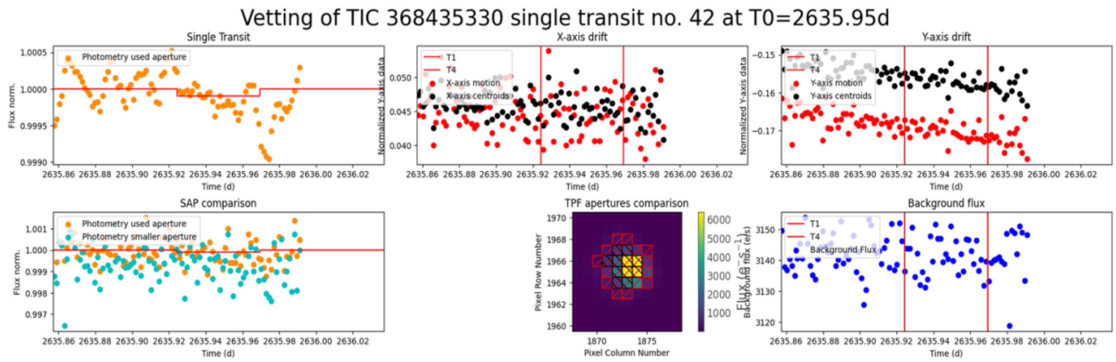

Figure B.50: TIC 368435330 vetting plots of the last transit.

Win_size	Period	P_err	N.Tra	Depth	T. dur	T0	SNR	SDE	FAP	Border	Match. OI	Harm.	Plan. rad	Rp/Rs	*a*	Habit.
PDCSAP	1.03913	0.000074	43	0.227	9.6	1900.2393	11.493	17.974	8.0032e-05	1.00	nan	-	1.72583	0.01126	0.02064	I
0.2000	1.03913	0.000055	43	0.098	64.7	1900.2414	14.768	93.080	8.0032e-05	0.98	nan	-	1.13238	0.00878	0.02064	I
0.3000	1.03913	0.000055	43	0.122	64.7	1900.2414	17.869	50.105	8.0032e-05	0.98	nan	-	1.26317	0.00994	0.02064	I
0.4000	1.03913	0.000074	43	0.141	64.7	1900.2414	20.286	30.005	8.0032e-05	0.98	nan	-	1.35958	0.01076	0.02064	I
0.5000	1.03913	0.000074	43	0.150	64.7	1900.2414	21.443	24.497	8.0032e-05	0.98	nan	-	1.40256	0.01111	0.02064	I
0.6000	1.03913	0.000074	43	0.155	64.7	1900.2414	21.943	21.217	8.0032e-05	0.98	nan	-	1.42463	0.01133	0.02064	I
0.7000	1.03913	0.000074	43	0.159	64.7	1900.2414	22.363	19.131	8.0032e-05	0.98	nan	-	1.44455	0.01148	0.02064	I
0.8000	1.03913	0.000074	43	0.160	64.7	1900.2414	22.222	16.602	8.0032e-05	0.98	nan	-	1.44676	0.01152	0.02064	I
0.9000	1.03913	0.000074	43	0.159	64.7	1900.2414	21.973	14.942	8.0032e-05	0.98	nan	-	1.44401	0.01151	0.02064	I
1.0000	1.03913	0.000074	43	0.228	6.5	1900.2383	10.147	14.367	8.0032e-05	1.00	nan	-	1.73098	0.01157	0.02064	I
1.1000	1.03913	0.000074	43	0.232	6.5	1900.2383	10.219	14.354	8.0032e-05	1.00	nan	-	1.74314	0.01168	0.02064	I

Elected signal with QUORUM algorithm from 11 VOTES –> NAME: 0 Period:1.0391321497522663 CORR_SDE: 190.0954314237361 SNR: 14.768032556426611 SDE: 93.0798541029267 FAP: 8.0032e-05 BORDER_SCORE: 0.9767441860465116 Proposed selection with BASIC algorithm was –> NAME: 0 Period:1.0391321497522663 SNR: 14.768032556426611 New best signal is good enough to keep searching. Going to the next run.

Table B.17: TIC 368435330 report log run 2.

Detrend no.	Period	Per_err	Duration	T0	Depth	SNR	SDE	FAP	Border_score	Matching OI	Harmonic	Plan. rad	Rp/Rs	*a*	Habit.
2	3.6452	0.00039	96.41	1902.87	0.648	60.68	57.79	0.000080	1.00	TOI 1797.01	-	2.91504	0.02047	0.04765	I
1	1.0391	0.00006	64.74	1900.24	0.098	14.77	93.08	0.000080	0.98	nan	-	1.13238	0.00878	0.02064	I
3	22.9398	0.00228	185.28	1901.48	0.105	15.85	141.99	0.000080	1.00	nan	-	1.17605	0.01507	0.16242	I
6	15.2110	0.00132	154.17	1906.61	0.253	14.05	269.79	0.000080	1.00	nan	-	1.82248	0.01441	0.12350	I

Table B.18: TIC 368435330 candidates report log.

B.10 TIC 14440192

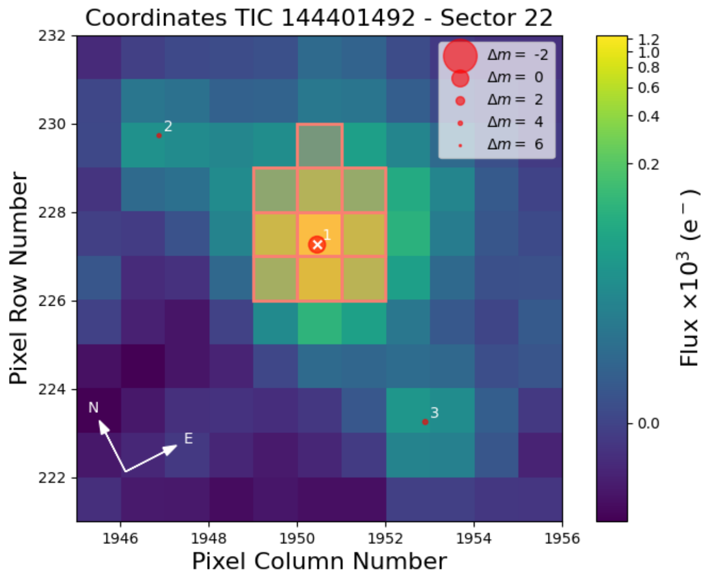

Figure B.51: TIC 14440192 Field of view plot sector 22.

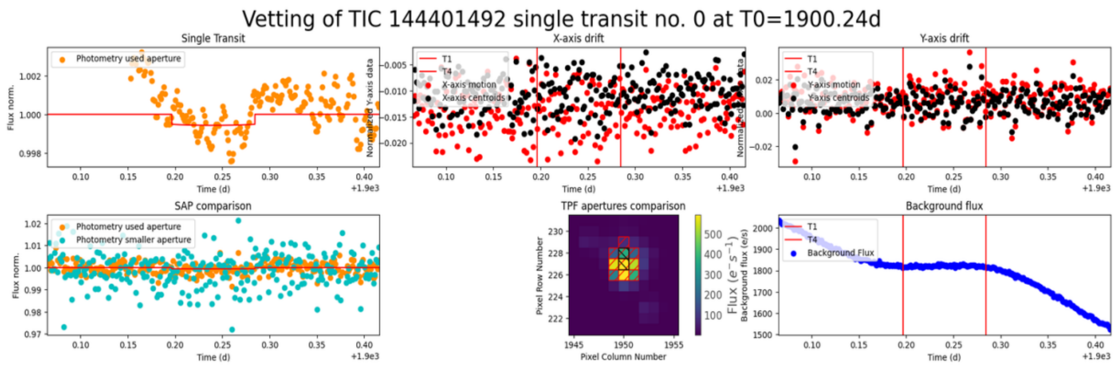

Figure B.52: TIC 14440192 vetting plots of the first transit.

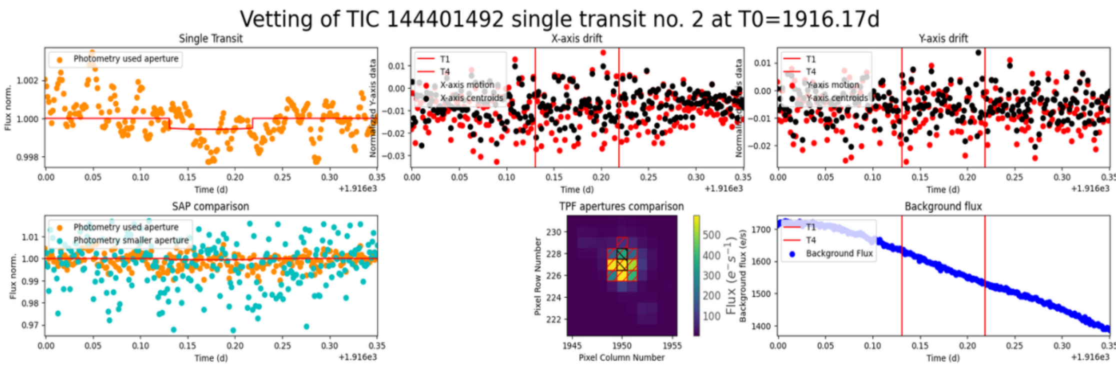

Figure B.53: TIC 14440192 vetting plots of the third transit.

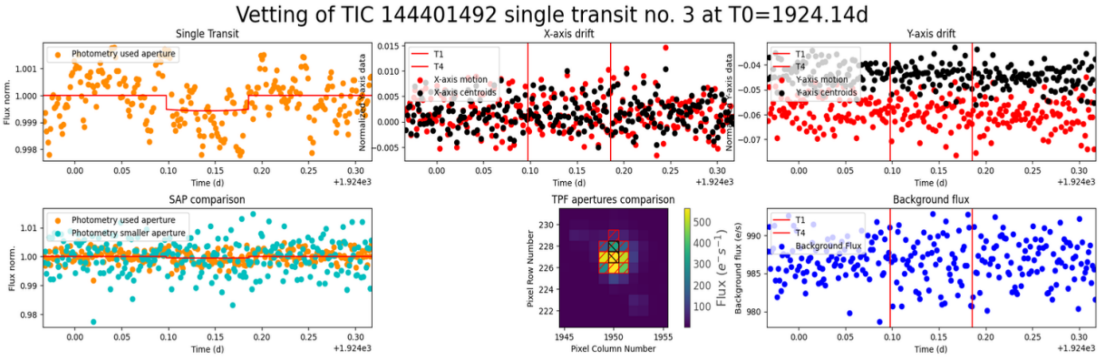

Figure B.54: TIC 14440192 vetting plots of the fourth transit.

Win_size	Period	P_err	N.Tra	Depth	T. dur	T0	SNR	SDE	FAP	Border	Match. OI	Harm.	Plan. rad	Rp/Rs	*a*	Habit.
PDCSAP	11.84470	0.230418	1	1.905	338.0	1903.0479	18.348	8.205	0.001040416	1.00	nan	-	3.28597	0.04260	0.09431	I
0.2000	3.73716	0.008265	8	0.441	102.3	1900.2499	10.268	8.509	0.000640256	0.88	nan	-	1.58060	0.02138	0.04371	I
0.3000	7.96709	0.017025	4	0.507	126.6	1900.2405	9.098	6.298	0.033053221	1.00	nan	-	1.69487	0.02362	0.07240	I
0.4000	7.96709	0.017025	4	0.514	126.6	1900.2405	9.194	5.909	0.065866347	1.00	nan	-	1.70683	0.02376	0.07240	I
0.5000	7.96709	0.017025	4	0.530	126.6	1900.2405	9.471	6.185	0.040736295	1.00	nan	-	1.73381	0.02413	0.07240	I
0.6000	7.96709	0.017025	4	0.545	126.6	1900.2405	9.741	6.606	0.018727491	1.00	nan	-	1.75804	0.02440	0.07240	I
0.7000	7.96709	0.017025	4	0.538	126.6	1900.2405	9.635	6.557	0.020488195	1.00	nan	-	1.74688	0.02426	0.07240	I
0.8000	7.96709	0.017025	4	0.542	126.6	1900.2405	9.719	6.799	0.01352541	1.00	nan	-	1.75334	0.02435	0.07240	I
0.9000	7.96709	0.017025	4	0.549	126.6	1900.2405	9.841	7.051	0.008563425	1.00	nan	-	1.76415	0.02451	0.07240	I
1.0000	7.96709	0.017025	4	0.562	126.6	1900.2405	10.047	7.397	0.004481793	1.00	nan	-	1.78419	0.02477	0.07240	I
1.1000	7.96709	0.017025	4	0.573	126.6	1900.2405	10.223	7.507	0.004001601	1.00	nan	-	1.80179	0.02498	0.07240	I

Elected signal with QUORUM algorithm from 9 VOTES –> NAME: 9 Period:7.967090151154406 CORR_SDE: 14.05923354926108 SNR: 10.223072634799072 SDE: 7.5073577204792175 FAP: 0.004001601 BORDER_SCORE: 1.0 Proposed selection with BASIC algorithm was –> NAME: 0 Period:3.7371551567944152 SNR: 10.267661743039634 New best signal is good enough to keep searching. Going to the next run.

Table B.19: TIC 144401492 report log run 3.

Detrend no.	Period	Per_err	Duration	T0	Depth	SNR	SDE	FAP	Border_score	Matching OI	Harmonic	Plan. rad	Rp/Rs	*a*	Habit.
4	12.8828	0.06456	177.12	1911.68	2.068	29.74	13.00	0.000080	1.00	TOI 1803.01	-	3.42354	0.04585	0.09974	I
10	6.2965	0.03732	141.69	1904.62	1.501	28.08	18.12	0.000080	1.00	TOI 1803.02	0.5*SOI1	2.91664	0.03880	0.06189	I
10	7.9671	0.01702	126.63	1900.24	0.573	10.22	7.51	0.004002	1.00	nan	-	1.80179	0.02498	0.07240	I
2	2.0727	0.00565	90.62	1901.31	0.389	9.57	6.12	0.044898	1.00	nan	0.25*SOI3	1.48466	0.01859	0.02950	I
10	4.1258	0.01176	35.13	1900.97	0.816	9.48	8.49	0.000640	1.00	nan	0.5*SOI3	2.14988	0.02167	0.04669	I

Table B.20: TIC 144401492 candidates report log.

B.11 TIC 306263608

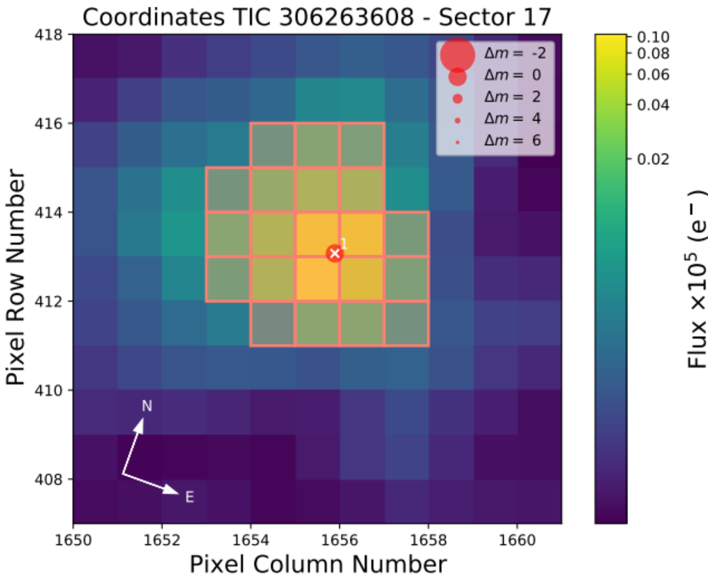

Figure B.55: TIC 306263608 Field of view plot sector 17.

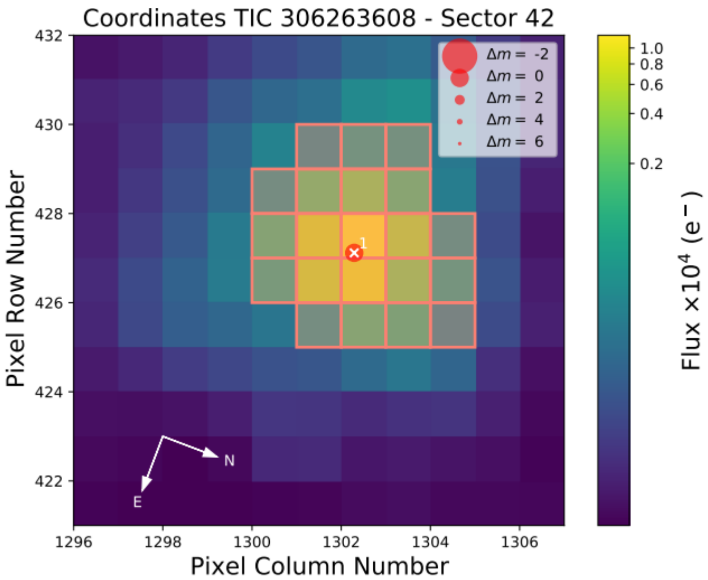

Figure B.56: TIC 306263608 Field of view plot sector 42.

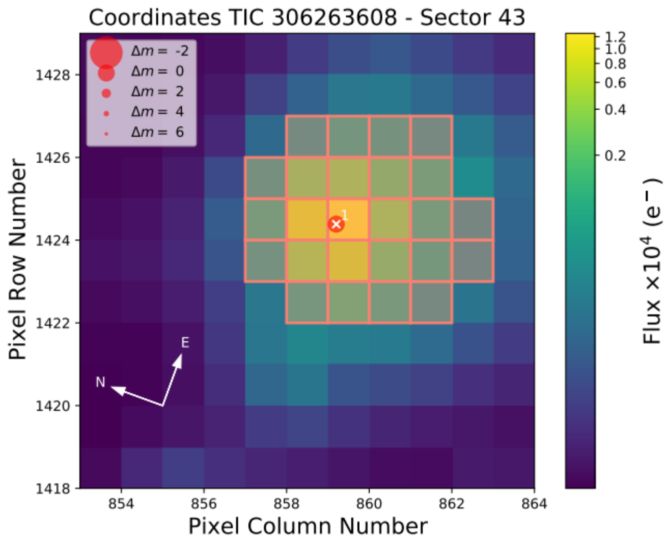

Figure B.57: TIC 306263608 Field of view plot sector 43.

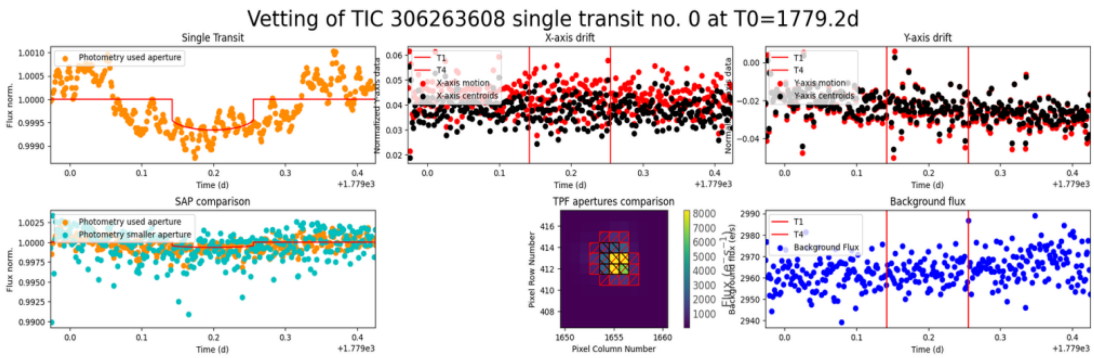

Figure B.58: TIC 306263608 vetting plots of the first transit.

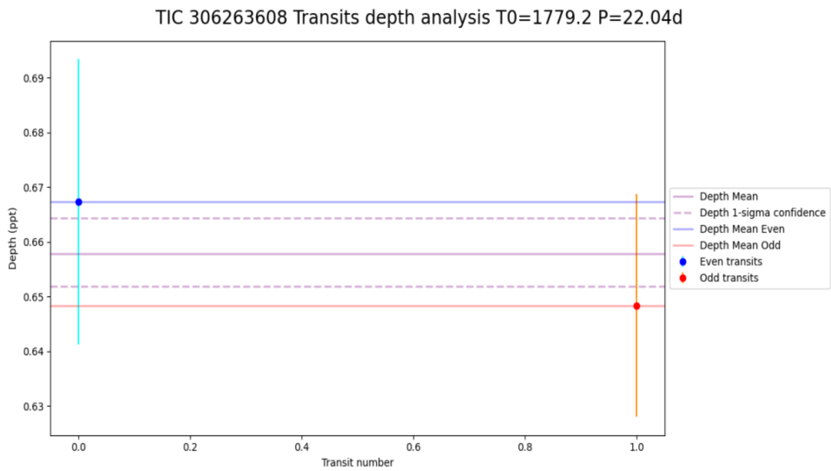

Figure B.59: TIC 306263608 single-transits depths plot.

Win_size	Period	P_err	N.Tra	Depth	T. dur	T0	SNR	SDE	FAP	Border	Match. OI	Harm.	Plan. rad	Rp/Rs	*a*	Habit.
PDCSAP	22.04249	0.004103	2	1.211	178.6	1779.1996	61.172	11.881	8.0032e-05	1.00	nan	-	3.67211	0.03145	0.15415	I
0.2000	35.96484	0.005910	2	0.102	201.5	1779.1220	6.224	10.932	8.0032e-05	0.50	nan	-	1.06332	0.01114	0.21364	I
0.3000	23.56323	0.002242	2	0.137	129.3	1779.2271	6.693	10.481	8.0032e-05	1.00	nan	-	1.23456	0.01123	0.16116	I
0.4000	22.04249	0.004103	2	0.419	162.7	1779.1989	22.463	14.070	8.0032e-05	1.00	nan	-	2.15935	0.01861	0.15415	I
0.5000	22.04249	0.004103	2	0.658	162.7	1779.1989	34.699	15.135	8.0032e-05	1.00	nan	-	2.70600	0.02279	0.15415	I
0.6000	22.04249	0.004103	2	0.777	162.7	1779.1989	40.470	14.881	8.0032e-05	1.00	nan	-	2.94064	0.02514	0.15415	I
0.7000	22.04249	0.004103	2	0.874	162.7	1779.1989	45.104	14.213	8.0032e-05	1.00	nan	-	3.11958	0.02705	0.15415	I
0.8000	22.04249	0.004103	2	0.976	162.7	1779.1989	49.914	13.640	8.0032e-05	1.00	nan	-	3.29640	0.02886	0.15415	I
0.9000	23.56323	0.004484	2	1.067	190.9	1779.1864	58.618	12.996	8.0032e-05	1.00	nan	-	3.44582	0.02927	0.16116	I
1.0000	22.04249	0.004103	2	1.135	178.6	1779.1996	59.590	12.641	8.0032e-05	1.00	nan	-	3.55399	0.03038	0.15415	I
1.1000	22.04249	0.004103	2	1.181	178.6	1779.1996	61.629	12.557	8.0032e-05	1.00	nan	-	3.62603	0.03096	0.15415	I

Elected signal with QUORUM algorithm from 8 VOTES –> NAME: 3 Period:22.042487873232716 CORR_SDE: 26.693223168733056 SNR: 34.699470490534424 SDE: 15.135332724539362 FAP: 8.0032e-05 BORDER_SCORE: 1.0 Proposed selection with BASIC algorithm was –> NAME: 3 Period:22.042487873232716 SNR: 34.699470490534424 New best signal is good enough to keep searching. Going to the next run.

Table B.21: TIC 306263608 report log run 1.

Detrend no.	Period	Per_err	Duration	T0	Depth	SNR	SDE	FAP	Border_score	Matching OI	Harmonic	Plan. rad	Rp/Rs	*a*	Habit.
4	22.0425	0.00410	162.70	1779.20	0.658	34.70	15.14	0.000080	1.00	nan	-	2.70600	0.02279	0.15415	I
10	48.6011	0.00883	220.79	1782.11	0.153	6.70	6.86	0.012085	1.00	nan	-	1.30584	0.01463	0.26113	I
7	44.5505	0.00524	195.31	1782.74	0.122	8.86	7.11	0.007843	1.00	nan	-	1.16643	0.01290	0.24641	I
6	10.4631	0.00152	123.42	1766.04	0.089	6.56	7.31	0.005362	1.00	nan	0.25*SOI3	0.99358	0.00999	0.09380	I
0	12.8650	0.00350	137.53	1766.35	0.185	8.95	37.73	0.000080	1.00	nan	0.25*SOI2	1.43564	0.01403	0.10766	I

Table B.22: TIC 306263608 candidates report log.